

ABSTRACT

Title of dissertation: ENERGY, STARS,
AND BLACK HOLES IN
EINSTEIN-AETHER THEORY

Christopher Thomas Eling
Doctor of Philosophy, 2007

Dissertation directed by: Professor Theodore Jacobson
Department of Physics

In recent years there have been hints of Lorentz violation in various approaches to quantum gravity. Lorentz violating physics has also been proposed as an explanation for unexpected observational anomalies such as atmospheric cosmic rays apparently observed above the GZK cutoff, the flatness of galactic rotation curves and the accelerating expansion of the universe. In this dissertation we will consider an alternative theory of gravity that exhibits Lorentz violation. This “Einstein-aether” theory is a four parameter class of theories where a dynamical unit timelike vector field (the “aether”) is coupled to gravity. We will focus particularly on energy, stars, and black holes in the theory. First, using pseudotensor methods we find expressions for the Einstein-aether energy. These are then applied to find the energy in both linear and non-linear regimes. Enforcing the energy positivity of linearized wave modes yields an important constraint on the four parameters. An expression for the energy of an asymptotically flat spacetime is also obtained, but a complete positive energy theorem remains elusive. Next, we study in detail non-linear spher-

ically symmetric solutions in the theory. The time independent asymptotically flat solutions fall into two classes depending on whether the aether is aligned with the timelike Killing vector. “Static” solutions aligned with the Killing vector describe the interior and vacuum regions of fluid stars. We characterize properties such as maximum masses and surface redshifts for candidate neutron star equations of state. Only tentative observational constraints on the theory are currently possible due to uncertainties in neutron star physics. Black hole solutions, which must be non-static, are shown to exist in a class of Einstein-aether theories using numerical integration. The geometry outside the horizon is very similar to the Schwarzschild solution of General Relativity, but there are qualitative differences inside. Finally, we investigate classical two-dimensional Einstein-aether theory as a toy model that could be used to study the Hawking effect and quantization in a Lorentz violating setting. We conclude by examining directions for future research.

Energy, stars, and black holes in Einstein-aether theory

by

Christopher Thomas Eling

Dissertation submitted to the Faculty of the Graduate School of the
University of Maryland, College Park in partial fulfillment
of the requirements for the degree of
Doctor of Philosophy
2007

Advisory Committee:

Professor Theodore Jacobson, Chair/Advisor

Professor Alessandra Buonanno

Professor M. Coleman Miller

Professor Charles Misner

Professor Christopher Reynolds

© Copyright by
Christopher Thomas Eling
2007

Preface

Portions of this dissertation appear in slightly altered form in the following publications:

Chapter 2 as C. Eling, “Energy in the Einstein-aether theory,” *Phys. Rev. D* **73**, 084026 (2006) [arXiv:gr-qc/0507059].

Chapter 3 and parts of Chapter 4 as C. Eling and T. Jacobson, “Spherical Solutions in Einstein-Aether Theory: Static Aether and Stars,” *Class. Quant. Grav.* **23**, 5625 (2006) [arXiv:gr-qc/0603058].

Parts of Chapter 4 as C. Eling, T. Jacobson, and M. C. Miller, “Neutron stars in Einstein-aether theory,” *Phys. Rev. D* to appear.

Chapter 5 as C. Eling and T. Jacobson, “Black holes in Einstein-aether theory,” *Class. Quant. Grav.* **23**, 5643 (2006) [arXiv:gr-qc/0604088].

Chapter 6 as C. Eling and T. Jacobson, “Two-dimensional gravity with a dynamical aether,” *Phys. Rev. D* **74**, 084027 (2006) [arXiv:gr-qc/0608052].

Acknowledgements

I want to thank my parents for their love and support while I was working on the various projects in this dissertation. I also would like to thank my friend Matthew Corne for his encouragement over the years and for taking the time to review this work for typographical and other errors.

I also acknowledge my colleagues David Brown and Brendan Foster for background discussions and Cole Miller and Chris Reynolds for suggesting the neutron star project to me and for their help on the astrophysical aspects of that project.

Finally, I give special thanks to my advisor, Ted Jacobson, for his advice, ideas, and patience while guiding this thesis.

Table of Contents

List of Tables	vii
List of Figures	viii
List of Abbreviations	xii
1 Introduction	1
1.1 A Brief Primer to Lorentz Violation	1
1.2 Einstein-aether theory and Gravitational Lorentz Violation	4
1.3 Related Work on ae-theory phenomenology	7
1.4 Outline of Thesis	10
2 Energy in Einstein-aether theory	14
2.1 Introduction	14
2.2 Field Equations	16
2.3 Weinberg Pseudotensor	17
2.4 Lagrangian Approach to Pseudotensors	20
2.4.1 Summary of Results	20
2.4.2 Basic Formalism	23
2.4.3 Application to GR and ae-theory	26
2.4.4 Relation to Noether Charge approach	30
2.5 Energy in Linearized Theory	33
2.6 Non-Linear Energy	38
2.7 Discussion	42
3 Spherical Solution Properties and Static Aether	44
3.1 Introduction	44
3.2 General Properties	45
3.2.1 Classification of stationary spherical solutions	48
3.2.2 Asymptotic Flatness	50
3.3 Static Aether	52
3.3.1 Field equations with static aether	52
3.3.2 Static aether solutions: general analysis	54
3.3.2.1 The GR limit: Schwarzschild solution	57
3.3.2.2 Static aether solutions for generic c_1	58
3.3.2.3 Charged dust interpretation	64
3.3.2.4 Solutions with $Y \in (Y_-, Y_+)$	67
3.4 Nonexistence of pure aether stars	68
3.5 Discussion	69

4	Fluid Stars	71
4.1	Introduction	71
4.2	Basic Properties of Stellar Solutions	74
4.2.1	Stellar Equations of Structure	77
4.2.1.1	Surface redshift	79
4.2.1.2	ISCO	80
4.3	Constant Density stars	81
4.4	Neutron Stars	84
4.4.1	Numerical Results	86
4.4.2	Maximum mass constraints	90
4.4.3	Surface redshift constraints	92
4.5	Discussion	94
5	Black Holes	96
5.1	Introduction	96
5.2	General properties of black holes in ae-theory	99
5.3	Field Redefinitions	103
5.4	Generic behavior of horizons and spatial infinity	105
5.4.1	Metric horizon expansion	106
5.4.2	Asymptotic expansion	108
5.4.3	Asymptotically flat solutions and spin-0 horizon regularity	110
5.5	Black holes with regular spin-0 horizons	115
5.5.1	Horizon expansion	115
5.5.2	Asymptotically flat black holes	117
5.5.2.1	Black hole mass	118
5.5.2.2	Horizons	119
5.5.2.3	Oscillations	120
5.5.2.4	Curvature singularity	121
5.5.2.5	Aether congruence	122
5.5.2.6	Surface gravity and the first law of black hole mechanics	124
5.5.2.7	Black hole properties for different values of c_1	126
5.6	Recent and related work on ae-theory black holes	128
5.6.1	Numerical simulations of gravitational collapse	128
5.6.2	Generalized second law violation	130
5.7	Discussion	133
6	Einstein-aether theory in two-dimensions	135
6.1	Introduction	135
6.2	1+1 dimensional action	137
6.3	Field equations and solutions	140
6.4	$\beta = 1$: Flat spacetime solutions	143
6.5	$0 < \beta \neq 1$ solutions	146
6.5.1	Non-constant curvature solution	146
6.5.2	Constant curvature solutions	147

6.5.2.1	$\beta < 1$: de Sitter solution in adapted coordinates . . .	149
6.5.2.2	$\beta > 1$: Anti-de Sitter solution	152
6.6	Discussion	154
7	Conclusion	155
7.1	Summary of Results	155
7.2	Reflections and Future Directions	158
	Bibliography	160

List of Tables

2.1	Wave Mode Speeds and Polarizations	34
3.1	Sphere radius and metric functions at special Y values.	57
5.1	Properties of black hole solutions for several c_1 values, in units with $r_h = 1$	127

List of Figures

3.1	Graph of r/r_{\min} vs. Y for $c_1 = 1$. The curves approach 1 asymptotically on both sides. The range $(Y_+, 0)$ defines a negative mass solution with naked singularity at $Y = Y_+$ and asymptotically flat region at $Y \rightarrow 0$. The range $(0, \infty)$ defines a positive mass solution, with a minimal 2-sphere as $Y \rightarrow \infty$. The range $(-\infty, Y_-)$ continues that solution to the other side of the minimal sphere, with a singularity at a sphere of infinite radius at $Y = Y_-$. This sphere lies at finite radial distance if $c_1 < 3/2$. There is no solution with timelike aether in the range (Y_-, Y_+) since the radial coordinate is timelike there (see Section 3.3.2.4).	56
3.2	Carter-Penrose diagram of the static aether solution. The left hand edge corresponds to spheres of infinite radius and is singular.	60
3.3	Plot of area radius r vs. proper length l for fixed mass M , in units with $2M = 1$, for $c_1 = 0, 0.1, 0.7$, and 1.9 . In the GR case $c_1 = 0$ this is the Einstein-Rosen bridge. For $c_1 = 0.1$ the radius flares out to infinity so quickly that the code used to make the plot halted at small radius. With increasing c_1 the throat widens, the flare-out inside is slower, and the proper length to the curvature singularity increases, becoming infinite for $c_1 \geq 3/2$	64
3.4	Plot of $r(l)$ and the norm of the Killing vector $\sqrt{N_s(l)}$ for GR and for $c_1 = 0.5$, for the solution with the same value of the total mass M , in units with $2M = 1$. In GR N_s vanishes at the bifurcation sphere at the center of the Einstein-Rosen bridge. In the ae-theory solution the Killing vector remains timelike at the throat, but at the internal $r = \infty$ curvature singularity both the norm and its slope vanish, indicating the presence of a singular extremal Killing horizon.	65
4.1	Total mass vs. central pressure P_0 in a constant density star, in units with $\rho = 1$ and $8\pi G = 1$, for several values of $c_{14} \equiv c_1$. The GR curve asymptotically approaches $M = (4\pi/3)(24/9)^{3/2}$. As c_{14} grows the maximum mass decreases, and the curve develops a sharp local maximum and a shallow local minimum.	82

4.2	Total mass vs. R for a constant density star, in units with $\rho = 1$ and $8\pi G = 1$, for P_0 up to 300 and several values of $c_{14} \equiv c_1$. For small pressures all the curves increase uniformly. For $c_{14} = 0.005$ the slope is nearly the same as in GR. For $c_{14} = 0.05$ a maximum occurs for a large central pressure. By $c_{14} = 0.6$, the first maximum occurs at much smaller pressures, and there is also a minimum. For $c_{14} = 1.6$ a second maximum has appeared.	84
4.3	Graphical representation of (4.22) (solid line) and (4.23) (dashed lines). The allowed region of the parameter space is below the solid curve, above $c_- = 0$ and to the left of $c_+ = 1$. The radiation damping constraint will restrict to a nearly one-dimensional subset of this region.	87
4.4	Total mass vs. central pressure P_0 for the Hm equation of state for c_{14} values 0, 0.05, 0.2, 0.5, and 1. The vertical axis is in units of solar masses and horizontal in $1/(100\text{km})^2$. As c_{14} grows from 0.05 to 1 the maximum mass decreases from near the GR value of 2.20 to less than 1.9.	88
4.5	Total mass versus R for the Hm equation of state for P_0 up to 100 and c_{14} values 0, 0.05, 0.2, 0.5, and 1. The vertical axis is units of solar masses and the horizontal in km. The GR curve reaches its maximum mass of 2.20 solar masses at slightly more than 10 km. For $c_{14} = 0.05$ the curve is slightly inside GR curve. As c_{14} increases to 1 the maximum masses decrease and the value of the radius at these maxima falls to about 9.5 km.	89
4.6	Maximum mass vs. c_{14} for the six equations of state. The hadronic models are plotted with solid lines, while the quark models are dashed. The thick solid horizontal lines represent the bare minimum constraint of 1.44 solar masses and a possible constraint value of $2 M_\odot$	90
4.7	Redshift factor z versus c_{14} for 1.8 solar mass neutron stars using the hardest equations of state. Hm (solid) is on top, Qh (dashed) is in the middle and Hh (solid) is on the bottom. Note that the GR value of 0.35 for the hardest eos, Hh, is consistent with the proposed redshift of 0.35 [84]. The Hm and Qh lines begin to curve up near $c_{14} = 1.1-1.2$ because the maximum mass for these equations of state is approaching 1.8 solar masses.	94

5.1	Solution for reduced theory (5.14) with $c'_1 = 0.051$ and $c'_2 = 0.116$, determined by data $N_1 = -1$ and $a_2 = -0.1$ at spatial infinity. There is both an outer and inner metric horizon where N vanishes, but f does not decrease enough to reach a spin-0 horizon. The functions N and f go to zero slightly inside $r = 1$ which would be the horizon radius of the corresponding Schwarzschild solution. As a_2 increases the minimum of $f(r)$ decreases until the solution acquires a spin-0 horizon, where is it generically singular.	113
5.2	Plots of f , N , B , a , and S (the Schwarzschild version of N) vs. $z = r - r_h$ for $c_1 = 0.3$, in units with $r_0 = 2$. The horizon radius is $r_h \approx 2.07$ for the ae-theory black hole, so $S = 0$ at $z \approx -0.07$. The solutions agree closely outside the horizon. Deviations are noticeable near the horizon and become significant in the interior, where N blows up more rapidly. Near the singularity f begins to oscillate rapidly. . .	118
5.3	Oscillations of $f = Na^2$ near the singularity inside the black hole solution shown in Figure 5.2, plotted vs. $z = r - r_h$ in units with $M = 1$	121
5.4	Plot of $\ln R_{abcd}R^{abcd}$ vs. $\ln r$ for $c_1 = 0.3$ ae-theory black hole (wiggly curve) and Schwarzschild black hole (straight line) of the same mass, in units with $M = 1$. r is plotted on a logarithmic scale. The slope for the GR case is -6 , while for the ae-theory case it alternates between roughly -6 and -4.5	122
5.5	Radial proper velocity $dr/d\tau$ of free-fall (lower, solid curve) and aether (upper, dashed curve) vs. $z = r - r_h$, in units with $M = 1$, for $c_1 = 0.3$. In contrast to the free-falling geodesics, the aether does not begin to fall significantly inward until close to the horizon.	124
5.6	Inward 3-velocity of the aether relative to free-fall inside the horizon for $c_1 = 0.3$. The velocity is initially negative and the aether lags behind the free-fall. Near the singularity the velocity oscillates between between faster and slower than free-fall.	125
6.1	Plot of the flow lines of (6.31) in Minkowski space with Cartesian coordinates t (increasing vertically) and x (increasing toward the right). The u^a field approaches the null vector ∂_v along the line $w = t - x = 0$, hence must be infinitely stretched there in order to maintain the unit constraint.	144
6.2	Plot of the flow lines of (6.33) in Minkowski space with Cartesian coordinates t and x . Here the aether is singular along the lines $w = t - x = 0$ and $v = t + x = 0$	145

- 6.3 Conformal diagram of 1+1 dS spacetime with the flow lines of the aether field. Horizontal lines at the top and bottom represent null infinity, while the two vertical lines at left and right are identified. The solid and dashed grey lines form the past and future horizons of the Killing horizon for the boost symmetry under which the aether is invariant. The slope of the flow lines is $-\beta^{-1/2}$ on all boundaries of the diagram which is drawn for the case $\beta = 0.1$ 152
- 6.4 Conformal diagram of 1+1 AdS spacetime with the flow lines of the aether field. The two vertical lines at left and right are at null infinity, and the diagram should be continued infinitely in the vertical direction. The aether is regular in the Poincaré patch bounded by the solid grey lines and null infinity. The dashed grey lines are the rest of the boost Killing horizon. The diagram is drawn for the case $\beta = 10$ 153

List of Abbreviations

c_{14}	$c_1 + c_4$
c_{123}	$c_1 + c_2 + c_3$
c_{13} or c_+	$c_1 + c_3$
c_-	$c_1 - c_3$

Chapter 1

Introduction

1.1 A Brief Primer to Lorentz Violation

For over a century Lorentz invariance has been a basic assumption in physics. It is the fundamental symmetry principle of Special Relativity, provides a part of the foundation of Quantum Field Theory and has been shown to hold in all accepted experiments. In this dissertation we will study the predictions of a certain class of theories that incorporate Lorentz violation (LV) into gravity. But why consider the possibility of LV at all? At a basic level, one reason is that the entire infinite parameter space of boosts can never be completely probed and without tests it is unreasonable to just assert the symmetry is exact. A more compelling motivation is that hints of LV effects have been seen in the various approaches to the problem of quantum gravity. Finally, there have been series of unexpected observations that may be explained as emerging from new physics. For example, the unconfirmed observation [1] of cosmic rays in the atmosphere above the Griesen-Zatsepin-Kuzmin (GZK) cutoff [2, 3] could be explained by LV, as was first discussed in [4]¹. In addition, theories with LV fields may be able also account for the flattening of galaxy rotation curves and structure formation [6, 7] without the hypothesis of dark

¹more recently the HiRes experiment [5] has reported an observation of the cutoff at the expected GZK energy

matter. These fields could also help explain other aspects of cosmology, such as the observed accelerating expansion of the universe [8, 9] and giving inflation without the “inflaton” field [10]

There are a number of possibilities for the fate of the symmetry. The first is that what we know as Lorentz invariance is only the low energy limit of some larger, more fundamental symmetry. In the absence of experimental evidence one would need profound concepts or physical principles to elucidate the nature of this symmetry. Since a new Einstein has not emerged, none currently exist.

Another possibility is that Lorentz symmetry is not replaced by a new fundamental symmetry and is only true to a good approximation. Examples of this type of possible LV have been seen in some proposals for a theory of quantum gravity. In Loop Quantum Gravity [11, 12] it has been argued that the semiclassical spacetime state has a polymer-like structure that exhibits dispersion and possibly noticeable LV effects in light propagation. Similar effects from the “foaminess” of spacetime [13] could be tested using observations of cosmological Gamma Ray Bursts [14]. One can also consider a fundamentally non-commutative structure for spacetime like the one studied by Connes and others in M-theory [15]. It has been shown [16] that Lorentz violation is intrinsic to non-commutative field theories.

An interesting analogy can be also made to condensed matter physics. In particular, work on some “analogue models” [17, 18, 19, 20] has suggested an analogy (at the level of kinematics) between macroscopic states of some fluids and aspects of the Lorentzian spacetime manifold such as event horizons. In a fluid, the inherently quantum mechanical degrees of freedom (“atoms”) at short wavelengths do not

respect the continuum symmetries that are only apparent when the degrees of freedom behave collectively in the hydrodynamic, long wavelength regime. Similarly, one might argue that the fundamental theory describing physics at high energies should not be Lorentz invariant and that the classical spacetime we observe emerges only as the hydrodynamic limit.

A different, more conservative point of view taken by some particle and string theorists is that Lorentz symmetry is fundamentally respected, but spontaneously broken at some large energy scale. In string theory Kostelecky and Samuel [21] have argued that the instability of the perturbative string vacuum is a mechanism for spontaneous LV. In this situation some fields acquire a non-zero vacuum expectation value that is not preserved by Lorentz symmetry.

Finally, another approach is to construct effective, low energy symmetry breaking models in order to investigate the phenomenology of LV. Effective field theories can be written down without specifying the fundamental physics of the symmetry breaking at high energies. Comparing to observations yields important constraints and some indirect information about the characteristics of physics at high energies. This has already been done in non-gravitational theories by studying extensions of the Standard Model [22] and modified particle dispersion relations [23]. Currently, all tests [24] tightly constrain these types of LV effects.

1.2 Einstein-aether theory and Gravitational Lorentz Violation

The story is different for gravitational Lorentz violation because the constraints discussed above do not apply and the literature in this area has been relatively sparse (although it continues to grow in recent years). Also, since gravity is weak at low energies, there is the interesting possibility that observational bounds on LV fields coupled only to gravity will not be nearly as strong. The model of gravitational LV we will consider in this dissertation is a classical vector-tensor theory of gravity, where the vector field is constrained to be unit and timelike. We will be agnostic about the fundamental mechanism for LV here, whether it be from loop quantum gravity, analogous to condensed matter physics, or from spontaneous symmetry breaking. The goal is to study the predictions of the theory, with an eye toward observational constraints or even ruling the theory out entirely.

The vector field can be thought of as the 4-velocity of a preferred frame throughout spacetime, which breaks local boost symmetry at every point. It has been dubbed by my collaborators as the “aether”, although it has nothing to do with the 19th century concept of a medium for electromagnetic waves. Since the aether is coupled to Einstein GR we refer to the theory as “Einstein-aether” theory or “ae-theory” for short. To preserve general covariance this field must be dynamical. In the spirit of effective field theory Jacobson and Mattingly [25] wrote down the action as the most general (up to total derivatives) diffeomorphism invariant functional of the spacetime metric and aether field u^a involving no more than two

derivatives [26],

$$S = \frac{1}{16\pi G} \int \sqrt{-g} L d^4x \quad (1.1)$$

where

$$L = -R - K^{ab}{}_{mn} \nabla_a u^m \nabla_b u^n - \lambda(g_{ab} u^a u^b - 1). \quad (1.2)$$

Here R is the Ricci scalar, $K^{ab}{}_{mn}$ is defined as

$$K^{ab}{}_{mn} = c_1 g^{ab} g_{mn} + c_2 \delta_m^a \delta_n^b + c_3 \delta_n^a \delta_m^b + c_4 u^a u^b g_{mn}, \quad (1.3)$$

where the c_i , ($i = 1, \dots, 4$) are dimensionless coupling constants, and λ is a Lagrange multiplier enforcing the unit timelike constraint. A term of the form $R_{ab} u^a u^b$ is not explicitly included as it is proportional to the difference of the c_2 and c_3 terms in (1.1) via integration by parts. The convention for the metric signature used throughout this dissertation is $(+---)$ and the units are chosen so that the speed of light c defined by the metric g_{ab} is unity. An important point is that (1.1) describes only the vacuum theory. It will be assumed any matter couples universally to g_{ab} . This issue will be discussed further in later chapters.

Jacobson and Mattingly were not the first researchers to consider vector-tensor theories of gravitation. A theory without the c_4 term in the action or the unit constraint was considered in the early 1970's by Will, Nordtvedt, and collaborators [27]. The theory acted as a toy model “sparring partner” used for comparisons with GR in weak field regimes and within the newly developed parameterized post-Newtonian (PPN) framework for solar system experiments. However, without the unit constraint, variations of the aether can be spacelike, leading to ghosts and other instabilities. In the mid-1980's Gasperini [28] was the first to study a unit

vector-tensor theory in the context of LV. Gasperini wrote the theory in terms of a tetrad “frame field” $e_A^a(x)$ where the capitalized A here is a Lorentz index. The tetrad field maps local Lorentz fields to the curved spacetime manifold. Thus, $u^a = e_A^a u^A$ for a Lorentz vector u^A which is unit with respect to the flat Minkowski metric, $\eta_{AB} u^A u^B = 1$. The Lagrangian for the theory is defined in terms of u^A , a Lorentz covariant derivative, and a spin connection ω_a^{AB} . The model is equivalent to Einstein-aether theory when it is rewritten in terms of g_{ab} and u^a . Gasperini primarily studied cosmological solutions in models where the coupling parameters are time dependent, finding a class with repulsive behavior that apparently avoided the big bang singularity ².

Before concluding this section it is appropriate to mention another set of popular gravitational LV models related to Einstein-aether theory. Like the work of Kostelecky and Samuel, these are effective field theories motivated by the idea that Lorentz invariance is spontaneously broken. However, the fundamental high energy physics behind the breaking is not specified. The so-called “ghost condensate” [29] theory is a simple model where the gradient of the scalar ghost field acquires a vacuum expectation value. The effective action for the Nambu-Goldstone fluctuations about the vacuum state contains wrong sign kinetic terms. When coupled to gravity and put in a cosmological setting these ghost terms yield an equation of state that acts like a cosmological constant. The theory also predicts a spin-dependent inverse square law force. Other models [30, 31, 32, 33] consider a potential term $V(u_a u^a)$ in the effective action instead of a rigid unit constraint. A number of predictions have

²I thank Brendan Foster and Ted Jacobson for bringing this point to my attention

been worked out, including the wave modes, non-linear dynamics and other velocity dependent effects. In [33] it was argued that Einstein-aether theory is a certain “decoupling” limit of one these models related to the potential term becoming more rigid and approaching the unit constraint. The consequences of this argument have yet to be fully examined.

1.3 Related Work on ae-theory phenomenology

A great deal of progress has been made on the observational and theoretical consequences of ae-theory over the past few years. The work described in this dissertation is a part of these advances. In this section we will summarize other results on PPN parameters, cosmology, waves and the complete set of observational constraints from our solar system and binary pulsar systems. This work provides important background and context to our research.

In [34] Carroll and Lim showed that Einstein-aether theory has a proper Newtonian limit for weak fields and slow motion. Specifically they found that the Newtonian potential produced by a mass M is $-G_N M/r$. Here $G_N = G(1 - c_{14}/2)^{-1}$, where G is the bare constant appearing in the action (1.1) and the notation $c_{14} = c_1 + c_4$. Since G_N is what we observe as the Newton constant, the only constraint is that $c_{14} < 2$ to preserve positivity. For further tests the PPN formalism [35] may be used. This is the standard method for comparing alternative theories of gravity to GR in a solar system. It is an expansion in the squared velocity of the bodies and a dimensionless gravitational potential. A completely general metric theory has 10

PPN parameters, but 5 of these vanish for theories described by a diffeomorphism invariant action principle. One other parameter is associated with a 3-body interaction that is clearly not present and it also vanishes. The remaining parameters relevant in ae-theory are denoted β , γ , and α_1 , α_2 . In the standard PPN gauge the parameter β is a measure of the lowest order non-linearity in the metric produced by an isolated source mass while γ characterizes the spatial curvature. $\alpha_{1,2}$ are associated with preferred frame effects, such as forces that depend on the velocity of the source mass with respect to a preferred frame. In [36] it was shown that $\beta, \gamma = 1$ as in GR. Later [37] worked out α_2 to lowest order in the c_i coupling constants. Both α_1 and α_2 were found in complete generality by Foster and Jacobson [38]. Bounds on these preferred frame parameters from solar system tests are tight: α_1 must be less than roughly 10^{-4} and α_2 less than 4×10^{-7} . In order to agree with observation they can be set to zero. These conditions reduce the full four parameter c_i theory space to a two parameter family. The most convenient choice is to write c_4 and c_2 in terms of (c_1, c_3) .

In cosmology, the Friedmann-Robertson-Walker equations in ae-theory were found in [39, 34]. Since the aether coincides with the 4-velocity of isotropic observers the aether contribution to the stress tensor is simplified. The net effect is to renormalize the Newton constant, $G_{\text{cosmo}} = G(1 + (c_1 + c_3 + 3c_2)/2)^{-1}$ and spatial curvature contribution. Since current observations tell us the universe is very nearly flat, the spatial curvature renormalization does not yield a new constraint. However, since G_{cosmo} and G_N are different, the expansion rate of the universe differs from that found in GR with the same matter content. Observations of primor-

dial ${}^4\text{He}$ abundance require $|G_{\text{cosmo}}/G_N - 1| < 1/8$. Remarkably it was shown in [38] that this relationship is automatically satisfied when $\alpha_{1,2}$ are forced to vanish. Additional work by Lim [40] considered the spectrum of primordial perturbations around deSitter spacetime and their interactions with an inflaton field. In order to check whether observations of the cosmic microwave background yield a constraint on ae-theory, the evolution of these perturbations to the surface of last scattering needs to be examined, probably with numerical methods.

Another important set of constraints on ae-theory discussed in [38] come from the linearized gravity-aether wave modes found in [41]. Stability requires that these modes have only real frequencies and they must also carry away positive energy (this will be discussed in much more detail in Chapter 2). Also, high energy matter traveling through the vacuum could engender gravitational and aetherial Cerenkov radiation in these modes. If these effects exist in the theory, observation puts extremely tight bounds (less than 10^{-15}) on the c_i [42]. To avoid them, the wave modes must all have speeds greater than 1. This condition, together with constraints from stability and energy positivity, reduces the allowed theories to the region of the (c_1, c_3) space,

$$\begin{aligned} 0 &< c_+ < 1 \\ 0 &< c_- < c_+/3(1 - c_+), \end{aligned} \tag{1.4}$$

where $c_{\pm} = c_1 \pm c_3$. This region is still large (order unity). Finally, Foster [43] studied radiation emitted from binary pulsar systems in the post-Newtonian weak field regime. In general, a radiative energy loss in ae-theory depends on time deriv-

atives of quadrupole, dipole, and monopole moments. However, observations of the Hulse-Taylor binary system have agreed very well with the quadrupole formula of GR. Only a narrow (order 10^{-3}) band of ae-theories in the 2d (c_1, c_3) space satisfying all the other constraints discussed above have radiative losses consistent with observation.

Foster [44] has recently noted that the radiation damping formula he derived only holds for small c_i because strong field effects inside the binary bodies cannot be neglected in all binary pulsar systems. To model a strongly gravitating system in ae-theory he considered the bodies to be point particles with velocity dependent interactions characterized by dimensionless “sensitivities”. The post-Newtonian equations of motion and radiation damping rate depend on the values of the sensitivities, which have not yet been determined. However, these sensitivities scale with the mass m and size d of the compact object like $f[c_i](G_N m/d)^2$, where $f[c_i]$ denotes some function of the coupling constants. From this scaling, Foster argues that if c_i is less than roughly 0.1 then theories passing all weak field tests also pass current strong field tests. Other phenomenology of ae-theory in the strong field regime is likely to yield further constraints.

1.4 Outline of Thesis

In this dissertation we study aspects of the phenomenology of Einstein-aether theory, focusing particularly on energy and the solutions of the full non-linear theory. It turns out that this phenomenology is very rich and for a certain class of

coupling parameters does not yet conflict with observation. We write down quantities that describe energy and establish weak field constraints on the theory from these. We also complete a full survey of the spherically symmetric solutions and use these results to discuss the current and future state of constraints on the theory from astrophysical observations of strongly gravitating compact objects. Finally, we completely characterize Einstein-aether theory in two-dimensions and show that the solutions could be of use as toy model for Lorentz violating quantum gravitational physics. Specifically:

Chapter 2 broadly considers energy in ae-theory. Pseudotensor methods are used to derive the energy densities of the linearized gravity-aether wave modes found by Jacobson and Mattingly [41]. An expression for the total non-linear energy of an asymptotically flat spacetime is also obtained. Demanding that the linearized energy densities have positive energy yields inequalities that constrain the theory. We discuss the form of the energy in certain limits and briefly address the possibility of a positive energy theorem.

Chapter 3 examines the basic structure of the time independent spherically symmetric field equations. Locally there is a three parameter family of solutions. Enforcing asymptotic flatness reduces the number of parameters to two. There is no Birkhoff's theorem in ae-theory and spherical solutions fall into distinct classes. We examine the asymptotic weak field solution and analytically solve the full "static" vacuum case where the aether is aligned with the timelike Killing vector.

Chapter 4 studies fluid stars in ae-theory. The exterior of the stars is described by the static solution found in Chapter 3. In the interior, the aether is also static,

but numerical methods are required to solve the field equations. As a warm-up we first consider the simple model of a constant density equation of state. Then we examine neutron stars given six equation of state models. We find the dependence of the maximum mass and surface redshift on the coupling constant combination c_{14} . Constraints are currently tentative because we lack good knowledge of the equation of state. Possible future observational constraints from these results are emphasized.

In Chapter 5, we turn to black hole solutions. These are defined as objects with horizons that trap all the gravity-aether modes in addition to any matter fields. Black holes do exist for c_i values that are not too large. In these solutions the aether is not aligned with the Killing vector. Outside they are very close to the Schwarzschild metric for a wide range of couplings and they have a spacelike singularity inside. We also briefly discuss recent work showing that if the c_i are again not too large these black holes are the end-state of a collapsing scalar field. We conclude by summarizing other recent work describing a classical process operating in black hole systems with a preferred frame that violates the generalized second law.

Chapter 6 describes ae-theory in two dimensions. Interestingly, the theory is not trivial. In addition to a flat spacetime with constant aether, there are constant curvature deSitter/anti-deSitter solutions with a uniformly accelerated aether that is singular on the horizons, and a non-constant curvature solution with no Killing vectors containing curvature singularities. The existence of dS/AdS horizons in such a simple model may allow issues in Lorentz violating black hole thermodynamics to be probed.

Chapter 7 summarizes the complete set of results and provides some reflections and possible directions for future research.

Chapter 2

Energy in Einstein-aether theory

2.1 Introduction

In this chapter we examine energy in the Einstein-aether theory. Energy in any field theory is defined as the value of the Hamiltonian, which acts as the generator of time translations. Although in diffeomorphism invariant theories there is generally no preferred notion of time (and thus energy), in asymptotically flat spacetimes one can naturally define the ADM and Bondi energies associated with asymptotic time translations at spatial and null infinity respectively. The ADM and Bondi definitions for GR have also been shown to satisfy positive energy theorems [45].

Since it has proven difficult to explicitly construct the full Hamiltonian for the theory, we instead consider the pseudotensor method of studying gravitational energy. Such an approach was first taken in a similar context by Lee, Lightman, and Ni [46], who derived pseudotensors for the unconstrained vector-tensor models studied by Will and collaborators [27] but did not evaluate them on solutions. Despite the non-covariance of pseudotensors, it is known that they give well-defined results for the spatially averaged energy carried by waves in linearized theory and the total energy of asymptotically flat spacetimes. In gravitational wave physics they can provide a simple and straightforward method for calculating averaged energy densities and the energy-momentum flux radiated away from sources. In addition,

Chang, Nester, and Chen [47] have shown that the superpotential associated with every pseudotensor corresponds to a (albeit non-covariant) quasi-local Hamiltonian boundary term.

We first discuss the Einstein-aether field equations and then motivate and construct the modified Weinberg pseudotensor expression. As the calculational and consistency check we also use a Lagrangian based method to derive the modified Einstein “canonical” pseudotensor and its associated superpotential. The relationship of these pseudotensors to Wald’s “Noether charge” formalism [48] is discussed. We then apply these expressions to solutions in both the linear and non-linear regimes. In the linearized theory the Einstein and Weinberg prescriptions give the same energy densities for the plane wave modes derived in [41]. Restricting these densities to be positive yields constraints on the model in terms of the coefficients of the aether part of the action. These constraints are also compared to results obtained in the limit where the metric and aether decouple [40]. In the full non-linear theory the Einstein-aether superpotential is used to obtain the total energy for an asymptotically flat spacetime. This result agrees with [49], where the total energy in the Einstein-aether theory is derived via the covariant Noether charge formalism. We conclude with a discussion of the status of positive energy in the non-linear regime and prospects for a positive energy theorem.

2.2 Field Equations

The Einstein-aether field equations from varying the action in (1.1) together with a matter action with respect to g^{ab} and u^a are given by

$$G_{ab} = T_{ab}^{(u)} + 8\pi GT^M{}_{ab} \quad (2.1)$$

$$\nabla_a J^a{}_m - c_4 \dot{u}_a \nabla_m u^a = \lambda u_m, \quad (2.2)$$

$$g_{ab} u^a u^b = 1. \quad (2.3)$$

where

$$J^a{}_m = K^{ab}{}_{mn} \nabla_b u^n \quad (2.4)$$

and

$$\dot{u}_a = u^b \nabla_b u_a. \quad (2.5)$$

Here we assume that there are no aether-matter couplings in the matter action. The aether stress tensor is given by

$$\begin{aligned} T^{(u)}{}_{ab} &= \nabla_m (J^m{}_{(a} u_{b)}) - J_{(a}{}^m u_{b)} + J_{(ab)} u^m \\ &+ c_1 [(\nabla_a u_m)(\nabla_b u^m) - (\nabla_m u_a)(\nabla^m u_b)] \\ &- c_4 \dot{u}_a \dot{u}_b \\ &- [u_n (\nabla_m J^{mn}) - c_4 \dot{u}^2] u_a u_b \\ &- \frac{1}{2} L_u g_{ab}, \end{aligned} \quad (2.6)$$

where $L_u = -K^{ab}{}_{mn} \nabla_a u^m \nabla_b u^n$ and $\dot{u}^2 = \dot{u}_a \dot{u}^a$. The Lagrange multiplier λ has been eliminated from (2.6) by solving for it via the contraction of the aether field (2.2)

with u^a . As we will see below, the form of the aether stress tensor and Einstein-aether Lagrangian will be important tools in derivation of the modified Weinberg and Einstein pseudotensors.

2.3 Weinberg Pseudotensor

Weinberg's pseudotensor construction [50] is based on the "field theoretic" approach to GR that treats gravity as a spin-2 field on a flat background spacetime. Using Greek indices to represent coordinate indices, we begin by writing the metric in coordinates such that $g_{\mu\nu} = \eta_{\mu\nu} + h_{\mu\nu}$, where $\eta_{\mu\nu}$ is the flat Minkowski metric and $h_{\mu\nu}$ is an symmetric tensor field with the asymptotic conditions $h_{\mu\nu} \sim O(1/r)$, $\partial_\sigma h_{\mu\nu} \sim O(1/r^2)$, $\partial_\tau \partial_\sigma h_{\mu\nu} \sim O(1/r^3)$. The Einstein tensor can be expanded into a series of parts linear, quadratic, and higher order in the field variable $h_{\mu\nu}$. Following Ch. 20 of Misner, Thorne, and Wheeler [51] the non-linear corrections to the Einstein tensor are defined as follows

$$16\pi G t_{\mu\nu} \equiv 2G_{\mu\nu}^{(1)} - 2G_{\mu\nu}, \quad (2.7)$$

where $G_{\mu\nu}^{(1)}$ and $G_{\mu\nu}$ are the linearized and full non-linear Einstein tensors respectively. Note that this splitting is non-unique because it depends on the coordinate system. Since the linearized Einstein tensor is symmetric and satisfies a linearized Bianchi identity $\partial^\mu G_{\mu\nu}^{(1)} = 0$, it can be rewritten in superpotential form

$$2G_{\mu\nu}^{(1)} = H_{\mu\alpha\nu\beta}{}^{,\alpha\beta} \quad (2.8)$$

where $H_{\mu\nu\alpha\beta}$ has the symmetries of the Riemann tensor $H_{\mu\nu\alpha\beta} = H_{[\mu\nu][\alpha\beta]} = H_{\alpha\beta\mu\nu}$ (see, for example [52]). Using (2.7) and (2.8) the full Einstein equation becomes

$$H_{\mu\alpha\nu\beta}{}^{,\alpha\beta} = 16\pi G (t_{\mu\nu} + T_{\mu\nu}). \quad (2.9)$$

Due to the symmetries of $H_{\mu\alpha\nu\beta}$, this implies that $\partial^\nu(t_{\mu\nu} + T_{\mu\nu}) = 0$. Therefore the integral of $t_{00} + T_{00}$ over a spacelike slice is a conserved quantity. This conserved quantity

$$\begin{aligned} \int (t_{00} + T_{00}) d^3x &= \frac{1}{16\pi G} \int H_{0\alpha 0\beta}{}^{,\alpha\beta} d^3x \\ &= \frac{1}{16\pi G} \oint H_{0\alpha 0\beta}{}^{,\alpha} n^\beta d^2x, \end{aligned} \quad (2.10)$$

where n^β is the unit normal to the surface at spatial infinity, is in fact the total energy, with t_{00} acting as the energy density of the gravitational field alone. To sharpen this point, consider the case where the gravitational field is weak everywhere, allowing use of the linearized theory. The leftmost member of (2.10) then gives the total matter energy, which in this case is the total energy. The rightmost member is insensitive to the interior volume, so replacement by arbitrary sources and strong fields in the interior will not affect the identification of (2.10) as the total energy.

The extension to the Einstein-Aether theory is straightforward. The metric field equations (2.1) take the form

$$\tilde{G}_{\mu\nu} = G_{\mu\nu} - T_{\mu\nu}^{(u)} = 8\pi G T_{\mu\nu}. \quad (2.11)$$

In addition to the metric, we now decompose the aether into background and dynamical parts by writing $u^\mu = \underline{u}^\mu + v^\mu$. Unlike normal matter fields the aether stress

$T_{\mu\nu}^{(u)}$ contains linear pieces in the perturbation v^μ due to the fact that the aether does not vanish in the background (since it is always a unit vector). These linear terms will modify the Weinberg pseudotensor and superpotential. Performing the split of the modified Einstein tensor \tilde{G}_{ab} as in (2.7) we find

$$16\pi G \tilde{t}_{\mu\nu} \equiv 2\tilde{G}_{\mu\nu}^{(1)} - 2\tilde{G}_{\mu\nu} \quad (2.12)$$

where $\tilde{G}_{\mu\nu}^{(1)} = G_{\mu\nu}^{(1)} - T_{\mu\nu}^{(1)(u)}$. $\tilde{G}_{\mu\nu}$ satisfies a Bianchi identity $\nabla^\mu \tilde{G}_{\mu\nu} = 0$ if the aether is uncoupled to the matter and if the aether field equation (2.2) is satisfied.

Therefore in the linearized case one can write

$$2\tilde{G}_{\mu\nu}^{(1)} = \tilde{H}_{\mu\alpha\nu\beta}{}^{,\alpha\beta} \quad (2.13)$$

along with

$$\tilde{H}_{\mu\alpha\nu\beta}{}^{,\alpha\beta} = 16\pi G(\tilde{t}_{\mu\nu} + T_{\mu\nu}). \quad (2.14)$$

By the same reasoning as before one could conclude that the total energy is given by

$$E = \frac{1}{16\pi G} \oint \tilde{H}_{0\alpha 0\beta}{}^{,\alpha} n^\beta d^2x. \quad (2.15)$$

However, unlike the GR case (2.9), it is not clear whether the new Weinberg superpotential $\tilde{H}_{\mu\alpha\nu\beta}{}^{,\alpha}$ can be expressed as a local function of the fields h_{ab} and u^a ¹. On the other hand, the pseudotensor $\tilde{t}_{\mu\nu}$ can be calculated directly via the non-linear pieces of $T_{\mu\nu}^{(u)}$ and $G_{\mu\nu}$ in $\tilde{G}_{\mu\nu}$. This will be used to compute the linearized wave energy densities. Evaluation of the total energy as a surface integral at spatial infinity requires a locally defined superpotential. Since we do not have knowledge

¹I thank an anonymous referee for pointing out this fact

of the aether corrections to the Weinberg superpotential we will instead consider the Einstein superpotential, which can be derived directly from the form of the Lagrangian. The Einstein formulation of gravitational energy-momentum will also provide a consistency check when we evaluate the energy density of the linearized plane wave modes.

2.4 Lagrangian Approach to Pseudotensors

2.4.1 Summary of Results

The gravitational energy pseudotensor originally derived by Einstein in 1916 shortly after his discovery of the field equations of GR is closely related to the familiar canonical stress tensor of matter fields in flat spacetime. In order to derive the corresponding expression for the Einstein-aether theory, we use a Lagrangian approach based upon the famous work of Noether relating symmetries to conservation laws. In flat spacetime, invariance of a Lagrangian under global space and time translations is associated with the conservation of energy-momentum expressed by the conservation of the canonical stress tensor

$$T_{\nu}^{\mu} = \frac{\partial \mathcal{L}}{\partial(\partial_{\mu}\psi)} \partial_{\nu}\psi - \delta_{\nu}^{\mu} \mathcal{L}, \quad (2.16)$$

where $\mathcal{L} = \mathcal{L}(\psi, \partial\psi)$ and ψ represents a general collection of fields with indices suppressed. In the case of local symmetries, such as the diffeomorphism invariance of the Einstein-Aether theory, the situation is more complex. In the subsections that follow we review a general formalism due to Julia and Silva [53] for constructing

Noether currents and superpotentials and apply it to the Einstein-aether theory. The relationship of these methods to Wald’s covariant Noether charge approach is also explored. In this subsection the final results needed to examine linearized and non-linear energy will be summarized for the reader.

The pseudotensor and superpotential have the following general form

$$t_\nu{}^\mu = \frac{\sqrt{-g}}{16\pi G} \left(\frac{\partial L}{\partial(\partial_\mu g_{\alpha\beta})} \partial_\nu g_{\alpha\beta} + \frac{\partial L}{\partial(\partial_\mu u^\alpha)} \partial_\nu u^\alpha - \delta_\nu^\mu L \right) \quad (2.17)$$

$$U_\nu{}^{\mu\gamma} = \frac{\sqrt{-g}}{16\pi G} \left(\frac{\partial L}{\partial(\partial_\mu g_{\alpha\beta})} (\delta_\alpha^\gamma g_{\nu\beta} + \delta_\beta^\gamma g_{\nu\alpha}) - \frac{\partial L}{\partial(\partial_\mu u^\alpha)} \delta_\alpha^\nu u^\gamma \right) \quad (2.18)$$

where L is the Lagrangian

$$L = -g^{\alpha\beta} (\Gamma_{\alpha\delta}^\eta \Gamma_{\eta\beta}^\delta - \Gamma_{\eta\delta}^\eta \Gamma_{\alpha\beta}^\delta) - K^{\alpha\beta}{}_{\mu\nu} \nabla_\alpha u^\mu \nabla_\beta u^\nu - \lambda (g_{\mu\nu} u^\mu u^\nu - 1). \quad (2.19)$$

Note that we have eliminated a surface term in the Einstein-Hilbert Lagrangian, replacing the Ricci scalar R with the Einstein-Schrodinger “ Γ^2 ” action, which depends only on the metric and its first derivatives. When evaluated on-shell the pseudotensor and superpotential obey the following relations

$$\partial_\mu t_\nu{}^\mu = 0 \quad (2.20)$$

$$t_\nu{}^\mu = -\partial_\gamma U_\nu{}^{\gamma\mu}. \quad (2.21)$$

To account for the presence of any non-aether matter sources one only has to make the replacement $t_\nu{}^\mu \rightarrow t_\nu{}^\mu + T_\nu{}^\mu$ in (2.20) and (2.21). Like the Weinberg construc-

tion, the pseudotensor $t_\nu{}^\mu$ is a conserved quantity and is related to the divergence of a superpotential.

The contributions from the pure GR Γ^2 Lagrangian are the *Einstein* pseudotensor

$$\begin{aligned} \text{einstein } t_\rho{}^\mu &= \frac{\sqrt{-g}}{16\pi G} \left(\delta_\rho{}^\mu (\Gamma_{\beta\gamma}^\alpha \Gamma_{\alpha\delta}^\beta - \Gamma_{\alpha\beta}^\alpha \Gamma_{\gamma\delta}^\beta) g^{\gamma\delta} \right. \\ &\quad + \Gamma_{\rho\alpha}^\beta \Gamma_{\gamma\beta}^\gamma g^{\mu\alpha} - \Gamma_{\rho\beta}^\beta \Gamma_{\gamma\alpha}^\gamma g^{\mu\alpha} + \Gamma_{\rho\alpha}^\alpha \Gamma_{\beta\gamma}^\mu g^{\beta\gamma} \\ &\quad \left. + \Gamma_{\rho\alpha}^\mu \Gamma_{\beta\gamma}^\beta g^{\alpha\gamma} - 2\Gamma_{\alpha\beta}^\mu \Gamma_{\rho\gamma}^\alpha g^{\beta\gamma} \right) \end{aligned} \quad (2.22)$$

and the *von Freud* superpotential (see, e.g. [54])

$$\text{fr } U_\beta{}^{\lambda\alpha} = \frac{1}{16\pi G} \frac{1}{\sqrt{-g}} g_{\beta\tau} \partial_\gamma \{ (-g) (g^{\lambda\tau} g^{\alpha\gamma} - g^{\alpha\tau} g^{\lambda\gamma}) \}. \quad (2.23)$$

To compute the additional aether modifications, we use the relation

$$\frac{\partial L}{\partial(\partial_\mu g_{\alpha\beta})} = \frac{1}{2} (g^{\alpha\nu} \delta_\gamma^\beta \delta_\delta^\mu + g^{\alpha\nu} \delta_\delta^\beta \delta_\gamma^\mu - g^{\mu\nu} \delta_\gamma^\alpha \delta_\delta^\beta) \frac{\partial L}{\partial(\Gamma_{\gamma\delta}^\nu)} \quad (2.24)$$

and $L_u = K^{\alpha\beta}{}_{\mu\nu} \nabla_\alpha u^\mu \nabla_\beta u^\nu$ in (2.17) and (2.18) since when evaluated on solutions any terms related to the unit constraint will vanish. We find the pseudotensor

$$\begin{aligned} \text{ae } t_\nu{}^\lambda &= \frac{1}{16\pi G} \left(2\sqrt{-g} J^\lambda{}_\rho \nabla_\nu u^\rho - \sqrt{-g} \{ (J^\lambda{}_\beta + J_\beta{}^\lambda) u^\alpha \right. \\ &\quad \left. - (J^\alpha{}_\beta + J_\beta{}^\alpha) u^\lambda + (J^{\lambda\alpha} - J^{\alpha\lambda}) u_\beta \} \Gamma_{\alpha\nu}^\beta \right. \\ &\quad \left. + \delta_\nu^\lambda \sqrt{-g} L_u \right). \end{aligned} \quad (2.25)$$

and the superpotential

$$\begin{aligned} \text{ae } U_\beta{}^{\lambda\alpha} &= \frac{1}{16\pi G} \sqrt{-g} \left((J^\lambda{}_\beta + J_\beta{}^\lambda) u^\alpha \right. \\ &\quad \left. - (J^\alpha{}_\beta + J_\beta{}^\alpha) u^\lambda + (J^{\lambda\alpha} - J^{\alpha\lambda}) u_\beta \right) \end{aligned} \quad (2.26)$$

where $J^a{}_\beta$ is defined in (2.4). The above decompositions of (2.17) and (2.18) into GR and aether pieces do not satisfy (2.20) and (2.21) independently. A key requirement when evaluating these pseudotensorial expressions is that the metric must be written in a coordinate system where the connection coefficients vanish like $O(1/r)$ or faster in the asymptotic limit. If the coordinate system is not chosen properly then these expressions will yield incorrect energies and momenta ². This condition was not well understood in the early literature on gravitational energy-momentum, but will be explained in Section 2.4.3 using an analysis of the boundary terms and conditions in an action.

2.4.2 Basic Formalism

In this subsection we will derive the Einstein pseudotensor and superpotential using the Noether current formalism of Julia and Silva [53] applied to Lagrangians that depend on the fields and their first and second derivatives. One can write a variation in the Lagrangian as

$$\delta L = \frac{\partial L}{\partial \psi} \delta \psi + \frac{\partial L}{\partial (\partial_\mu \psi)} \delta (\partial_\mu \psi) + \frac{\partial L}{\partial (\partial_\mu \partial_\nu \psi)} \delta (\partial_\mu \partial_\nu \psi) \quad (2.27)$$

and then integrate by parts to isolate the equations of motion E and a symplectic current θ^μ ,

$$\delta L = E \delta \psi + \partial_\mu \theta^\mu, \quad (2.28)$$

²For example, if one uses the Schwarzschild metric in spherical polar coordinates $ds^2 = (1 - \frac{2M}{r})dt^2 - (1 - \frac{2M}{r})^{-1}dr^2 - r^2d\Omega^2$, the von Freud superpotential will yield an incorrect total energy. After re-expressing the metric in Cartesian coordinates (t, x, y, z) , the pseudotensor expression gives $E = M$.

where

$$\begin{aligned} \partial_\mu \theta^\mu &= \partial_\mu \left(\frac{\partial L}{\partial(\partial_\mu \psi)} \delta\psi - \partial_\nu \left(\frac{\partial L}{\partial(\partial_\mu \partial_\nu \psi)} \right) \delta\psi \right. \\ &\quad \left. + \frac{\partial L}{\partial(\partial_\mu \partial_\nu \psi)} \partial_\nu(\delta\psi) \right). \end{aligned} \quad (2.29)$$

If the action associated with L is invariant under a continuous transformation of the fields, $\delta L = \partial_\mu S^\mu$. Thus, we have the equation

$$\partial_\mu (S^\mu - \theta^\mu) = E \delta\psi. \quad (2.30)$$

This identifies the on-shell ($E = 0$) conserved Noether current,

$$\begin{aligned} J^\mu &= \theta^\mu - S^\mu = \frac{\partial L}{\partial(\partial_\mu \psi)} \delta\psi - \partial_\nu \left(\frac{\partial L}{\partial(\partial_\mu \partial_\nu \psi)} \right) \delta\psi \\ &\quad + \frac{\partial L}{\partial(\partial_\mu \partial_\nu \psi)} \partial_\nu(\delta\psi) - S^\mu. \end{aligned} \quad (2.31)$$

We now want to consider a gauge transformation of the fields that involves derivatives of the generator $\xi^A(x)$. Here we will focus on the special case restricting attention to only the first derivative. Following the analysis and notation of [53] the gauge transformation is parameterized as

$$\delta\psi = \xi^A \Delta_A + (\partial_\nu \xi^A) \Delta_A^\nu \quad (2.32)$$

where A is an internal or spacetime index and Δ is a transformation matrix. The quantity S^μ can be expressed similarly as

$$S^\mu = \xi^A \Sigma_A^\mu + (\partial_\nu \xi^A) \Sigma_A^{\mu\nu} + (\partial_\tau \partial_\nu \xi^A) \Sigma_A^{\mu(\tau\nu)}. \quad (2.33)$$

Inserting these forms into (2.31) and combining terms, we find that on-shell

$$\partial_\mu \left(\xi^A J_A^\mu + \partial_\nu \xi^A U_A^{\mu\nu} + \partial_\tau \partial_\nu \xi^A V_A^{\mu(\nu\tau)} \right) = 0, \quad (2.34)$$

where

$$\begin{aligned}
J_A^\mu &= \left(\frac{\partial L}{\partial(\partial_\mu \psi)} - \partial_\nu \left(\frac{\partial L}{\partial(\partial_\mu \partial_\nu \psi)} \right) \right) \Delta_A \\
&\quad + \left(\frac{\partial L}{\partial(\partial_\mu \partial_\nu \psi)} \right) \partial_\nu \Delta_A - \Sigma_A^\mu
\end{aligned} \tag{2.35}$$

$$\begin{aligned}
U_A^{\mu\nu} &= \left(\frac{\partial L}{\partial(\partial_\mu \psi)} - \partial_\tau \left(\frac{\partial L}{\partial(\partial_\mu \partial_\tau \psi)} \right) \right) \Delta_A^\nu \\
&\quad + \left(\frac{\partial L}{\partial(\partial_\mu \partial_\tau \psi)} \right) \partial_\tau \Delta_A^\nu + \frac{\partial L}{\partial(\partial_\mu \partial_\nu \psi)} \Delta_A \\
&\quad - \Sigma_A^{\mu\nu}
\end{aligned} \tag{2.36}$$

$$V_A^{\mu(\tau\nu)} = \frac{\partial L}{\partial(\partial_\mu \partial_\tau \psi)} \Delta_A^\nu - \Sigma_A^{\mu(\tau\nu)}. \tag{2.37}$$

Since ξ^A and its derivatives should be arbitrary and independent, this single equation decomposes into 4 equations

$$\partial_\mu J_A^\mu \approx 0 \tag{2.38}$$

$$J_A^\mu + \partial_\nu U_A^{\nu\mu} \approx 0 \tag{2.39}$$

$$U_A^{(\mu\nu)} + \partial_\tau V_A^{\tau(\mu\nu)} = 0 \tag{2.40}$$

$$V_A^{(\mu\nu\tau)} = 0. \tag{2.41}$$

The first two equations hold on-shell, while the last two are identities (since there are no second or third derivatives of ξ^A on the right hand side of (2.29)).

The gauge symmetry implies that J_A^μ is conserved and equal to the divergence of the superpotential $U_A^{\mu\nu}$. Since $\xi^A = \xi^A(x)$, the Noether current J^μ (2.31) will now be parameter dependent. Let us consider a one parameter subgroup of the local gauge or diffeomorphism symmetry where ξ^A has the decomposition,

$$\xi^A(x) = \epsilon(x) \xi_0^A, \tag{2.42}$$

and ξ_0^A is fixed. Inserting this form into (2.39) produces

$$J_{\xi_0}^\mu + \partial_\nu(U_{\xi_0}^{\nu\mu}) = 0, \quad (2.43)$$

with $J_{\xi_0}^\mu = \xi_0^A J_A^\mu$ and $U_{\xi_0}^{\nu\mu} = \xi_0^A U_A^{\nu\mu}$. The conserved charge is

$$Q = \int J_{\xi_0}^0 d^3x = \oint \xi_0^A U_A^{\nu 0} n_\nu d^2x \quad (2.44)$$

Q depends on the choice of ξ_0^A and can be expressed in terms of the gauge fields using (2.36). If ξ_0^A is an asymptotic translation in an asymptotically flat spacetime, then the conserved charge will be a total energy or momentum.

2.4.3 Application to GR and ae-theory

Now assume that the Lagrangian density $\mathcal{L}(\psi, \partial\psi, \partial^2\psi)$ is invariant under diffeomorphisms and is a combination of a scalar density $\tilde{\mathcal{L}}$ and a total divergence $\partial_\mu W^\mu$,

$$\mathcal{L}(\psi, \partial\psi, \partial^2\psi) = \tilde{\mathcal{L}}(\psi, \partial\psi, \partial^2\psi) + \partial_\mu[W^\mu(\psi, \partial\psi)]. \quad (2.45)$$

If W^μ is a vector density then the total divergence is a scalar density, but we allow for a non-covariant total divergence. For a variation that is an infinitesimal diffeomorphism generated by a vector field ξ^μ , we have $\delta\tilde{\mathcal{L}} = \partial_\mu(\xi^\mu\tilde{\mathcal{L}})$ since $\tilde{\mathcal{L}}$ is a scalar density and $\delta(\partial_\mu W^\mu) = \partial_\mu(\delta W^\mu)$. Therefore the surface term S^μ in (2.30) has the form

$$S^\mu = \xi^\mu\tilde{\mathcal{L}} + \delta W^\mu. \quad (2.46)$$

Now consider the Einstein-Hilbert action

$$S_{\text{EH}} = \int \sqrt{-g} R d^4x \quad (2.47)$$

of pure GR. The Ricci scalar R has a dependence on second derivatives of the metric. In light of this, Einstein exploited a property of the Hilbert action that allows it to be separated into a bulk and a surface term

$$\int \sqrt{-g} R d^4x = \int \sqrt{-g} L_{\text{bulk}} + \partial_\mu V^\mu d^4x. \quad (2.48)$$

This decomposition of the Ricci scalar takes the following form

$$L_{\text{bulk}} = g^{\alpha\beta} \{ \Gamma_{\alpha\delta}^\eta \Gamma_{\eta\beta}^\delta - \Gamma_{\eta\delta}^\eta \Gamma_{\alpha\beta}^\delta \} \quad (2.49)$$

$$V^\mu = \sqrt{-g} \{ \Gamma_{\alpha\beta}^\mu g^{\alpha\beta} - \Gamma_{\alpha\beta}^\beta g^{\mu\alpha} \}. \quad (2.50)$$

where Γ is the Levi-Civita connection. One can eliminate the total divergence by adding its negative to the Einstein-Hilbert action

$$\int \sqrt{-g} L_{\text{bulk}} = \int \sqrt{-g} R d^4x - \partial_\mu V^\mu d^4x. \quad (2.51)$$

The elimination does not affect the equations of motion and is consistent with the general action (2.45) with $\tilde{\mathcal{L}} = \sqrt{-g} R$ and $W^\mu = -V^\mu$. The result of this is a loss of diffeomorphism invariance since the remaining L_{bulk} in the “ Γ^2 ” action is not a scalar. We have allowed for this possibility with the non-covariant $\partial_\mu W^\mu$ term in (2.45).

With $\mathcal{L}(\psi, \partial\psi, \partial^2\psi)$ the bulk part of the Einstein-Hilbert action plus the aether terms in (1.1), we arrive at the Einstein-aether form of (2.30) on shell

$$\partial_\mu \left(\frac{\partial \mathcal{L}}{\partial(\partial_\mu g_{\alpha\beta})} \delta g_{\alpha\beta} + \frac{\partial \mathcal{L}}{\partial(\partial_\mu u^\alpha)} \delta u^\alpha - S^\mu \right) = 0. \quad (2.52)$$

The second derivative terms in (2.31) vanish in this case. Under a diffeomorphism generated by a vector field ξ^ν the variation of the metric and the aether is simply

the Lie derivative, $\delta g_{\alpha\beta} = \xi^\nu \partial_\nu g_{\alpha\beta} + \partial_\alpha \xi^\nu g_{\nu\beta} + \partial_\beta \xi^\nu g_{\alpha\nu}$ and $\delta u^\alpha = \xi^\gamma \partial_\gamma u^\alpha - u^\gamma \partial_\gamma \xi^\alpha$.

It follows from (2.46) that $S^\mu = \xi^\mu L_{bulk} - \sqrt{-g}(\partial_\delta \partial_\nu \xi^\mu g^{\delta\nu} - \partial_\delta \partial_\nu \xi^\nu g^{\mu\delta})$. Inserting these forms into (2.52) produces

$$t_\nu^\mu = \sqrt{-g} \left(\frac{\partial L}{\partial(\partial_\mu g_{\alpha\beta})} \partial_\nu g_{\alpha\beta} + \frac{\partial L}{\partial(\partial_\mu u^\alpha)} \partial_\nu u^\alpha - \delta_\nu^\mu L \right) \quad (2.53)$$

$$U_\nu^{\mu\gamma} = \sqrt{-g} \left(\frac{\partial L}{\partial(\partial_\mu g_{\alpha\beta})} (\delta_\alpha^\gamma g_{\nu\beta} + \delta_\beta^\gamma g_{\nu\alpha}) - \frac{\partial L}{\partial(\partial_\mu u^\alpha)} \delta_\nu^\alpha u^\gamma \right) \quad (2.54)$$

$$V_\nu^{\mu(\gamma\lambda)} = \sqrt{-g} \left(\delta_\nu^\mu g^{\lambda\gamma} - \frac{1}{2} \delta_\nu^\gamma g^{\lambda\mu} - \frac{1}{2} \delta_\nu^\lambda g^{\gamma\mu} \right) \quad (2.55)$$

as coefficients of ξ^μ , $\partial\xi^\mu$ and $\partial^2\xi^\mu$ respectively. t_ν^μ and $U_\nu^{\mu\gamma}$, and $V_\nu^{\mu(\gamma\lambda)}$ are the analogs of J_A^μ , $U_A^{\mu\nu}$, $V_A^{\mu(\gamma\lambda)}$ in (2.35)-(2.37). The resulting equations due to the arbitrariness and independence of the derivatives of ξ^μ are

$$\partial_\mu t_\nu^\mu \approx 0 \quad (2.56)$$

$$t_\nu^\mu \approx -\partial_\gamma U_\nu^{\gamma\mu} \quad (2.57)$$

$$U_\nu^{(\gamma\mu)} + \partial_\lambda V_\nu^{\lambda(\mu\gamma)} = 0 \quad (2.58)$$

$$V_\nu^{(\lambda\nu\gamma)} = 0. \quad (2.59)$$

Following (2.42), one can keep the ξ^ν vector fixed (and determine it later for each conserved charge) by choosing $\xi^\nu = \epsilon(x)\xi_0^\nu$. The main result, as before, is

$$\xi_0^\nu t_\nu^\mu = -\partial_\gamma (\xi_0^\nu U_\nu^{\gamma\mu}) \quad (2.60)$$

showing that a Noether charge is again obtained as a surface term. Einstein effectively chose the ξ_0^ν vector to be a constant in (2.60), reducing the pseudotensor to a form consistent with the flat spacetime canonical stress tensor (2.16).

The choice of generator everywhere throughout the spacetime introduces a coordinate system. This can be seen by examining the variational principle ($\delta S = 0 \rightarrow$ equations of motion). For the “ Γ^2 ” action this requires the vanishing of the surface term in the asymptotic region,

$$\int_{S_\infty} \frac{\partial \mathcal{L}}{\partial(\partial_\mu g_{\alpha\beta})} \delta g_{\alpha\beta} + \frac{\partial \mathcal{L}}{\partial(\partial_\mu u^\alpha)} \delta u^\alpha. \quad (2.61)$$

Therefore we have Dirichlet boundary conditions $\delta g_{\alpha\beta} = 0$ and $\delta u^\alpha = 0$ on the metric and the aether at infinity. Inserting the Lie derivatives for the variations above, we see that as $r \rightarrow \infty$

$$\nabla_{(\alpha} \xi_{\beta)} \rightarrow 0 \quad (2.62)$$

$$\mathcal{L}_\xi u^\alpha \rightarrow 0. \quad (2.63)$$

If ξ_0^ν were chosen to be the generator of asymptotic time translations, these conditions would be automatically satisfied. However, since ξ^ν has been chosen to be constant everywhere and u^α is asymptotically constant, the connection coefficients must vanish as one approaches spatial infinity. This amounts to the following splitting of the metric: $g_{\alpha\beta} = \eta_{\alpha\beta} + h_{\alpha\beta}$ where $h_{\alpha\beta}$ vanishes as $h_{\alpha\beta} \sim O(1/r)$, $\partial_\sigma h_{\alpha\beta} \sim O(1/r^2)$ or faster. Thus, one typically computes the Einstein pseudotensor and its corresponding superpotential in an asymptotically Cartesian coordinate system (t, x, y, z) . If, for example, one instead uses spherical polar coordinates (t, r, θ, φ) , the superpotential will yield an incorrect total energy.

2.4.4 Relation to Noether Charge approach

We now will digress to discuss how this work is related to the well-known formalism of Wald [48]. Working with general diffeomorphism invariant Lagrangians, he found a formula for the total canonical energy of an asymptotically flat spacetime in terms of the ‘‘Noether charge’’. To avoid fixing a volume element on spacetime he represented tensor densities of type (k, l) and weight 1 by tensors of type $(k, l + n)$,

$$T_{\nu_1 \dots \nu_l}^{\mu_1 \dots \mu_k} \epsilon_{\alpha_1 \dots \alpha_n}, \quad (2.64)$$

where the last n indices are antisymmetric. These are denoted as (k, l) tensor valued n -forms \mathbf{T} . In this equivalent formalism (2.28) becomes

$$\delta \mathbf{L} = \mathbf{E} \delta \psi + d\mathbf{\Theta} \quad (2.65)$$

for the 4-form Lagrangian $\mathbf{L} = L \epsilon_{abcd}$ and 3-form symplectic current $\mathbf{\Theta} = \theta^a \epsilon_{abcd}$. Similarly, (2.31) is

$$\mathbf{J} = \mathbf{\Theta} - \xi \cdot \mathbf{L} \quad (2.66)$$

where the centered dot represents the contraction on the first index of the form with ξ^a . The 3-form $\mathbf{S} = d(\xi \cdot \mathbf{L})$ for diffeomorphism invariant Lagrangians. On-shell $d\mathbf{J} = 0$, which implies [55] that there exists a Noether charge \mathbf{Q} locally constructed from fields ψ and ξ such that $\mathbf{J} = d\mathbf{Q}$. Wald’s general algorithm [55] can then be used to find \mathbf{Q} given a \mathbf{J} linear in derivatives of ξ^a (an example being (2.34)). The algorithm reduces the highest number of derivatives appearing in \mathbf{J} by one. However, the algorithm for the Noether charge is not unique since one can always add an exact 4-form to the Lagrangian, an exact 3-form to the symplectic current, and a closed

(and hence exact [55]) 2-form to \mathbf{Q} itself. Up to these ambiguities, the form of \mathbf{Q} is equivalent to the ξ^a dependent superpotential $U_{\xi_0}^{\nu\mu}$ in (2.43). For example, an exact form can be added to the superpotential derived from the Einstein-Hilbert Lagrangian using the “cascade” method [53] in order to give

$$\mathbf{Q}_{ab} = -\frac{1}{16\pi G}\epsilon_{abcd}\nabla^c\xi^d, \quad (2.67)$$

which is the Komar form derived in [48].

Wald found that Hamilton’s equation of motion generated by ξ^a are

$$\delta H = \delta \int_C \mathbf{J} - \int_\infty \xi \cdot \Theta \quad (2.68)$$

where the integration is over a Cauchy surface with an asymptotically flat region and compact interior. Typically the asymptotic conditions ensuring δH is convergent imply that any exact form added to the currents will not contribute. Thus Eqn. (2.68) is independent of the ambiguities in the currents and Noether charge. A Hamiltonian exists if and only if there is a (possibly non-covariant) 3-form \mathbf{B} such that at infinity

$$\delta \int_\infty \xi \cdot \mathbf{B} = \int_\infty \xi \cdot \Theta. \quad (2.69)$$

Then

$$H = \int_\infty (\mathbf{Q} - \xi \cdot \mathbf{B}). \quad (2.70)$$

when evaluated on-shell.

The need for the additional \mathbf{B} term is related to the requirement of a well-defined variational principle discussed above in Section 2.4.3. A covariant action constructed only out of metric (e.g. Hilbert action) must contain 2nd or higher

derivatives of the metric. But then a variation leads to boundary terms that are integrals of the symplectic current over the boundary and involve $\delta(\partial g_{\mu\nu})$. These will not vanish for the usual asymptotically flat boundary conditions

$$\begin{aligned} g_{\mu\nu} &= \eta_{\mu\nu} + O(1/r) \\ g_{\mu\nu,\alpha} &= O(1/r^2) \\ \delta g_{\mu\nu} &= O(1/r), \end{aligned} \tag{2.71}$$

where we have assumed a Cartesian coordinate system at infinity. This is why the Noether charge (2.67) alone gives an incorrect total energy for an asymptotically flat spacetime and $\int_{\infty} \xi \cdot \mathbf{B}$ is required. Note that since the aether part of the Einstein-aether Lagrangian is first order in metric and aether derivatives, boundary terms are consistent with the asymptotic flat boundary conditions on the metric and now also the aether,

$$\begin{aligned} u^{\nu} &= \underline{u}^{\mu} + O(1/r) \\ \delta u^{\nu} &= O(1/r), \end{aligned} \tag{2.72}$$

so no modification to the GR 3-form \mathbf{B} is required. In the approach above in Section 2.4.3 the issue of a well-defined variational principle was addressed ab initio by adding appropriate non-covariant boundary terms to the Hilbert action. This produces the “ Γ^2 ” form of the action which is first order in metric derivatives, but forces one into the regime of pseudotensors. Nevertheless, the work in Section 2.4.3 is consistent with the Noether charge methods, giving the same results for conserved quantities.

2.5 Energy in Linearized Theory

Equipped with the modified Einstein and Weinberg pseudotensors we can now calculate the energy density of the linearized plane wave solutions to the Einstein-Aether theory. The plane wave solutions in the absence of matter are found by linearizing the field equations above, (2.1)-(2.3), with $g_{\mu\nu} = \eta_{\mu\nu} + h_{\mu\nu}$ and $u^\mu = \underline{u}^\mu + v^\mu$. This gives

$$\partial_\alpha J^{(1)\alpha}_\beta = \lambda \underline{u}_\beta \quad (2.73)$$

$$G^{(1)}_{\alpha\beta} = T^{(1)}_{\alpha\beta} \quad (2.74)$$

$$v^0 = -\frac{1}{2}h_{00}. \quad (2.75)$$

Cartesian coordinates are used in the flat background, $\eta_{\mu\nu} = (1, -1, -1, -1)$ and $\underline{u}^\mu = (1, 0, 0, 0)$. Since the background value of the Lagrange multiplier vanishes, λ in (2.73) represents a perturbation. The superscript (1) represents quantities written to first order in the perturbation. Jacobson and Mattingly [41] then proceed to analyze these equations using the gauge choice

$$h_{0i} = 0 \quad (2.76)$$

$$v_{i,i} = 0 \quad (2.77)$$

which they prove to be accessible. Inserting plane wave solutions

$$h_{\mu\nu} = \epsilon_{\mu\nu} e^{ik_c x^c} \quad (2.78)$$

$$v^\mu = \epsilon^\mu e^{ik_c x^c} \quad (2.79)$$

into the equations of motion, imposing the four gauge conditions (2.76)-(2.77), and choosing coordinates such that the wave-vector is $(k_0, 0, 0, k_3)$ (travelling in the z

direction), it is found [41] that the mode polarizations and speeds are completely determined. The result is a total of 5 wave modes falling into spin 2, spin 1, and spin 0 types as shown in Table 2.1.³ The notation I in subscript refers to the

Table 2.1: Wave Mode Speeds and Polarizations

Mode	Squared Speed s^2	Polarizations
spin-2	$1/(1 - c_{13})$	$h_{12}, h_{11} = h_{22}$
spin-1	$(c_1 - \frac{1}{2}c_1^2 + \frac{1}{2}c_3^2)/c_{14}(1 - c_{13})$	$h_{I3} = [c_{13}/(1 - c_{13})s]v_I$
spin-0	$c_{123}(2 - c_{14})/c_{14}(1 - c_{13})(2 + c_{13} + 3c_2)$	$h_{00} = -2v_0,$ $h_{11} = h_{22} = -c_{14}v_0,$ $h_{33} = [2c_{14}(c_2 + 1)/c_{123}]v_0$

transverse components of the metric and aether while $c_{14} = c_1 + c_4$, etc. The 2 spin-2 TT metric modes look exactly like the usual GR case, except for the modification of the speed. The 2 spin-1 transverse aether modes and 1 spin-0 trace mode are new modes coming from the constrained aether, which is characterized by 3 degrees of freedom.

In order to determine the energy, note that in the absence of matter the

³Unlike (for example) the Lorentz gauge in GR, the residual gauge of (2.76)-(2.77) is not compatible with the equations of motion (2.73)-(2.75) so it is not clear how to fix the remaining gauge in a simple way. However, it is possible to argue for the existence of 5 wave modes by counting gauge inequivalent degrees of freedom. Consider a theory with N field variables and M gauge symmetries. One can always use the M constraint equations to solve for the M variables whose time derivative does not appear in the equations of motion. This reduces the number of degrees of freedom to $N - M$. Then the remaining M gauge functions can be used to further reduce to $N - 2M$. In the case of the aether theory the metric has 10 degrees of freedom and the constrained vector has 3, making 13 field variables. There are 4 diffeomorphism symmetries, and $13 - 2 \times 4 = 5$.

Weinberg prescription (2.10) reduces to

$$E = \frac{1}{16\pi G} \oint \widetilde{H}_{0\alpha 0\beta}{}^{\alpha} n^{\beta} d^2x = \int \widetilde{t}_{00} d^3x, \quad (2.80)$$

which clearly produces infinite total energy for plane wave modes. One could reformulate the problem in terms of wavepackets with the appropriate asymptotic fall-off conditions, but a far more direct approach is to simply evaluate the plane wave energy density \widetilde{t}_{00} . This quantity is meaningless at a point for plane waves, but the average over a cycle is well-defined. Consider a large, but finite region with nearly plane waves. There are “surface effects”, but the contribution to $\int \widetilde{t}_{00} d^3x$ is dominated by the volume. Thus, \widetilde{t}_{00} gives an effective energy density.

The 3 general classes of modes were analyzed separately using the Riemann tensor package [56] in Maple. The package allows the user to enter the components of the metric and aether vector, calculate curvature tensors, and to define new tensors involving both ordinary and covariant derivatives. In this case the linearized metric and aether were entered, where $h_{\mu\nu}$ and v^{μ} take the plane wave forms. A polarization was written as

$$A \exp(ik_3(z - st)) + \bar{A} \exp(-ik_3(z - st)) \quad (2.81)$$

where s are speeds shown in Table 2.1 and A is a complex-valued function. Using this metric we calculated the explicit form of the Weinberg pseudotensor \widetilde{t}_{00} (2.12) up to quadratic order. Higher order terms will be small in the linearized theory and oscillatory terms proportional to \bar{A}^2 and A^2 can be neglected in the usual time averaging process. These energy densities were then compared with the modified Einstein pseudotensor ${}^{\text{einstein}}t_0^0 + {}^{\text{æ}}t_0^0$ from (2.22) and (2.25) again up to quadratic

order in the perturbations. Note that while (2.20) holds at quadratic order when the linearized equations of motion are imposed, (2.21) does not. Therefore, one must use the modified Einstein pseudotensor directly to compute the energy densities. The results of the Weinberg and Einstein prescriptions agreed and are displayed below:

$$\mathcal{E}_{\text{spin-2}} = \frac{1}{8\pi G} k_3^2 |A|^2 \quad (2.82)$$

$$\mathcal{E}_{\text{spin-1}} = \frac{1}{8\pi G} k_3^2 |A|^2 \frac{c_3^2 - c_1^2 + 2c_1}{1 - c_1 - c_3} \quad (2.83)$$

$$\mathcal{E}_{\text{spin-0}} = \frac{1}{8\pi G} k_3^2 |A|^2 c_{14}(2 - c_{14}) \quad (2.84)$$

These results have been independently verified in [43] by imposing a flat background metric in the Noether charge method and employing a decomposition of u^a into irreducible pieces.⁴ The lack of c_i dependence in (2.82) and the simplicity of (2.83)-(2.84) is striking considering the complicated form of the pseudotensor expressions. The energy of the spin-2 mode is positive definite, like pure GR, while for the other 2 modes the sign of the energy density depends upon a combination of c_1 , c_3 , and c_4 . Note that when the c_i 's are zero, (2.83) and (2.84) are zero as expected. This set of results for the coefficients also holds for exponentially growing modes (i.e. when $s^2 < 0$)

$$A \cos(kz + \varphi) \exp(kst) \quad (2.85)$$

when we average over the spatial oscillations. Restricting $s^2 > 0$ in Table 2.1 to

⁴Note that Foster chose the gauge $h_{0i,i} = 0$ instead of $h_{0i} = 0$. In this gauge the spin-1 polarization differs from that shown in Table 2.1. The energy density is gauge invariant, but the definition of the amplitude of the spin-1 modes here and in [43] differ by a factor of $(1 - c_{13})^{-1}$.

eliminate the unstable modes and enforcing positivity in the energy densities in (2.82)-(2.84) restricts the c_i values in the Einstein-aether theory.

In [40], Lim worked in the limit where the aether and metric perturbations decouple, with the aether propagating in flat spacetime. Mathematically this amounts to tuning $c_i, G \rightarrow 0$ while holding the ratio c_i/G fixed in the action (1.1). If we then expand the metric as $g = \eta + \sqrt{G} h$ and take the limit, the action reduces to that of linearized gravity plus aether terms coupled only to η_{ab} . In this limit the linearized constraint reduces to $v^0 = 0$ and we can decompose v^i into spin-0 and spin-1 parts via $v^i = \partial^i S + N^i$ where $N^i_{;i} = 0$. By examining the Hamiltonian of these modes they found $c_1 > 0$ for positivity in both cases, neglecting c_4 . We can make contact with this result simply by examining in the small c_i limit of the wave solutions. The trace and transverse aether energy waves then correspond to the flat spacetime spin-0 and spin-1 modes. To lowest order in c_i/G we find that

$$c_{14} > 0 \tag{2.86}$$

$$c_1 > 0 \tag{2.87}$$

for positive energy densities of the spin-0 and spin-1 modes respectively. Restoring c_4 in the flat spacetime analysis yields complete agreement. Note that for small c_i the $s^2 > 0$ criteria for stable, non-exponentially growing modes reduce to $c_1/c_{14} \geq 0$ for the spin 1 aether-metric mode and $c_{123}/c_{14} \geq 0$ for the spin 0 trace mode. Thus, modes with positive energy are stable if $c_{123} > 0$.

2.6 Non-Linear Energy

In this section we will attempt to extend the criteria for positive energy from linearized theory into the non-linear regime. As a first step, we will consider the total energy of an asymptotically flat spacetime in the full non-linear theory. Integrating (2.21) over a spacelike slice in the presence of non-aether matter gives the total energy

$$\int T_{\text{eff}0}{}^0 = \int \partial_\lambda {}^{\text{tot}}U_0{}^{\lambda 0} = \oint_\infty {}^{\text{tot}}U_0{}^{\lambda 0} n_\lambda dS \quad (2.88)$$

where ${}^{\text{tot}}U = {}^{\text{ae}}U + {}^{\text{gr}}U$ are the aether and von-Freud superpotentials, (2.26) and (2.23), and $T_{\text{eff}} = t + T$ is total matter and gravitational energy-momentum. The problem now is to calculate the superpotentials for the asymptotically flat solutions to the Einstein-Aether theory. We will use Cartesian coordinates throughout since these have the required asymptotic behavior discussed at the end of Section 2.4.1. Therefore, the surface element is $dS = r^2 d\Omega^2$ and the unit normal is $(\sqrt{2}, x/r, y/r, z/r)$ where $r = \sqrt{x^2 + y^2 + z^2}$. For asymptotically flat boundary conditions we will assume that as $r \rightarrow \infty$

$$g_{\mu\nu} = \eta_{\mu\nu} + O(1/r) + \dots \quad (2.89)$$

$$u^\mu = \underline{u}^\mu + O(1/r) + \dots \quad (2.90)$$

where $\underline{u}^\mu = (1, 0, 0, 0)$ with respect to the Minkowski metric $\eta_{\mu\nu} = (1, -1, -1, -1)$. Equation (2.88) will only be affected by terms in the metric and aether up to $O(1/r)$. Using the analysis of the Newtonian limit [34] and applying the unit constraint, we

find that far from the source in any asymptotically flat solution

$$g_{00} = 1 - \frac{r_0}{r} + \dots \quad (2.91)$$

$$g_{ij} = -1 - \frac{r_0}{r} + \dots \quad (2.92)$$

$$g_{0i} = O(1/r^2) + \dots \quad (2.93)$$

$$u^t = 1 + \frac{r_0}{2r} + \dots \quad (2.94)$$

$$u^i = O(1/r^2) + \dots \quad (2.95)$$

The constant value at infinity and $1/r$ fall-off term in the aether are due to the unit timelike constraint. Thus, unlike ordinary fields, the aether will contribute to the energy expression directly. Inserting (2.91)-(2.95) into the von Freud superpotential (2.23) and aether superpotential (2.26) yields the usual ‘ADM mass’ of GR

$$E_{\text{GR}} = \frac{1}{16\pi G} \oint_{\infty} (g_{jk,k} - g_{kk,j}) n_j d^2 S = \frac{r_0}{2G} \quad (2.96)$$

and the aether modification

$$E_{\text{æ}} = \frac{c_{14}}{8\pi G} \oint_{\infty} \partial^i u^t n_i d^2 S = -\frac{c_{14}}{2} \frac{r_0}{2G}. \quad (2.97)$$

Combining, we find

$$E_{\text{tot}} = \frac{r_0}{2G} \left(1 - \frac{c_{14}}{2}\right). \quad (2.98)$$

This shows that the aether contribution effectively renormalizes the $r_0/2G$ value we usually find for the total energy of an asymptotically flat spacetime in GR. This renormalization can also be understood as a rescaling of Newton’s constant of the form $G_N = G/(1 - c_{14}/2)$. This agrees with the result of [34] and shows the total energy is the gravitating mass that appears in the Newtonian potential.

Equation (2.98) implies that if $c_{14} < 2$ then the total energy of the Einstein-aether theory is positive if the ADM mass $r_0/2G$ is positive. However, the positive energy theorem for GR [45] requires a stress-tensor that satisfies the dominant energy condition. The aether stress-tensor (2.6) does not appear to generally satisfy this condition, so the proof does not go through. However, it is important to note that this does not necessarily mean a positive energy theorem could not be formulated. For example, while the energy density of the aether $T_{tt}^{(u)}$ is negative *everywhere* in the “static” aether solution that will be discussed in Chapter 3, the solution has positive total energy.

Despite the difficulties in formulating a general positive energy theorem, there are examples that are simple enough for calculations of the energy, yet still give important results. One sector of interest is the non-linear decoupled limit. As discussed above in Section 2.5 this formal limit allows one to essentially replace g_{ab} with the flat Minkowski metric η_{ab} in the aether parts of (1.1). One significant example is $c_2 = c_3 = c_4 = 0, c_1 \neq 0$ theory. In this case the Lagrangian density for the aether is

$$L = c_1 \eta^{ab} \eta_{mn} \partial_a u^m \partial_b u^n + \lambda(u^2 - 1) \quad (2.99)$$

This corresponds to a nonlinear sigma model on the unit hyperboloid, which has a stress tensor satisfying the dominant energy condition. A simple way to see this is to note that the derivatives of the individual scalar components u^μ and are contracted with $\eta_{\mu\nu}$, which is positive definite on the unit hyperboloid. Returning to the linearized plane wave energy densities of Section 2.5 we see that in this special

case of (2.82)-(2.84), if $0 < c_1 < 1$, energy is positive in both the linearized and decoupled non-linear regimes of the theory.

Another application of the decoupling limit relevant for our analysis of energy is the work of Clayton [57]. Clayton examined the Maxwell-like simplified theory where $c_1 = -c_3$, $c_2 = c_4 = 0$ in the decoupled version of non-linear Lagrangian (1.1), yielding

$$L = \int d^3x \left\{ \frac{1}{2}(\partial_t u_i - \partial_i u_0)^2 - \frac{1}{4}F_{ij}^2 + \frac{1}{2}\lambda(u_0^2 - \vec{u}^2 - 1) \right\}. \quad (2.100)$$

where $F_{\mu\nu} = \partial_\mu u_\nu - \partial_\nu u_\mu$. The standard calculation of the Hamiltonian and the constraint equations then produces the following on-shell value for the Hamiltonian

$$H = \int d^3x \left\{ \frac{1}{2}\vec{P}^2 + P^i \partial_i u_0 + \frac{1}{4}(F_{ij})^2 \right\}. \quad (2.101)$$

Unlike the electromagnetic case, the second term cannot be turned into a total divergence since now $\nabla \cdot \vec{P} = -\lambda u_0$ on-shell. This implies that for some solutions the value of the Hamiltonian is negative. For example, as initial data choose u_i to be the gradient of a scalar field and $P_i = -\partial_i u_0$. Evaluating the Hamiltonian then yields

$$E = -1/2(\partial_i u_0)^2, \quad (2.102)$$

which can be made arbitrarily negative by an appropriate choice of u_0 .

Moreover, as Clayton points out, the negative energies are not restricted to this special case. In particular, allowing $c_2 \neq 0$ does not affect the $\vec{P} \cdot \vec{\partial} u_0$ term in the Hamiltonian and even produces additional questionable terms. The indefinite nature of the decoupled Hamiltonian contrasts with the wave energy densities of

Section 2.5, which clearly can be made positive definite in the Maxwell-like case. The key point is that the wave results are in the linearized theory and associated with quadratic parts of the Hamiltonian, while the indefinite terms appear at higher orders. For example, the linearized constraint equation $v^0 = 0$ eliminates $\vec{P} \cdot \vec{\partial} u_0$ from the Maxwell-like Hamiltonian and forces the u_0 in (2.102) to be quadratic or higher in the perturbation. Thus, the indefinite pieces begin to appear at quartic order in the Hamiltonian. This indefiniteness at higher orders implies that the decoupled, linearized results of Lim and the “coupled”, linearized analysis of this paper generally do not detect possible energies of arbitrary sign in the fully non-linear decoupled Einstein-aether theory.

2.7 Discussion

In this chapter we have derived two energy-momentum pseudotensor expressions for the Einstein-aether theory and used them to compute the energy densities of weak gravitational waves and the total energy of an asymptotically flat solution. The constraints of Section 2.5 show that a sector of this LV model satisfies the important theoretical condition of positive energy in the linearized case. This result is a key component in the full set of weak field constraints summarized by [38]. A remaining open question is whether the energy remains positive when we consider the full non-linear theory. We have argued that in the decoupled limit the $c_1 \neq 0$ non-linear sigma model is immune to the sickness of energies of indefinite sign. However, in the full theory this particular special case is not consistent with

the vanishing of the PPN parameter α_2 and is ruled out observationally. Meanwhile other special cases of the coupling constants yield negative energy solutions even when the linearized theory has positive energy. But since solutions in the decoupled limit will not generally be solutions in the full theory, this does not imply that there is no positive energy theorem. Perhaps energy positivity can only be formulated (for some range of the coupling constants) in the preferred frame defined everywhere by the aether field. Currently a complete answer to the question of positivity of energy in the full non-linear theory is not yet in hand.

Chapter 3

Spherical Solution Properties and Static Aether

3.1 Introduction

As described in Chapter 1, the study of linearized and weak-field behavior of ae-theory has led to a rich phenomenology and constraints on the theory. Also important for determining theoretical viability and observational constraints on ae-theory are the properties of non-linear solutions. In this chapter and the following two chapters (devoted to stars and black holes) we complete a general survey of the time-independent spherically symmetric solutions. Some of these solutions were previously obtained in the special case where the aether dynamics is Maxwell-like [25]. It was shown in [25] that the Reissner-Nordstrom metric in a spherically symmetric static gauge with fixed norm is a solution, and it was claimed (incorrectly, as shown here) that this is the only solution in that special case. The asymptotic weak field limit of the general case was studied in [36], where it was found that there is a two-parameter family of asymptotically flat spherical, static solutions. A thorough examination of the fully nonlinear solutions has not been carried out before.

In Section 3.2 we start by specializing the vacuum action for ae-theory to time independent spherical symmetry. We review some general properties and examine the structure of the field equations as ordinary differential equations. We show that locally there is a three parameter family of vacuum solutions. There is no Birkhoff's

theorem for spherical solutions in ae-theory. Imposing asymptotic flatness reduces the number of parameters to two. Some of the details of the asymptotic solutions are also discussed in this section.

In Section 3.3 the general vacuum solution in which the aether vector is aligned with the timelike Killing field is found. Being a unit vector, the aether is completely determined by the metric in this case. This solution is asymptotically flat and described by one free total mass parameter. For negative total mass there is a naked singularity at the origin. The positive mass solution has a wormhole-like spatial geometry, reaching a minimum area 2-sphere at some radius like the Schwarzschild solution. Unlike in the Schwarzschild solution this throat is not on a horizon. Inside the throat the spheres re-expand to infinitely large size in finite affine parameter along a radial null geodesic and finite or infinite proper distance depending on the coupling parameters in the Lagrangian. When the distance is finite the internal infinity is singular, and it occurs at a would-be extremal Killing horizon. When the distance is infinite the metric is asymptotically singular. We conclude in Section 3.4 by showing that no regular solutions corresponding to spherically symmetric “stars” made from lumps of pure aether can exist in the theory.

3.2 General Properties

The vacuum Einstein-aether Lagrangian compactly written in terms of the kinetic term $K^{ab}{}_{mn}$ (1.2) can be expanded out into

$$L = -R - c_1(\nabla_a u_b)(\nabla^a u^b) - c_2(\nabla_a u^a)^2 - c_3(\nabla_a u_b)(\nabla^b u^a)$$

$$-c_4(u^c \nabla_c u^a)(u^d \nabla_d u_a) - \lambda(g_{ab} u^a u^b - 1). \quad (3.1)$$

In spherical symmetry the c_4 term in the action can be absorbed by the change of coefficients

$$\begin{aligned} c_1 &\rightarrow c_1 + c_4 \\ c_3 &\rightarrow c_3 - c_4. \end{aligned} \quad (3.2)$$

To see why, note that any spherically symmetric vector field is hypersurface orthogonal, hence the twist

$$\omega_a = \epsilon_{abcd} u^b \nabla^c u^d \quad (3.3)$$

of the aether vanishes. The identity

$$\dot{u}^2 = -\omega_a \omega^a + \nabla_a u_b \nabla^a u^b - \nabla_a u_b \nabla^b u^a, \quad (3.4)$$

valid for u^a satisfying $u^2 = 1$, can be used to trade the \dot{u}^2 term in the Lagrangian (3.1) for an ω^2 term together with the substitution (3.2). Since the twist occurs quadratically and vanishes in spherical symmetry, that term will not contribute to the field equations, hence the $c_4 \dot{u}^2$ term simply modifies the coefficients as indicated in (3.2). Thus we henceforth set $c_4 = 0$ in this chapter without loss of generality, as it can be reintroduced at the end via the replacements (3.2). (Although substitution of the identity (3.4) will not change the content of the field equations, it will change the value of the lagrange multiplier λ for a given solution.)

As a reminder to the reader, the vacuum field equations are

$$G_{ab} = T_{ab}^{(u)} \quad (3.5)$$

$$\nabla_a J^a_m - c_4 \dot{u}_a \nabla_m u^a = \lambda u_m, \quad (3.6)$$

$$g_{ab} u^a u^b = 1. \quad (3.7)$$

where

$$J^a_m = K^{ab}{}_{mn} \nabla_b u^n \quad (3.8)$$

and

$$\dot{u}_a = u^b \nabla_b u_a. \quad (3.9)$$

The aether stress tensor is given by

$$\begin{aligned} T^{(u)}{}_{ab} &= \nabla_m (J^m{}_{(a} u_{b)}) - J_{(a}{}^m u_{b)} + J_{(ab)} u^m \\ &+ c_1 [(\nabla_a u_m)(\nabla_b u^m) - (\nabla_m u_a)(\nabla^m u_b)] \\ &- c_4 \dot{u}_a \dot{u}_b \\ &- [u_n (\nabla_m J^{mn}) - c_4 \dot{u}^2] u_a u_b \\ &- \frac{1}{2} L_u g_{ab}, \end{aligned} \quad (3.10)$$

where $L_u = -K^{ab}{}_{mn} \nabla_a u^m \nabla_b u^n$ and $\dot{u}^2 = \dot{u}_a \dot{u}^a$.

Some words about terminology are in order. Spacetimes admitting a timelike Killing vector field ξ^a are generally called *stationary*. In the special case where ξ^a is hypersurface orthogonal, and therefore invariant under a time reflection $t \rightarrow -t$, the spacetime is said to be *static*. A stationary aether field u^a on a stationary spacetime is one whose Lie derivative with respect to ξ^a vanishes. If the spacetime is static, one might be tempted to say the aether is “static”, however this is not really appropriate since the aether itself breaks the Killing time reflection symmetry. The solutions studied in this paper involve a static metric coupled to a stationary aether. This

general situation will be called here “stationary spherical symmetry”. An important special case occurs when the aether is parallel to the Killing vector. We refer to this special case as “static aether”. Such an aether changes sign under the Killing time reflection, however the action (1.1) is invariant under $u^a \rightarrow -u^a$ so the sign of u^a has no physical meaning. Note that regular black holes (see Chapter 5) cannot have static aether fields since the Killing vector is null, not timelike on the horizon.

3.2.1 Classification of stationary spherical solutions

In GR stationary spherically symmetric solutions describe, for example, a black hole or the exterior of a time-independent star. In spherical symmetry all stationary metrics are static [58]. The line element can be written in Schwarzschild type coordinates,

$$ds^2 = e^{A(r)} dt^2 - B(r) dr^2 - r^2 d\Omega^2, \quad (3.11)$$

and the aether field takes the form

$$u = a(r)\partial_t + b(r)\partial_r. \quad (3.12)$$

The unit constraint on u^a becomes

$$e^{A(r)} a(r)^2 - B(r) b(r)^2 = 1, \quad (3.13)$$

which can be used for example to eliminate $b(r)$. This ansatz for the metric and aether can then be used in the field equations (3.5) and (3.6) to generate a system of ordinary differential equations (ODE’s). The t -component of the aether field equation (3.6) can be used to solve for λ in this case, and the remaining field equations

reduce to five ODE's: the tt , rr , tr , and $\theta\theta$ components of the metric field equation and the r component of the aether field equation. These five equations involve the eight functions $\{A'', A', A, B', B, a'', a', a\}$, where prime denotes differentiation with respect to the argument r which is suppressed. The equations are too complicated to be worth writing down here, so we shall just describe their structure. Using the tt and $\theta\theta$ metric equations along with the r component of the aether equation, one can solve for A'' , a'' , and B' in terms of the remaining five functions $\{A', A, B, a', a\}$. It turns out that only one additional piece of information remains in the tr and rr equations, which can be used to solve (for example) for B in terms of $\{A', A, a', a\}$. Finally, $A(r_0)$ at any given value $r = r_0$ can be chosen at will by allowing for an appropriate scaling of the t coordinate. At a given r_0 value, the remaining three values $\{A'(r_0), a'(r_0), a(r_0)\}$ then determine a (local) solution by integration with respect to r . This shows that there is in general a three-parameter family of spherically symmetric stationary solutions.

To illustrate this reasoning in a more familiar setting, we apply it to the field equations of pure GR in Schwarzschild coordinates,

$$G_{tt} \propto rB' - B + B^2 = 0 \tag{3.14}$$

$$G_{rr} \propto rA' - B + 1 = 0 \tag{3.15}$$

$$G_{\theta\theta} \propto 2rA''B + A'(2B - rB') + rA'^2B - 2B' = 0. \tag{3.16}$$

These can be used to solve for B' , B , and A'' in terms of A' and A . Using the freedom to scale t the initial value $A(r_0)$ can be fixed at will, so we recover the well-known fact that static spherically symmetric solutions in GR are characterized

by one free parameter, in this case the value of $A'(r_0)$. In the Einstein-aether theory the aether vector and its derivative provide two additional degrees of freedom at each point.

Birkhoff's theorem in GR states that the only spherically symmetric solution is static and given (up to coordinate freedom) by the Schwarzschild metric. The radial tilt of the aether provides another local degree of freedom in ae-theory, so spherical solutions need not be time-independent. But, as we have seen, even restricting to stationary spherical symmetry ae-theory has more solutions. In this chapter we will focus primarily on the static aether solutions, which form a one-parameter family. Black hole solutions, which comprise a different family, are studied in Chapter 5.

3.2.2 Asymptotic Flatness

Numerical integration of the ae-theory field equations as ODE's out from some arbitrary point r_0 with generic initial conditions yields singularities in $A(r)$, $B(r)$, and $a(r)$. However, there is a two-parameter family of asymptotically flat solutions. This was first found in Ref. [36] using a perturbative expansion about infinity. Asymptotic flatness can be imposed there by assuming regular power series expansions for the metric functions about $x = 1/r = 0$, where r is the Schwarzschild radial coordinate. To begin, the field equations are rewritten in terms of the new variable x . Around $x = 0$ the functions $N_s(x) = e^{A(x)}, B(x), b(x)$ will have power series behavior in the form of

$$N_s(x) = 1 + N_1x + N_2x^2 + N_3x^3 + N_4x^4 \quad (3.17)$$

$$B(x) = 1 + B_1x + B_2x^2 + B_3x^3 + B_4x^4 \quad (3.18)$$

$$b(x) = b_0 + b_1x + b_2x^2 + b_3x^3 + b_4x^4, \quad (3.19)$$

where at this stage it is convenient to use the constraint equation (3.13) to eliminate $a(x)$ in favor of the radial component $b(x)$. It turns out that asymptotic flatness and spherical symmetry generally require the aether to have no radial component at infinity ($a_0 = 1, b_0 = 0$) except in the Einstein-Maxwell-like case ($c_3 = -c_1, c_2 = c_4 = 0$) where the action takes a special form with an additional gauge symmetry. The first order coefficient N_1 determines the Newtonian gravitational potential, while the post-Newtonian corrections to this are associated with the B_1 and N_2 coefficients. The higher order coefficients are post-post Newtonian (and beyond). Substituting the above forms of the functions into the equations of motion and performing a series expansion in Maple around the point $x = 0$ ultimately gives a set of algebraic equations that can be solved to produce the local power series solutions for the fields.

We note tangentially that these series solutions split into two classes depending on whether combination of coupling constants $c_{123} = c_1 + c_2 + c_3$ vanishes or not. The $c_{123} = 0$ special case seems to be degenerate. For example, the preferred frame parameter α_2 diverges [37, 38] implying a post-Newtonian expansion is not valid. The speed of spin-0 waves vanishes in this case because spatial gradient kinetic terms in the action are missing for those modes. Thus, there is no well-defined static limit. For the generic $c_{123} \neq 0$ we are interested in here, there are two free parameters, namely N_1 and b_2 in this gauge. As we have seen from the study of total non-linear

energy in Section 2.6, the metric parameter N_1 is determined by the total mass of the presumed central object generating the field. The additional aether parameter b_2 cannot be associated with a “charge” as in the special case of Einstein-Maxwell due to the $1/r^2$ fall off.

Asymptotic flatness can also be imposed using the “shooting method”. This is simple to implement here since it is only necessary to tune one of the three initial values at an interior point $\{A'(r_0), a'(r_0), a(r_0)\}$ so that, for example, $A(r)$ approaches a constant value as $r \rightarrow \infty$. The asymptotic field equations then automatically enforce the remaining flatness conditions. In GR, by contrast, asymptotic flatness is a consequence of the vacuum field equations without any tuning of initial data, so the one-parameter family of local (Schwarzschild) solutions is automatically asymptotically flat.

3.3 Static Aether

In this section we obtain the static aether solution, where the aether vector u^a is proportional to the timelike Killing field ξ^a and therefore entirely determined by the metric.

3.3.1 Field equations with static aether

Using the Schwarzschild type coordinates in (3.11) and (3.12), the static aether has $b(r) = 0$ and $a(r) = \exp(-A(r)/2)$, i.e.

$$u = e^{-A/2} \partial_t. \tag{3.20}$$

In this case the c_2 and c_3 terms drop out of the field equations. To see why, note that (3.20) implies $\nabla_a u^a = 0$, so all variations of the c_2 term in the action (3.1) vanish. In addition, the normalization $u_a u^a = 1$ implies $u_b \nabla_a u^b = 0$. These conditions together with spherical symmetry imply that the derivative of u^b has the form

$$\nabla_a u^b = u_a s^b, \quad (3.21)$$

where s^b is a radial vector orthogonal to u^a . (We note in passing that contraction of (3.21) with u^a reveals that s^b is the acceleration of the aether worldlines.) Therefore $(\nabla_a u^b)(\nabla_b u^a)$ vanishes, so the variation of the volume element in the c_3 term of the action (3.1) vanishes. The remaining variation of the c_3 term is proportional to $u_a s^b \delta(\nabla_b u^a) = s^b \delta(u_a \nabla_b u^a)$, which vanishes for all variations $(\delta g_{ab}, \delta u^a)$ preserving the normalization $g_{ab} u^a u^b = 1$. Moreover, as explained in Section 3.2, in spherical symmetry the c_4 term can be absorbed into the c_1 and c_3 terms, hence the solutions with static aether are fully characterized by the case with only c_1 non-zero.

When only c_1 is nonzero the aether field equation (3.6) reduces to

$$c_1 \nabla^a \nabla_a u^b = \lambda u^b. \quad (3.22)$$

Using (3.21) this becomes

$$c_1 u^a \nabla_a s^b = \lambda u^b. \quad (3.23)$$

Contraction of the left hand side of (3.23) with s_b is proportional to $u^a \nabla_a s^2$, which vanishes since s^2 is a scalar that must be constant along the Killing direction parallel to u^a . Therefore both sides are parallel to u^b , so the aether equation only determines λ . Contracting both sides of (3.23) with u_b one finds

$$\lambda = -c_1 s^2, \quad (3.24)$$

having made use of (3.21) and $u^b \nabla_a s_b = -s^b \nabla_a u_b$, which follows from $u^b s_b = 0$.

The metric field equation is $E_{ab} = G_{ab} - T_{ab}^u = 0$, and the tt , rr , and $\theta\theta$ components of E_{ab} are given by

$$E_{tt} = (e^A/r^2 B) \left[(-1 + B + rB'/B) - \nu(8rA' + r^2 A'^2 - 2r^2 A'B'/B + 4r^2 A'') \right] \quad (3.25)$$

$$E_{rr} = r^{-2}(1 - B + rA' + \nu r^2 A'^2) \quad (3.26)$$

$$E_{\theta\theta} = B^{-1} \left[(2rA' - 2rB'/B + r^2 A'^2 - r^2 A'B'/B + 2r^2 A'')/4 - \nu r^2 A'^2 \right], \quad (3.27)$$

where for notational convenience we have introduced the symbol

$$\nu = \frac{c_1}{8}. \quad (3.28)$$

Using the E_{rr} equation one can solve for B ,

$$B = 1 + rA' + \nu r^2 A'^2, \quad (3.29)$$

Substituting this solution for B into the E_{tt} and E_{rr} equations, we find that the equations are redundant and the system is described by the second order ODE

$$r^2 A'' + 2rA' + r^2 A'^2 + \nu r^3 A'^3 = 0. \quad (3.30)$$

A constant shift of A can be absorbed by a scaling of the t coordinate, hence there is just a one parameter family of solutions. As in GR, the solutions in this family are all asymptotically flat.

3.3.2 Static aether solutions: general analysis

To solve (3.30) we define the function $Y(r)$ by

$$Y = rA', \quad (3.31)$$

in terms of which the solution for B becomes

$$B = 1 + Y + \nu Y^2 \tag{3.32}$$

and Eqn. (3.30) for A becomes

$$dY/dr = -(Y/r)(1 + Y + \nu Y^2) \tag{3.33}$$

The problem is thus reduced to quadratures: integration of this equation yields $Y(r)$, which also directly yields B via (3.32). To determine A we combine (3.31) and (3.33) to obtain

$$dA/dY = -1/(1 + Y + \nu Y^2), \tag{3.34}$$

which yields $A(Y)$ by integration.

The character of the solutions is evidently controlled by the roots of B ,

$$Y_{\pm} = (-1 \pm \sqrt{1 - 4\nu})/(2\nu), \tag{3.35}$$

in terms of which we have

$$B = \nu(Y - Y_-)(Y - Y_+). \tag{3.36}$$

The nature of the roots depends on the value of ν . We consider here only positive ν , since as was shown in Section 2.5 that is required by positivity of the energy of linearized spin-0 waves, and we restrict to $\nu < 1/4$ since the Newton constant $G_N = G/(1 - c_{14}/2)$ becomes negative beyond this limit. In the pure c_1 case also the stability [41] or positive energy of linearized waves requires $c_1 < 1$ or $\nu < 1/8$. One can visualize the roots graphically: they are the intersections of the line $Y + 1$ with the inverted parabola $-\nu Y^2$. When $\nu = 1/4$ the parabola is tangent to the line,

and the two roots coincide at $Y = -2$. The larger root approaches -1 as $\nu \rightarrow 0$, while the smaller root approaches $-\infty$, hence in the range $0 \leq \nu < 1/4$ the roots fall within the ranges

$$-\infty \leq Y_- < -2, \quad -2 < Y_+ \leq -1. \quad (3.37)$$

Note that $Y_- = 1/(\nu Y_+)$, and $\nu = -(1 + Y_+)/Y_+^2$.

One can integrate (3.34) and (3.33) to find both A and Y using the factorization (3.36) and partial fractions. The result is

$$N_s = e^A = \left(\frac{1 - Y/Y_-}{1 - Y/Y_+} \right)^{\frac{-Y_+}{2+Y_+}} \quad (3.38)$$

and

$$\frac{r_{\min}}{r} = \left(\frac{Y}{Y - Y_-} \right) \left(\frac{Y - Y_-}{Y - Y_+} \right)^{\frac{1}{2+Y_+}}, \quad (3.39)$$

where r_{\min} is an integration constant. The graph of r/r_{\min} vs. Y is plotted in Fig. 3.1, for the case $c_1 = 1$. The values of the sphere radius r and metric functions B and N at the special values of Y are given in Table 3.1.



Figure 3.1: Graph of r/r_{\min} vs. Y for $c_1 = 1$. The curves approach 1 asymptotically on both sides. The range $(Y_+, 0)$ defines a negative mass solution with naked singularity at $Y = Y_+$ and asymptotically flat region at $Y \rightarrow 0$. The range $(0, \infty)$ defines a positive mass solution, with a minimal 2-sphere as $Y \rightarrow \infty$. The range $(-\infty, Y_-)$ continues that solution to the other side of the minimal sphere, with a singularity at a sphere of infinite radius at $Y = Y_-$. This sphere lies at finite radial distance if $c_1 < 3/2$. There is no solution with timelike aether in the range (Y_-, Y_+) since the radial coordinate is timelike there (see Section 3.3.2.4).

Table 3.1: Sphere radius and metric functions at special Y values.

Y	Y_-	Y_+	0	$\pm\infty$
r	∞	0	∞	r_{\min}
B	0	0	1	∞
N	0	∞	1	> 0

3.3.2.1 The GR limit: Schwarzschild solution

To help to interpret the general case, we consider first the pure GR limit $c_1 = 0$, for which $Y_+ = -1$ and $Y_- = -\infty$. The solution is then

$$B = 1 + Y \tag{3.40}$$

$$N_s = 1/(1 + Y) \tag{3.41}$$

$$r_{\min}/r = Y/(1 + Y). \tag{3.42}$$

This is just the Schwarzschild solution, with $Y = 1/(r - r_{\min})$ and $r_{\min} = 2M$. Spatial infinity corresponds to $Y = 0$, and as $Y \rightarrow \infty$ the radius decreases to r_{\min} at the bifurcation surface of the horizon. The other side of the wormhole is here labelled by the same values of Y . The range $-\infty < Y < -1$ corresponds to the future wedge of the black hole interior, where the Killing vector is spacelike. The remaining range $-1 < Y < 0$ is also significant. It corresponds to the negative mass Schwarzschild solution.

3.3.2.2 Static aether solutions for generic c_1

For generic values of c_1 the limit $Y \rightarrow 0$ still corresponds to an asymptotically flat spatial infinity, where the limiting form of the solution is

$$B = 1 + Y + \dots \quad (3.43)$$

$$N_s = 1 - Y + \dots \quad (3.44)$$

$$Y = 2M/r + \dots, \quad (3.45)$$

and the mass M is related to the minimum radius by

$$r_{\min}/2M = (-Y_+)^{-1}(-1 - Y_+)^{(1+Y_+)/(2+Y_+)}. \quad (3.46)$$

This ratio grows smoothly from 1 for $c_1 = 0$, to about 1.23 for $c_1 = 1$, and reaches $e/2 \approx 1.4$ for $c_1 = 2$.

Series solution in powers of $x = 2M/r$ yields

$$B = 1 + x + (1 + \nu)x^2 + \dots \quad (3.47)$$

$$N = 1 - x - (\nu/6)x^3 + \dots \quad (3.48)$$

$$Y = x + x^2 + (1 + \nu/2)x^3 + \dots \quad (3.49)$$

In this case the additional asymptotic aether parameter discussed in Section 3.2.2 is set to zero and the solution is completely described by the total mass. This completes our characterization of the asymptotically flat region. What happens when we follow the solution to smaller values of r ?

The answer depends on the range of Y considered. For $Y \in (Y_+, 0)$, equation (3.39) or its graph in Fig. 3.1 indicate that r_{\min} must be *negative*, which according to

(3.46) implies a negative total mass $M < 0$. In this case there is a naked singularity at $Y = Y_+$ ($r = 0$) connected to an asymptotically flat region at $Y = 0$ ($r = \infty$), like in the negative mass Schwarzschild solution.

For positive Y the solution is different. It is seen again from (3.33) or its graph that Y grows monotonically as r decreases. As $Y \rightarrow \infty$ the r.h.s. of (3.39) goes to 1, so this limit for Y corresponds to a minimum radius r_{\min} , just as in the case of the Schwarzschild solution. However, the solution behaves quite differently from Schwarzschild. First, instead of $N(r_{\min}) = 0$ we have

$$N_s(r_{\min}) = \left(\frac{Y_+}{Y_-} \right)^{-Y_+/(2+Y_+)}, \quad (3.50)$$

so the minimal 2-sphere does not sit at a Killing horizon. The value of $N_s(r_{\min})$ grows smoothly from 0 for $c_1 = 0$ to about 0.083 for $c_1 = 1$ and reaches $e^{-2} \approx 0.135$ for $c_1 = 2$. (Recall that in the GR limit we have $Y_- \rightarrow -\infty$.) Another difference due to the finiteness of Y_- is that the solution continues with negative Y values, with the two values $Y = \pm\infty$ identified. According to (3.33), as Y grows from $-\infty$ up to Y_- , r increases from r_{\min} to ∞ . Therefore the “interior” of the minimal 2-sphere flares out to infinite radius as in the Schwarzschild solution. But unlike the Schwarzschild case, now two values of Y correspond to each r , and the “interior” geometry is not equivalent to the exterior. In fact the difference is quite dramatic: at the internal infinity both N and B go to zero, whereas they both approach one in the asymptotically flat region.

The Carter-Penrose diagram for this solution is the square diamond in Fig. 3.2 with asymptotically flat past and future null infinity on the lower and upper edges

bounding the right hand side and a singularity on both edges S^\pm and at S^0 bounding the left hand side. S^\pm are singular Killing horizons with vanishing surface gravity. The proper distance to S^0 along a constant t surface is finite if $0 < c_1 < 3/2$ and infinite if $3/2 < c_1 < 2$, while for any c_1 the affine parameter to S^\pm along a radial light ray is finite, as we now demonstrate.

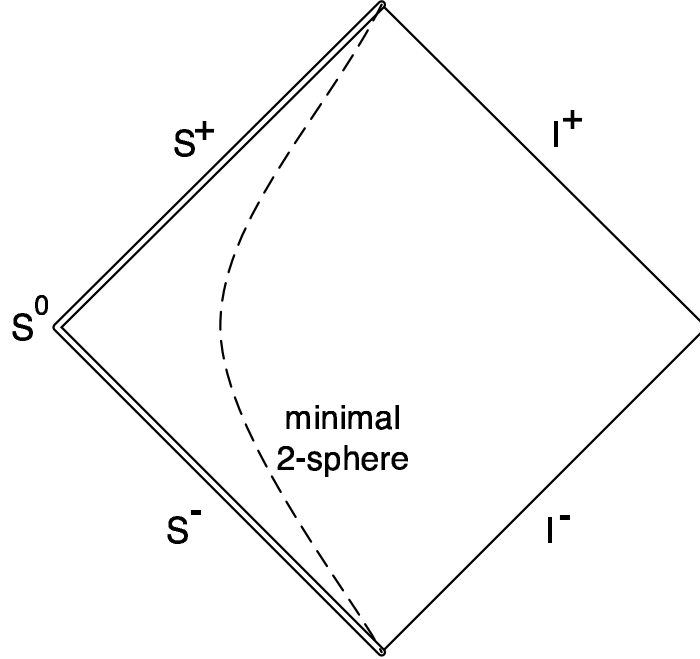


Figure 3.2: Carter-Penrose diagram of the static aether solution. The left hand edge corresponds to spheres of infinite radius and is singular.

As the internal infinity at Y_- is approached, the proper radial distance on a constant t surface behaves as

$$\frac{dl}{dr} = B^{1/2} \sim (Y_- - Y)^{1/2}. \quad (3.51)$$

On the other hand (3.39) shows that in this limit the relation between Y and r is

$$(Y_- - Y) \sim r^{\frac{2+Y_+}{1+Y_+}}, \quad (3.52)$$

so we have

$$\frac{dl}{dr} = r^{\frac{2+Y_+}{2+2Y_+}}. \quad (3.53)$$

The exponent of r in (3.53) is always negative, and it is equal to -1 when $Y_+ = -4/3$, which corresponds to $\nu = 3/16$, i.e. $c_1 = 3/2$. For $c_1 < 3/2$ the radial distance to S^0 is finite and there is a curvature singularity at $r = \infty$ that shows up, for example, in the square of the Riemann tensor.

Along a radial null geodesic the quantity $N_s \dot{t} = N_s dt/d\lambda$ is conserved, where λ is an affine parameter. Together with the lightlike condition $N_s \dot{t}^2 - Br^2 = 0$ this implies that as the internal infinity is approached the affine parameter behaves as

$$d\lambda/dr = (N_s B)^{1/2} \sim (Y_- - Y)^{1/(2+Y_+)} \sim r^{1/(1+Y_+)}. \quad (3.54)$$

The affine parameter distance to S^\pm is therefore finite for all $Y_+ \in (-2, -1)$, corresponding to all $c_1 \in (0, 2)$.

Note that since the minimal 2-sphere is not hidden by a horizon, a spherical congruence of null rays will converge towards the minimal sphere and exit the other side with a positive expansion. The Raychaudhuri equation shows that this can happen only if $R_{ab}k^a k^b < 0$ somewhere along the congruence, so we infer that the aether stress tensor must violate the null energy condition in this solution. We computed the curvature for this solution and found that $G_{tt} = -\nu Y^2/Br^2$, so the energy density of the aether ($\propto G_{tt}$) is negative *everywhere*. The solution nevertheless has positive total mass, which may at first seem to be inconsistent but it is not. The total mass of an asymptotically flat spacetime is given by a surface integral at spatial infinity, which for stationary spacetimes is proportional to the

volume integral $\int_{\Sigma} R_{ab}n^a\xi^b dV$, plus a surface term if there is an inner boundary [58]. Since $R_{ab} \propto T_{ab} - (1/2)Tg_{ab}$, it is not the energy density that figures in the total energy but rather R_{tt} . Quite surprisingly, it turns out that R_{tt} vanishes everywhere in the static aether solution. (The only nonzero component of the Ricci tensor is R_{rr} .) Hence the energy integrand vanishes identically, as in Schwarzschild spacetime. This does not mean the total energy vanishes however, since there is a contribution from the inner boundary. In Schwarzschild that inner boundary may be pushed off to the asymptotic region on the other side of the Einstein-Rosen bridge, but the static aether solution is singular on the other side of the throat. One can think of the mass as determined by a boundary condition at this singularity.

Let us briefly consider solutions for c_1 in the range $3/2 < c_1 < 2$, corresponding to $3/16 < \nu < 1/4$. In this case the distance to the internal infinite radius sphere is infinite, and all the algebraic and differential invariants that we checked (including R , $R_{ab}R^{ab}$, $R_{abcd}R^{abcd}$, $R_{ab}u^a u^b$, and $(\nabla_a u^b)(\nabla_b u^a)$) are asymptotically zero. However, the curvature component $R_{ab}k^a k^b$ blows up asymptotically, when k^a is the tangent to an affinely parameterized radial null geodesic approaching the internal infinity. The invariant $u^a k_a$ blows up as $N_s^{-1/2}$, since $N^{1/2}u^a$ is the Killing vector ξ^a and $k^a \xi_a$ is conserved along the geodesic. This suggests that the above-mentioned invariants vanish because the tensor structure of the curvature, the aether, and all derivatives is determined by a single null vector pointing in the future radial null direction opposite to k^a , i.e. pointing away from the internal area-infinity.

Returning now to the generic solution for $0 < c_1 < 1$, we examine more closely the behavior at the throat and at the internal infinity. Since the spherical radius r is

not a good coordinate at the minimal area sphere, nor at the internal area-infinity, we adopt instead the proper length coordinate l , in terms of which the line element takes the form

$$ds^2 = N_s(l)dt^2 - dl^2 - r(l)^2 d\Omega^2 \quad (3.55)$$

To get an idea of how the throat geometry depends on c_1 , we fix the mass M of the solution and plot in Fig. 3.3 the numerically computed function $r(l)$ for several different values of c_1 . There is a discontinuity at $c_1 = 0$ where the solution abruptly changes from a singular flare-out in finite proper distance to a perfectly regular Einstein-Rosen bridge. The singularity approaches the throat as $c_1 \rightarrow 0$, but in the same limit the curvature becomes finite and the other half of the bridge suddenly appears.

To more fully compare the Schwarzschild and aether solutions we plot together in Fig. 3.4 the radius $r(l)$ and the norm of the Killing vector $\sqrt{N_s(l)}$ for the two solutions with the same value of the total mass M . At the internal singularity the norm of the Killing vector goes to zero, and the Killing vector is tangent to the constant r surfaces, so the singularity is a “would-be” Killing horizon. The surface gravity of the horizon is given by $d\sqrt{N_s}/dl$ at the horizon. The behavior is easily found using the previous formulae:

$$d\sqrt{N_s}/dl = (1/2)(N_s/B)^{1/2}(Y/r) \propto (Y - Y_-)^{2(1+Y_+)/(2+Y_+)}. \quad (3.56)$$

The exponent is positive, so the derivative of the norm vanishes as $Y \rightarrow Y_-$. The surface gravity is therefore zero, so the would-be Killing horizon is extremal.

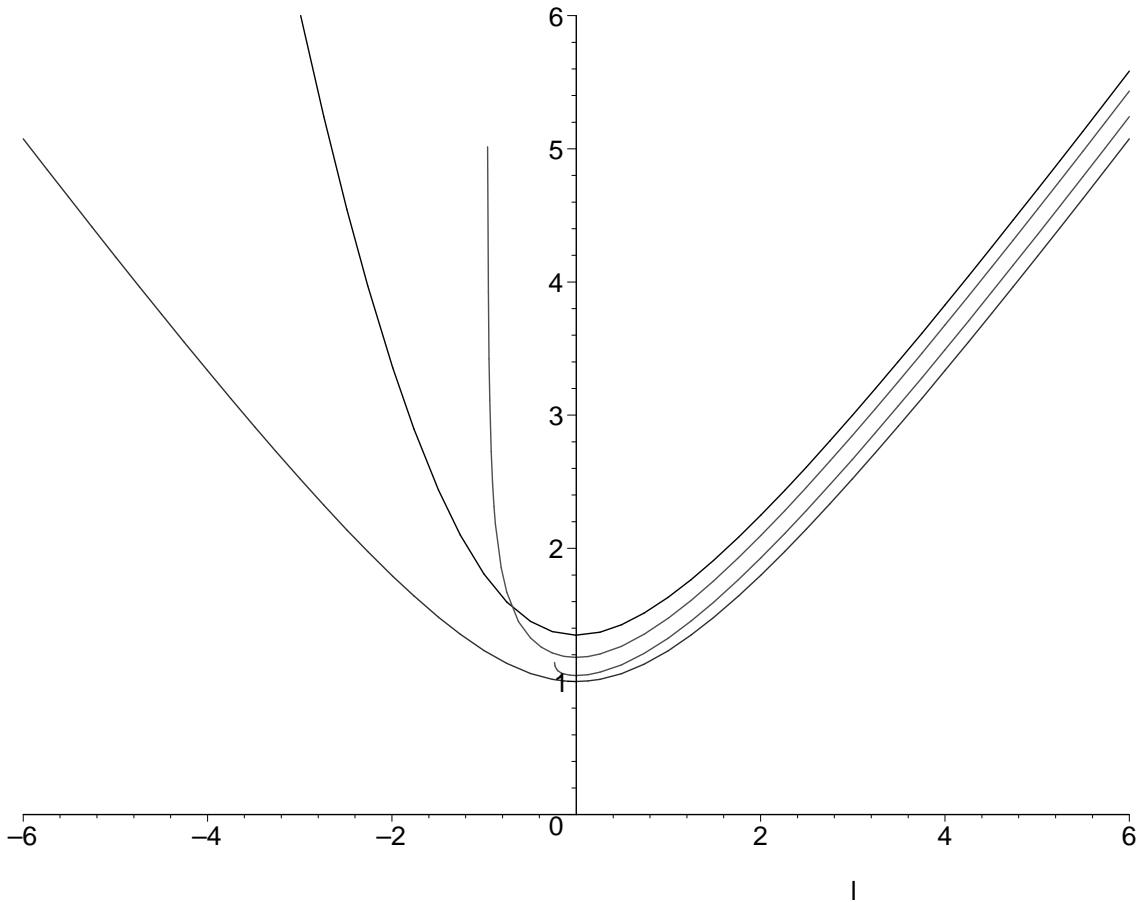


Figure 3.3: Plot of area radius r vs. proper length l for fixed mass M , in units with $2M = 1$, for $c_1 = 0, 0.1, 0.7$, and 1.9 . In the GR case $c_1 = 0$ this is the Einstein-Rosen bridge. For $c_1 = 0.1$ the radius flares out to infinity so quickly that the code used to make the plot halted at small radius. With increasing c_1 the throat widens, the flare-out inside is slower, and the proper length to the curvature singularity increases, becoming infinite for $c_1 \geq 3/2$.

3.3.2.3 Charged dust interpretation

We argued at the beginning of this section that the c_2 and c_3 terms in the action do not contribute to the field equations in the case of static, spherical symmetry and static aether, and the c_4 term can be absorbed into a simultaneous shift of c_1 and c_3 . This enabled us to reduce the general case to the one with only c_1 non-zero. One can nevertheless choose to include a c_3 term in the action, and by so doing

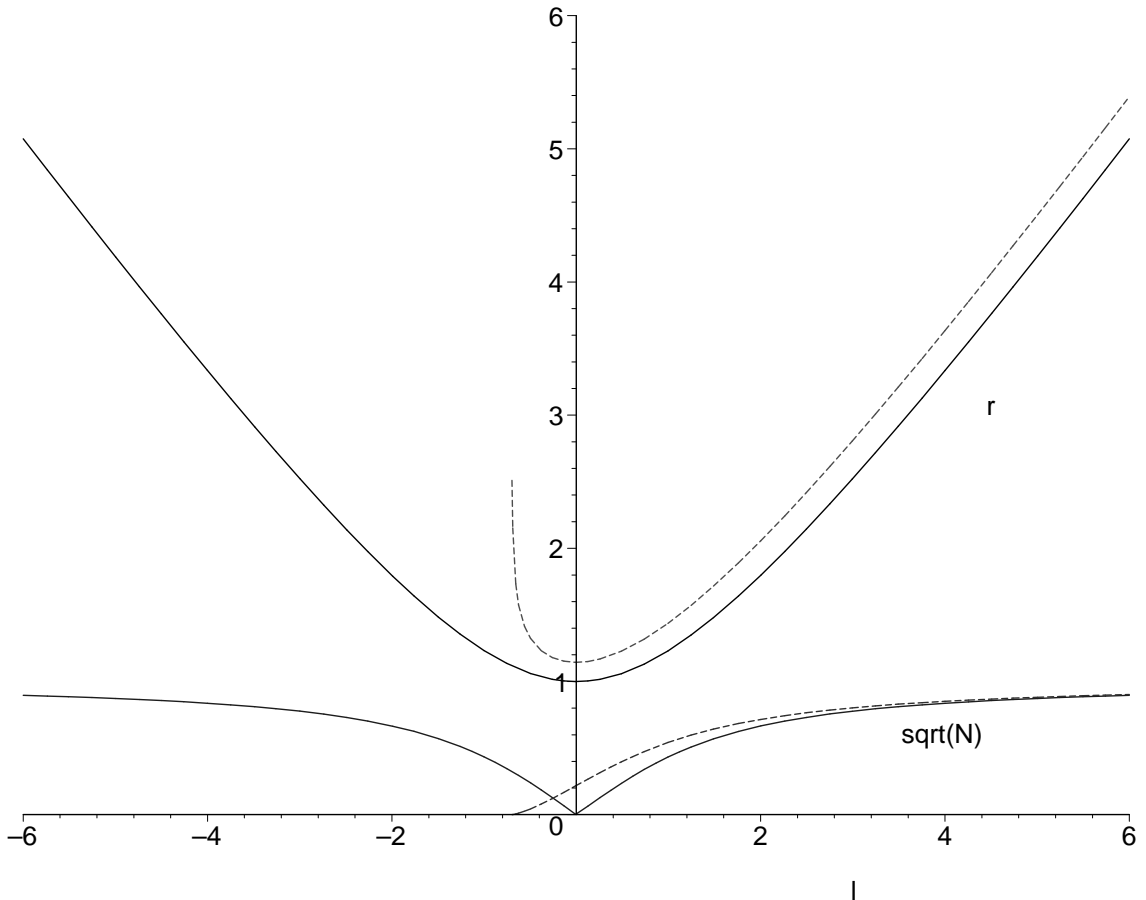


Figure 3.4: Plot of $r(l)$ and the norm of the Killing vector $\sqrt{N_s(l)}$ for GR and for $c_1 = 0.5$, for the solution with the same value of the total mass M , in units with $2M = 1$. In GR N_s vanishes at the bifurcation sphere at the center of the Einstein-Rosen bridge. In the ae-theory solution the Killing vector remains timelike at the throat, but at the internal $r = \infty$ curvature singularity both the norm and its slope vanish, indicating the presence of a singular extremal Killing horizon.

re-express the content of the field equations in an interesting way. In particular, if one choose $c_3 = -c_1$, then the c_1 and c_3 terms combine to make $(c_1/2)F_{ab}F^{ab}$, where $F_{ab} = \nabla_a u_b - \nabla_b u_a$. This is just the Maxwell Lagrangian for a vector potential u_a , up to a constant factor. We have been treating the contravariant vector u^a as the independent field variable, but in this Maxwell-like case it is natural to adopt instead the covariant vector u_a as independent. This change just amounts to an invertible

field redefinition, hence yields the same equations of motion when the metric and aether field equations are taken together. With this choice of field variable the theory with $c_3 = -c_1$ and $c_2 = c_4 = 0$ looks quite similar to Maxwell theory, the only difference being the constraint term $\lambda(g^{ab}u_a u_b - 1)$ in the Lagrangian. It was shown in [25] that this is equivalent to the Einstein-Maxwell-charged dust system, with a constant charge to mass ratio fixed by c_1 , and restricted to the sector in which there exists a gauge choice for which the vector potential is parallel to the dust 4-velocity. (This is a real restriction.)

It must be possible to interpret the strange static aether wormhole solution as a charged dust solution, but it is at first hard to see what could stabilize the dust unless it is extremally charged, which corresponds to the case $c_1 = 2$. In fact it was argued in Ref. [25], invoking prior results [59] for the charged dust problem, that there is no static solution with static aether and general c_1 . However, our result here shows that argument cannot be correct. The contradiction is resolved by the observation that the prior results invoked in Ref. [25] apply only if the dust mass density is positive, whereas in the solution at hand this mass density turns out to be negative. (In Ref. [60] the charged dust system with negative mass density and constant charge to mass ratio was studied (among other cases) in static axisymmetry, and it was shown that every harmonic function determines a solution. Presumably among these solutions is the static aether solution found here.) This is related to the negative energy density that we already inferred above must be present. With a negative mass density, the dust is gravitationally repulsive, and though it has the same sign charge it is electrically attractive. (In Newtonian terms, a force \mathbf{F}

produces an acceleration \mathbf{F}/m which is opposite to \mathbf{F} when m is negative.) Thus the gravitational and electric forces exchange their usual roles. The fact that the dust does not then just collapse on itself is perhaps due to the associated cost in (positive) electric field energy when the dust is squeezed together. Although static, the solution is not regular, since there is an internal singularity.

3.3.2.4 Solutions with $Y \in (Y_-, Y_+)$

So far we have discussed the solution for Y in all ranges except for $Y \in (Y_-, Y_+)$. In this range the metric function B is negative, so ∂_r is timelike. Therefore, in order for the metric signature to be Lorentzian, ∂_t must be spacelike. But in this static solution the aether is parallel to ∂_t (cf. (3.20)), so cannot be timelike. Hence there is no Lorentzian solution with timelike aether corresponding to this range of Y .

As a mathematical curiosity, if we allow $N > 0$, so there are two timelike dimensions, there would still be a further restriction for a real solution, since the ratio in (3.38) is negative and raised to the power $-Y_+/(2 + Y_+)$. In order for N to be real and positive this power must be an even integer m , which implies $\nu = (1/4)(1 - 1/m^2)$. The ratio in (3.39) is also negative, and is raised to the different power $1/(2 + Y_+)$, which can not also be an integer since Y_+ is not an integer. However, the integration constant r_{\min} can be complex, thus balancing the phase of the right hand side of (3.39), and yielding a real solution with signature $(++--)$.

3.4 Nonexistence of pure aether stars

In this section we show that there are no everywhere regular vacuum aether solutions. The reason for investigating this issue is that spherically symmetric self-gravitating “solitons” appear in a number of field systems coupled to gravity. For example there are boson star solutions in the Einstein-Klein-Gordon system [61] and Einstein-Yang-Mills theory possesses the Bartnik-McKinnon solutions [62, 63]. It is therefore natural to ask whether such “aether star” solutions might exist in the vacuum Einstein-Aether theory. The static aether solution studied in the previous section is the unique solution with static aether (remember, this means aether aligned with the timelike Killing vector), and does not have a regular origin. Thus the only way a regular aether star might exist is if the aether has a radial component. We now examine this possibility and show that it cannot occur.

The analysis of Section 3.2.1 showed that local solutions around a general $r = r_0$ are characterized by three free parameters which may be taken to be $A'(r_0)$, $a(r_0)$ and $a'(r_0)$. If we apply this result at the origin $r_0 = 0$ the parameter freedom is restricted. Spherical symmetry implies that at the origin the radial component of the aether vanishes, $b(0) = 0$. The normalization constraint (3.13) therefore fixes $a(0) = e^{-A_0/2}$, and the r -derivative of this constraint implies that $A'(0)$ and $a'(0)$ are not independent, but rather are related by $A'(0) = -2a'(0)/a(0)$. Thus there is a one parameter family of solutions regular at the origin.

These solutions cannot be asymptotically flat, for the following reason. The asymptotically flat boundary condition discussed in Section 3.2.2 would require fixing

the one free parameter, leaving a unique solution. However, pure ae-theory is scale invariant, so there must be at least a one parameter family of solutions much like the Schwarzschild solutions of different mass in GR. (By contrast, Einstein-Yang-Mills theory is *not* scale invariant, and admits a discrete family of soliton and black hole solutions.) We conclude that no regular aether stars exist. This conclusion was verified empirically by integrating out from the origin with different initial parameters, and attempting unsuccessfully to tune to an asymptotically flat solution. While no spherically symmetric vacuum aether stars exist in ae-theory, in the next chapter it is shown there are solutions describing a fluid star. The vacuum exterior of these stars turns out to be the static aether solution described in Section 3.3.

3.5 Discussion

In this chapter we analyzed the Einstein-aether theory assuming stationary spherical symmetry. We determined the number of free parameters in the corresponding solutions to the field equations, and classified the asymptotically flat ones. The vacuum solution with static aether, i.e. aether aligned with the timelike Killing vector, was found analytically up to inversion of a transcendental equation. It has a wormhole-like structure, with a minimal 2-sphere and a singular internal area-infinity which lies at finite affine parameter along a radial null geodesic and finite proper distance if $c_1 < 3/2$. Finally, it was argued that no aether solitons can exist.

A few directions for further work are suggested by these results. One issue is whether the pure static aether wormhole solution is stable. Seifert [64] has made sig-

nificant progress on this problem by employing a “generalized variational principle” [65] for static spherically symmetric spacetimes. He found in the asymptotic region away from the wormhole the local stability conditions for the static aether spacetime are the same as those for linearized stability about flat spacetime (i.e. that the wave modes have real frequencies). In the interior, near the wormhole throat, a definitive determination could not be made. However, direct investigation of the variational principle by numerical techniques indicates the squared frequency remains positive, showing there are apparently no stability problems.

The static solutions studied here also may be of some help on the unresolved question of energy positivity in ae-theory discussed in Chapter 2. It is known for what ranges of the coefficients c_i the energy of linearized solutions is positive, and it is known that for the decoupled Maxwell-like special case ($c_3 = -c_1$, $c_2 = c_4 = 0$) nonsingular negative energy initial data exist. The positive mass static aether solutions on the other hand have positive energy despite having everywhere negative energy density and an interior singularity, as explained in Section 3.3.2.2. It would be interesting to see whether a positive energy result can be established for these solutions.

Chapter 4

Fluid Stars

4.1 Introduction

In this Chapter we investigate non-rotating stellar solutions in ae-theory. Although there are no regular vacuum aether stars, we show globally regular solutions exist in the presence of a static, spherically symmetric perfect fluid with no aether couplings. Characterizing the properties of these solutions is important because, unlike solar system experiments and binary pulsar observations, robust tests of theoretical predictions for systems where gravitational fields are strong are not currently available. For astrophysical stars under strong gravity this is largely because their properties involve other uncertain physics, particularly knowledge of the stellar equations of state for highly dense matter. However, more robust tests may be available in the future. Larger-area X-ray detectors such as *Constellation-X* [66] may allow for more precise measurements of absorption spectra and the shapes of X-ray burst oscillations. This could allow mass versus radius relations to be mapped out, constraining both the equation of state models [67] and the particular gravitational theory.

It is therefore desirable for current and future data to have theoretically motivated alternatives to or generalizations of GR in strong gravity. Past work has examined scalar-tensor theories, which are the simplest alternatives to GR. In the

case of the well-known Jordan-Brans-Dicke theory it has been shown [68] that the predictions of the theory in both the weak and strong field regimes deviate from GR by a parameter that is tightly constrained by post-Newtonian Solar System experiments. Thus, the properties of compact objects such as neutron stars in Brans-Dicke theories that pass these weak field tests must be very close to those found in GR. However, Damour and Esposito-Farese [69] found a wide class of other scalar-tensor theories exhibiting “spontaneous scalarization,” where weak field constraints are met, but the properties of compact objects have significant deviations from GR in the strong field regime. Recently, [70] studied the properties of non-rotating neutron stars in these theories, finding larger stellar masses than in GR and larger surface redshifts for a given equation of state. These results were then used to put an observational constraint on one of the parameters of the model.

The main objective of this chapter is to study the same set of properties in ae-theory and, if possible, to use these results to obtain new constraints on the theory. The stellar solutions depend on the c_{14} combination of the theory’s coupling parameters. We consider the simple model of a constant density star and then six candidate neutron star equations of state, three with purely nucleonic degrees of freedom and different hardness, and three involving quark matter with different bag constants. By numerical solution of the field equations interior to the star we obtain the maximum mass, relation between mass and radius, and (for the neutron star models) surface redshifts, all as a function of the coupling parameter.

In all equation of state models it turns out that the maximum neutron star mass is less than in the case of GR, and is smaller for larger values of c_{14} . Thus, if

the equation of state is known well enough, it is possible to place an upper bound on the coupling parameter by observations of neutron star masses. Nonstandard relations between mass and surface redshift also occur, providing another possibility for interesting phenomenology and constraining the coupling parameter. We also examine the location of the innermost stable circular orbit (ISCO) as a function of mass, to determine whether that might provide further useful observables distinguishing GR and ae-theory. We find however that the ISCO is nearly unchanged for reasonable coupling parameters.

In Section 4.2 we consider some basic properties of the stellar solutions. It is shown that in the presence of a perfect fluid, regular asymptotically flat star solutions exist and are parameterized (for a given equation of state) by the central pressure. The equations of structure are also presented. Next in Section 4.3 for the case of constant density the star solutions are found by matching numerical integration for the interior to the vacuum solution discussed previously in Section 3.3. As in GR, for a given density there is a maximum mass. Utilizing the critical behavior of the mass as a function of stellar radius R it is shown that if they are stable at small mass, these stars are unstable beyond the maximum mass.

In Section 4.4 we turn to the six neutron star equation of state models. Using the exterior static solution, expressions are obtained for the surface redshift and ISCO radius that can be employed with the numerical solutions to obtain the observable quantities. The numerical results for maximum masses and redshifts are presented together with the possible constraints on the coupling parameter that can be obtained with these results. We conclude with a brief discussion of prospects for

further constraints from more precise neutron star measurements.

4.2 Basic Properties of Stellar Solutions

A matter lagrangian L_{matter} coupled to the vacuum Einstein-aether Lagrangian (3.1)

$$\begin{aligned}
 L = & -R - c_1(\nabla_a u_b)(\nabla^a u^b) - c_2(\nabla_a u^a)^2 - c_3(\nabla_a u_b)(\nabla^b u^a) \\
 & - c_4(u^c \nabla_c u^a)(u^d \nabla_d u_a) - \lambda(g_{ab} u^a u^b - 1)
 \end{aligned} \tag{4.1}$$

generically will be a functional of a collection of matter fields (denoted as ψ) along with g_{ab} and u^a . However, following the observational constraints, we assume here when studying the neutron star solutions that the only significant coupling of u^a to matter is through a universal ‘‘matter metric’’ $g_{ab}^{\text{matter}} = g_{ab} + \sigma u_a u_b$, where σ is a constant. Replacing g_{ab} by g_{ab}^{matter} as the independent metric field in the action returns an action with the same form as (4.1) but with new values of the constants $c_{1,2,3,4}$ that depend on σ [71]. Hereafter we assume that such a field redefinition has already been performed, so that g_{ab} is the metric to which matter couples universally, so that $L_{\text{matter}}(g_{ab}, \psi)$. The absence of any other coupling of u^a to matter has no theoretical justification in this purely phenomenological approach, and may be regarded as unnatural. However our goal here is just to explore consequences of gravitational Lorentz violation in a phenomenologically viable setting. It remains an open question whether this can emerge as an approximation to a more fundamental underlying theory.

Working in Schwarzschild coordinates

$$ds^2 = e^{A(r)} dt^2 - B(r) dr^2 - r^2 d\Omega^2 \quad (4.2)$$

$$u^a = a(r) \partial_t + b(r) \partial_r, \quad (4.3)$$

the fluid stress tensor appearing in the metric field equation (3.5) is

$$T_{ab}^M = (\rho(r) + P(r)) v_a v_b - P(r) g_{ab} \quad (4.4)$$

where $v^a = e^{-A/2} (\partial_t)^a$ is the fluid 4-velocity, $\rho(r)$ its mass density, and $P(r)$ its pressure. The metric field equation and the Bianchi identity together imply that the sum of the aether and fluid energy-momentum tensors is divergenceless. In addition, since the aether does not couple directly to the fluid, its stress tensor is independently divergenceless when its field equation and unit constraint are satisfied. Therefore the fluid stress tensor is also independently divergenceless in any solution. Thus, an appropriate system of equations for the aether plus fluid case is the (i) metric field equation, (ii) aether field equation, (iii) radial component of $\nabla^a T_{ab}^M = 0$, which is the hydrostatic equilibrium equation for the fluid

$$P' + \frac{1}{2} A' (\rho + P) = 0, \quad (4.5)$$

and (iv) an equation of state $\rho = \rho(P)$.

The count of parameters that can be freely specified when integrating out from a regular origin is the same as for the vacuum aether solution of Section 3.4, except for the addition of a central value for the pressure $P_0 = P(0)$. For a fixed central pressure, there is just one parameter which can be tuned to obtain an asymptotically flat solution. Now there is no contradiction with scale invariance, since the central

pressure sets the scale and determines the total mass of the solution. That these asymptotically flat star solutions have a static aether can be inferred as follows. The field equations can be integrated out from the origin with the aether assumed static. The pressure drops to zero at some value $r = R$, the surface of the star, where the static interior solution can be matched to the static vacuum aether solution discussed in Section 3.3. This solution is asymptotically flat, so it must be the unique asymptotically flat solution whose existence is indicated by the parameter count. Thus, everywhere the aether takes the form

$$u^a = e^{-A(r)/2} \partial_t. \quad (4.6)$$

consistent with the unit constraint.

The aether here is at rest with respect to the static frame at infinity, which means that the star is taken to be at rest with respect to the aether. When comparing theory and observation, it is typically assumed that the background aether frame coincides with that of the cosmological fluid. Any particular star will of course have some proper motion with respect to this frame, so strictly speaking the physically relevant solutions are not of the form (4.2, 4.6). However, assuming a relative velocity of order 10^{-3} , this discrepancy should not be significant for comparisons of much less precision such as concern us here.

A similar worry is whether it is appropriate to focus on non-rotating stars, since neutron stars have been observed to be rotating. It turns out this restriction is adequate since the effect of rotation on the maximum mass, surface redshift, and ISCO is very small for the observationally relevant spins. For example, presuming

the fractional change in maximum mass scales with the square of the spin, Tables 4 and 5 in Ref. [72] indicate that even for a one millisecond period the increase of maximum mass is less than 5% in GR. Barring an unexpected much greater sensitivity to a small spin in ae-theory, the results we find here for non-rotating stars should be quite reliable except for the fastest spinning stars.

4.2.1 Stellar Equations of Structure

It was shown in Section 3.2 that for configurations of the form (4.2, 4.6) the c_2 and c_3 terms in the action (4.1) and their variations are zero, and thus they do not contribute to the field equations. Also, the effect of the c_4 term can be absorbed by the replacement $c_1 \rightarrow c_1 + c_4$. Hence the only coupling relevant to these solutions is $c_{14} \equiv c_1 + c_4$.

It turns out that the aether field equation (3.6) has only a t component, which just determines the Lagrange multiplier λ . The tt , rr , and $\theta\theta$ metric field equations are

$$0 = -1 + B + r \frac{B'}{B} - \nu(8rA' + r^2A'^2 - 2r^2A' \frac{B'}{B} + 4r^2A'') - \rho r^2 B \quad (4.7)$$

$$0 = 1 - B + rA' + \nu r^2 A'^2 - Pr^2 B \quad (4.8)$$

$$0 = \frac{1}{4}(2rA' - 2r \frac{B'}{B} + r^2A'^2 - r^2A' \frac{B'}{B} + 2r^2A'') - \nu r^2 A'^2 - PB, \quad (4.9)$$

where the symbol

$$\nu = \frac{c_{14}}{8} \quad (4.10)$$

is introduced to compactify the notation, and we have adopted units with $8\pi G = 1$.

Equation (4.8) can be used to solve for B ,

$$B = (1 + r^2 P)^{-1} (1 + r A' + \nu r^2 A'^2). \quad (4.11)$$

After substituting this result into (4.7) and (4.9), A'' can be eliminated from this pair of equations, yielding an equation involving A , A' , P , P' , and $\rho(P)$. Due to its complexity it does not seem illuminating to display it here. This equation combined with (4.5) can then be numerically integrated to solve for $P(r)$ and $A(r)$ starting with initial values at the origin $r = 0$. (It is possible to eliminate A' , leaving one Tolman-Oppenheimer-Volkoff (TOV) type equation for $P(r)$. Since this TOV equation is quite complicated and doesn't aid the numerical integration procedure we will not display it here.)

To numerically integrate outward we find the power series solution to the equations (4.5) and (4.7,4.8,4.9) in the vicinity of $r = 0$, which is a singular point for the equations. In this solution the central value for the pressure $P(0) = P_0$ is the only free parameter to be specified ($A(0)$ is arbitrary due to scaling freedom of the t coordinate, so can just be set to unity). The numerical integration can then be started at a small value of r using the power series for initial data, and continued to the value $r = R$, which is the surface of the star where the pressure and mass density drop to zero. There $A'(r)$ is continuous so one can use it to match to the vacuum solution discussed in Section 3.3.2. The total mass M can be read off from (3.46)

$$r_{\min}/r_g = (-Y_+)^{-1} (-1 - Y_+)^{(1+Y_+) / (2+Y_+)}, \quad (4.12)$$

where $r_g = 2G_N M$, together with (3.39)

$$\frac{r_{\min}}{r} = \left(\frac{Y}{Y - Y_-} \right) \left(\frac{Y - Y_-}{Y - Y_+} \right)^{\frac{1}{2+Y_+}}, \quad (4.13)$$

using the definition $Y(R) = RA'(R)$. The area of the 2-spheres in such a star solution is strictly increasing as r increases from zero to the surface of the star where P vanishes. At that point $P' \leq 0$, so according to (4.5) $A' \geq 0$ (assuming positive fluid energy density ρ). Thus (3.31) implies $Y \geq 0$, which means that we always match to the static aether solution *outside* of the minimal area 2-sphere. A “throat” never occurs in such a star solution. In the subsections below we use the static aether vacuum solution to obtain useful formulas for the surface redshift and innermost stable circular orbit (ISCO).

4.2.1.1 Surface redshift

The light emitted from the surface of a star is redshifted as it climbs away to a distant observer. From (4.2), the surface redshift factor z is given by

$$z = [N_s(R)]^{-1/2} - 1, \quad (4.14)$$

which can be evaluated directly from the numerical solution using (3.38)

$$N_s = e^A = \left(\frac{1 - Y/Y_-}{1 - Y/Y_+} \right)^{\frac{-Y_+}{2+Y_+}}, \quad (4.15)$$

and (3.31).

4.2.1.2 ISCO

The orbits in the metric (4.2) have conserved energy $e = N_s \dot{t}$ and angular momentum $\ell = r^2 \dot{\phi}$, where $N_s = e^A$ and the overdot stands for derivative with respect to proper time. Since the parameter is proper time, the four-velocity has unit norm. This condition can be expressed in the form

$$\dot{r}^2 = V(r) = B^{-1}W, \quad (4.16)$$

with

$$W = W(r; e, \ell) = N_s^{-1}(r)e^2 - r^{-2}\ell^2 + 1. \quad (4.17)$$

The ISCO is determined by the conditions $V = V' = V'' = 0$, or equivalently, $W = W' = W'' = 0$, where the prime stands for derivative with respect to r . Thus the metric function B plays no role. These equations determine r , e and ℓ at the ISCO. After some manipulation of the equations we obtain

$$Y_{\text{ISCO}} = \frac{-1 + \sqrt{1 + \nu}}{\nu} \quad (4.18)$$

With this result, the radius of the ISCO can be found from (3.39) and (3.46) given the mass. Expanding in $\nu = c_{14}/8$ one finds (in units with $G_N M = 1$)

$$r_{\text{ISCO}} \simeq 6(1 + [\ln(3/2) - 1/6]\nu) \simeq 6(1 + 0.24\nu), \quad (4.19)$$

dropping $O(\nu^2)$ terms. This linear approximation is extremely accurate: the relative error grows monotonically from 0 to only about 0.3% over the entire allowed range of c_{14} from 0 to 2.

The angular frequency of an orbit with respect to time at infinity is given by $\omega = \dot{\phi}/\dot{t} = (\ell/e)(N/r^2)$. The circular orbit condition yields $N\ell/e = (N'r^3/2)^{1/2} =$

$r(YN/2)^{1/2}$, so $\omega = r^{-1}(YN/2)^{1/2}$. Expanding again in ν , the frequency at the ISCO is found (in units with $G_N M = 1$) to be

$$\omega_{\text{ISCO}} \simeq \frac{1}{6\sqrt{6}}(1 + [-2\ln(3/2) + 1/2]\nu) \simeq \frac{1}{6\sqrt{6}}(1 - 0.31\nu), \quad (4.20)$$

dropping $O(\nu^2)$ terms.

Thus, even for the maximum value $c_{14} = 2$ (as discussed in Chapter 1 any higher would give a negative G_N), the location of the ISCO is only about 6% larger than its value in GR for a star of the same mass, and the orbital frequency is about 8% smaller. Since ae-theory agrees so closely with GR on these quantities, it is unlikely that in the near future any useful constraints can be obtained from their behavior.

4.3 Constant Density stars

To get a sense of the nature of the static aether star solutions we consider here the simplest example, stars with constant energy density interior. Although this does not closely describe realistic stars, it turns out to be adequate for indicating the general behavior of maximum mass limits and the stability properties of equilibrium configurations. The discontinuity in the mass density at the surface entails via the field equations a jump in A'' , but A' remains continuous so can be used to match to the vacuum solution as described above.

Graphs of total mass M versus the central pressure P_0 for the equilibrium configurations are displayed in Figure 4.1.

In GR the mass tends asymptotically to a maximum value as the central

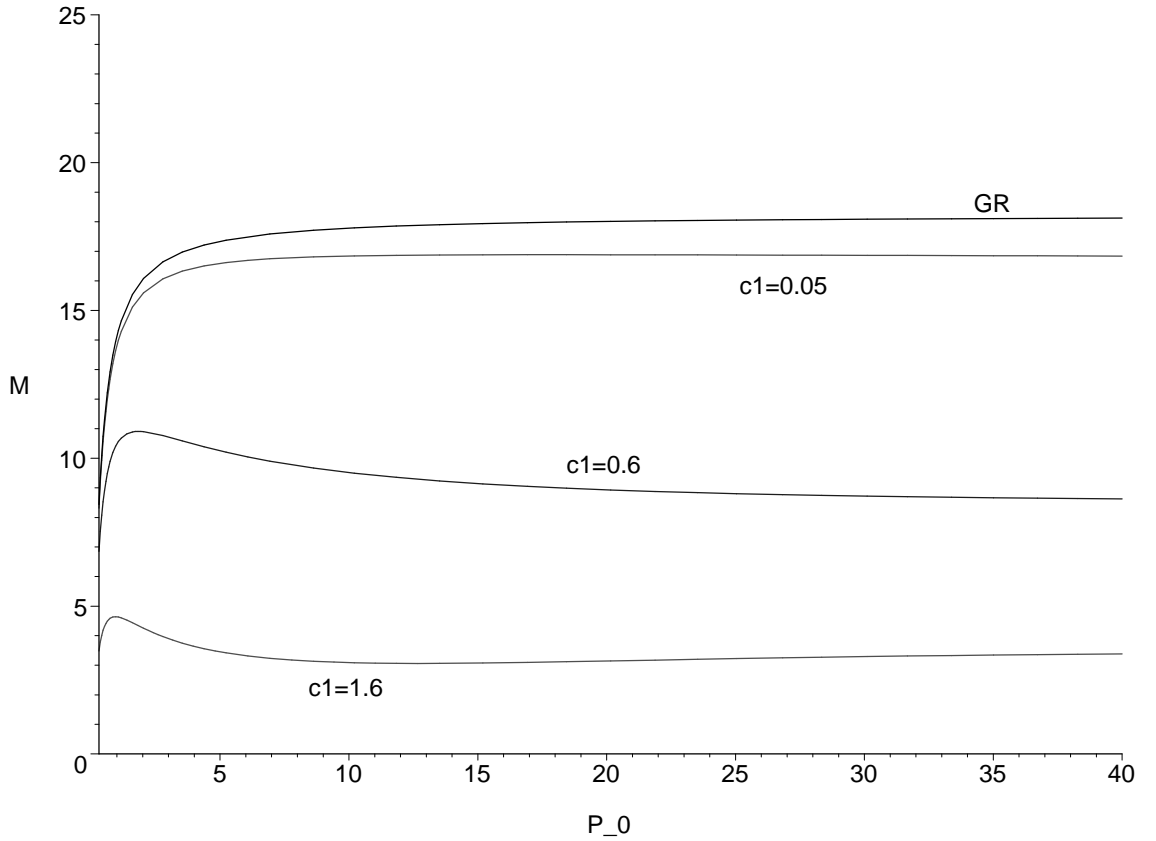


Figure 4.1: Total mass vs. central pressure P_0 in a constant density star, in units with $\rho = 1$ and $8\pi G = 1$, for several values of $c_{14} \equiv c_1$. The GR curve asymptotically approaches $M = (4\pi/3)(24/9)^{3/2}$. As c_{14} grows the maximum mass decreases, and the curve develops a sharp local maximum and a shallow local minimum.

pressure goes to infinity. Physically, an infinite central pressure would be required to maintain equilibrium for a greater mass. As c_{14} increases in the Einstein-aether case the maximum mass limit decreases, and the mass curve develops a local maximum and a very shallow local minimum that is only apparent for larger values of c_{14} . For sufficiently large c_{14} a second local maximum occurs. (We have not attempted to determine the behavior at arbitrarily high pressures and for c_{14} approaching 2. Perhaps the series of maxima and minima continues.)

The presence of stationary points in the mass versus pressure curves is an

indication that the stability character of the equilibrium may be changing [73]. The connection with linearized stability arises as follows. If the squared frequency of a mode is positive then the corresponding perturbation of the star is oscillatory, while if it is negative the perturbation grows exponentially in time. In the borderline case of zero frequency the mode has zero energy, hence corresponds to a variation between two static solutions with the same mass. Transitions between stability and instability therefore occur at extrema of the mass versus R plot shown in Figure 4.5, where a small displacement of R does not change the mass to first order.

In the GR limit there is no critical point. The mass increases monotonically with central pressure, as seen in Fig. 4.1, so there is no onset of instability. In aether theory even flat space is not necessarily stable. The conditions on the c_i for which all linearized plane wave modes have positive squared frequency were found in [41]. For example in the pure c_1 case they are $-2 < c_1 < 1$. If we assume the values of c_i are such that very small mass stars are stable, then instability can only set in at a critical point of the mass function. As c_1 grows larger, the curves in Fig. 4.5 exhibit extremal points corresponding to the local maxima and minima of Fig. 4.1. At the maximum mass the lowest mode becomes unstable. At the following local minimum another zero frequency mode occurs, corresponding to the next mode becoming unstable. (It cannot be the lowest mode becoming stable again, since R is increasing with increasing central pressure, implying the presence of a node in the corresponding radial mode [73].) Therefore, beyond the maxima shown in Figure 4.5 constant mass density stars in the Einstein-aether theory are unstable. For small values of c_{14} the central pressure has to be very large compared to the density for the

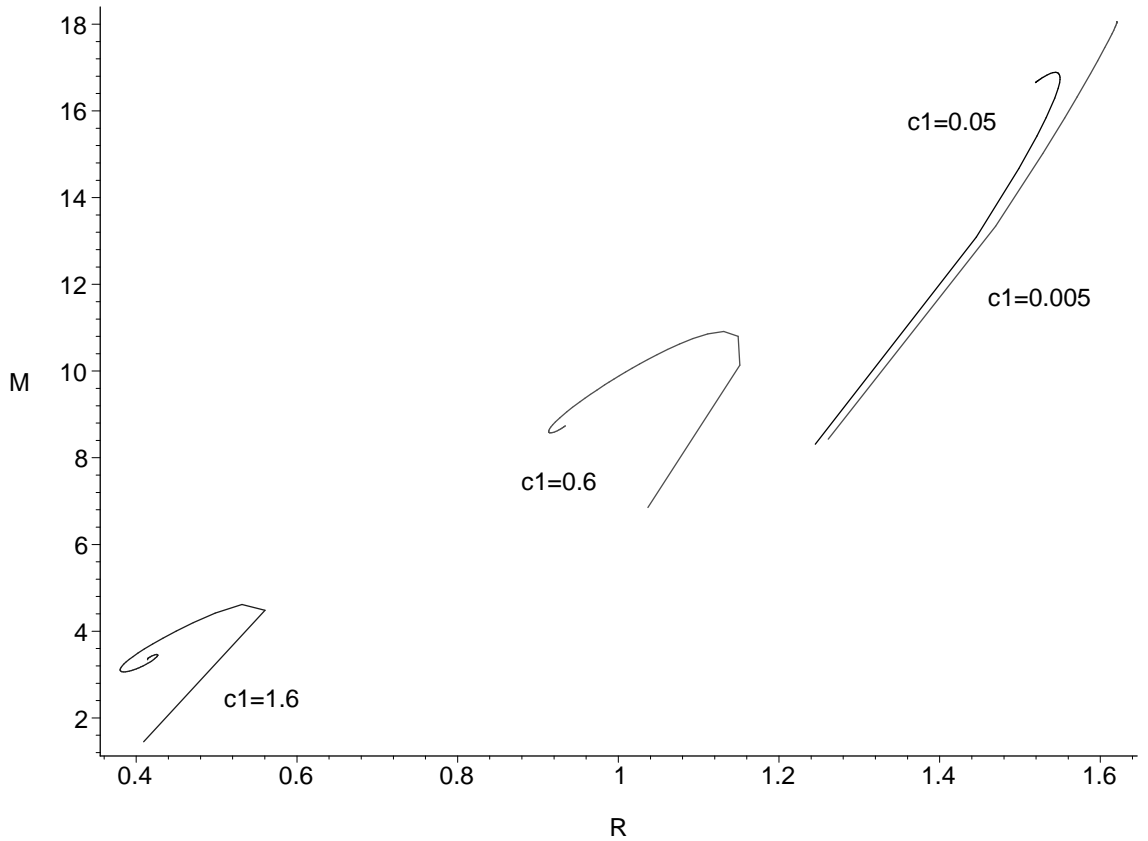


Figure 4.2: Total mass vs. R for a constant density star, in units with $\rho = 1$ and $8\pi G = 1$, for P_0 up to 300 and several values of $c_{14} \equiv c_1$. For small pressures all the curves increase uniformly. For $c_{14} = 0.005$ the slope is nearly the same as in GR. For $c_{14} = 0.05$ a maximum occurs for a large central pressure. By $c_{14} = 0.6$, the first maximum occurs at much smaller pressures, and there is also a minimum. For $c_{14} = 1.6$ a second maximum has appeared.

star to reach the instability, implying a violation of the dominant energy condition.

For $c_{14} = 1$ the pressure at the onset of instability is about 1.28 times the density.

4.4 Neutron Stars

We now turn to realistic models of non-rotating neutron stars. The ultimate goal is to compare the properties of these models to stars in GR and ultimately astrophysical observations with the goal of constraining the theory. Therefore here

we will briefly review the known constraints on ae-theory and discuss the possible effect of additional constraints coming from neutron star observations.

As we discussed in Section 1.3, all PPN parameters except the preferred frame parameters $\alpha_{1,2}$ agree with those of GR for any choice of the c_i . Observations impose strong constraints on α_1 (less than 10^{-4}) and α_2 (less than 4×10^{-7}). These parameters can be set to zero in Einstein-aether theory by imposing two conditions, on the c_i , which can be solved to determine [38]

$$\begin{aligned} c_2 &= (-2c_1^2 - c_1c_3 + c_3^2)/3c_1 \\ c_4 &= -c_3^2/c_1. \end{aligned} \tag{4.21}$$

The stability, positive energy, and vacuum Čerenkov constraints then impose the inequalities (1.4) [38]

$$\begin{aligned} 0 &< c_+ < 1 \\ 0 &< c_- < c_+/3(1 - c_+), \end{aligned} \tag{4.22}$$

where $c_{\pm} = c_1 \pm c_3$.

We also noted in Section 1.3 that further constraints have been obtained using radiation damping in binary pulsar systems [43]. An analysis neglecting strong self-gravitating effects found that when (4.21) hold, just one condition $\mathcal{A}(c_1, c_3) = 1$ makes the lowest order radiation rate in ae-theory identical to that of GR. This condition is satisfied entirely in the region allowed by (4.22).¹ However, the neutron star sources are strongly self-gravitating. It turns out [44] that as long as c_i is less

¹In [43], the $\mathcal{A} = 1$ curve does not fall entirely in the otherwise allowed region, but this is due to an error in the analysis there that has since been corrected [44].

than roughly 0.1, the strong field corrections are negligible, but for larger coupling values the precise radiation damping constraints are not yet worked out. They will lead to a modified condition $\mathcal{A}'(c_1, c_3) = 1$ that will depend on the nature of the compact objects in the binary.

Non-rotating neutron star structure constraints along the lines discussed in the present paper should eventually be able to restrict c_{14} , which is given by

$$c_{14} = 2c_+c_-/(c_+ + c_-) \quad (4.23)$$

when the PPN equivalence conditions (4.21) hold. The only previous constraint on c_{14} was the requirement that it be less than 2 in order to maintain positivity of Newton's constant. Fig. 4.3 shows the region in the (c_+, c_-) parameter space allowed by the above constraints (other than the radiation damping constraint), along with c_{14} contours. Note that without a constraint on c_{14} , c_- can grow arbitrarily large as $c_+ \rightarrow 1$. Any upper bound on c_{14} will cut off this region however. A c_{14} contour intersects the right hand boundary ($c_+ = 1$) of the allowed region at $c_- = c_{14}/(2 - c_{14})$, and intersects the upper boundary at $c_- = (4/3)c_{14}/(2 - c_{14})$.

4.4.1 Numerical Results

Here we will compare the properties of neutron stars in GR and ae-theory using three hadronic and three quark equations of state (EOS). We label these according to whether they are softer (s), medium (m), or harder (h), by

$$\text{Hs, Hm, Hh} \leftrightarrow \text{A18, A18}\delta v\text{UIX, A18UIX} \quad (4.24)$$

$$\text{Qs, Qm, Qh} \leftrightarrow (90, 0), (60, 200), (60, 0). \quad (4.25)$$

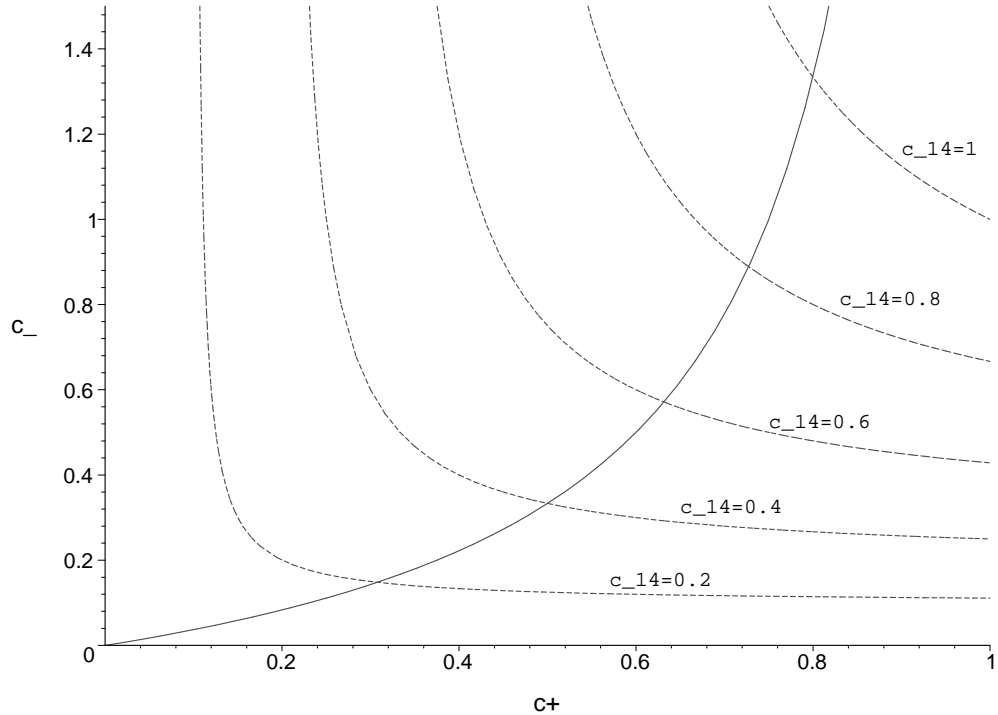


Figure 4.3: Graphical representation of (4.22) (solid line) and (4.23) (dashed lines). The allowed region of the parameter space is below the solid curve, above $c_- = 0$ and to the left of $c_+ = 1$. The radiation damping constraint will restrict to a nearly one-dimensional subset of this region.

The hadronic models are discussed in [74], and the quark models are MIT bag models [75] determined by two parameters (B, m_s), with the bag constant B measured in MeV/fm^3 and the strange quark mass m_s in MeV .

We converted the pressure and mass density data tables for these models [76] from cgs units to geometrized units, i.e. replacing the energy density ρ and pressure p by $G_N \rho / c^4$ and $G_N p / c^4$ respectively, yielding quantities with dimension inverse length squared. We then used a curve fitting procedure to generate an equation of state function $\rho(P)$ suitable for the numerical integration. The field equations (4.7-4.9) are written in units with $8\pi G = c = 1$, so to apply them we first multiply the density and pressure in the above geometrized units by $8\pi G / G_N = 8\pi(1 - c_{14}/2)$.

In GR five of the six equations of state have associated M versus P_0 curves containing a maximum mass extremum and regions of stability and instability. The exception is the softest quark EOS, Q_s , which appears to asymptote to its maximum mass value. The GR maximum mass values for the Hm and Hs equations of state we find here ($2.20M_\odot$ and $1.67M_\odot$ respectively) agree very well with the results obtained in [74]. An example is shown in Fig. 4.4 for the Hm equation of state.

As in the constant mass density case, Fig. 4.4 shows the maximum mass value

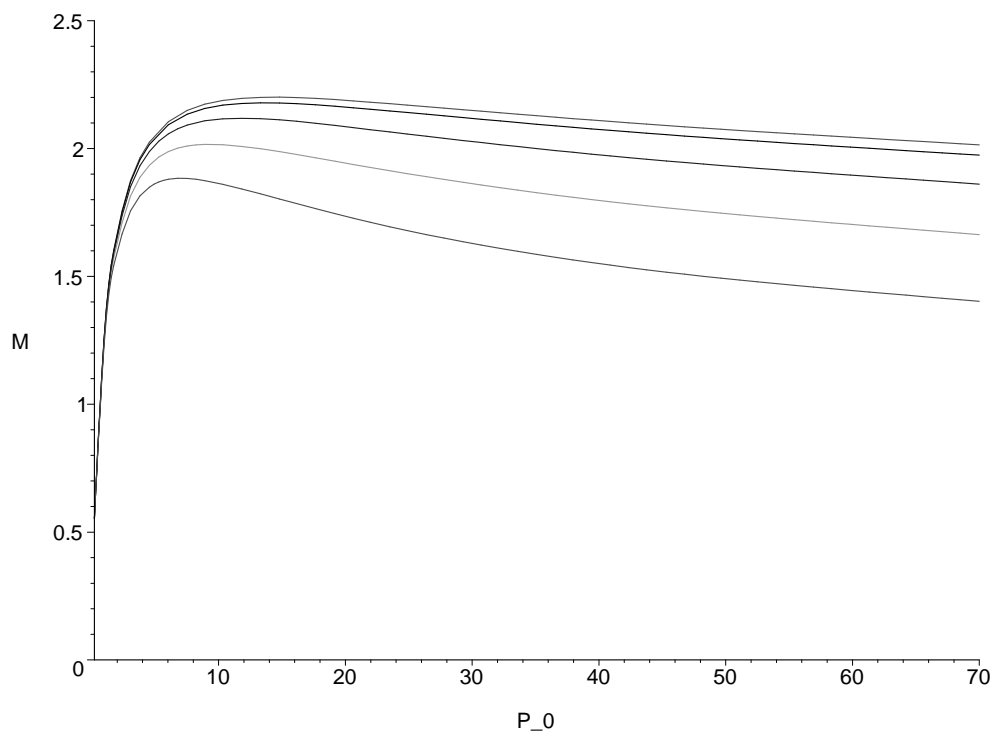


Figure 4.4: Total mass vs. central pressure P_0 for the Hm equation of state for c_{14} values 0, 0.05, 0.2, 0.5, and 1. The vertical axis is in units of solar masses and horizontal in $1/(100\text{km})^2$. As c_{14} grows from 0.05 to 1 the maximum mass decreases from near the GR value of 2.20 to less than 1.9.

in ae-theory grows smaller and occurs at smaller values of central pressure as c_{14} is increased. For the Q_s EOS extrema begin to develop in the curve as c_{14} approaches 1. Fig. 4.5 is a plot of M vs. R , each point being determined by a value of P_0 ,

for several values of c_{14} .

As P_0 increases the mass values increase sharply to

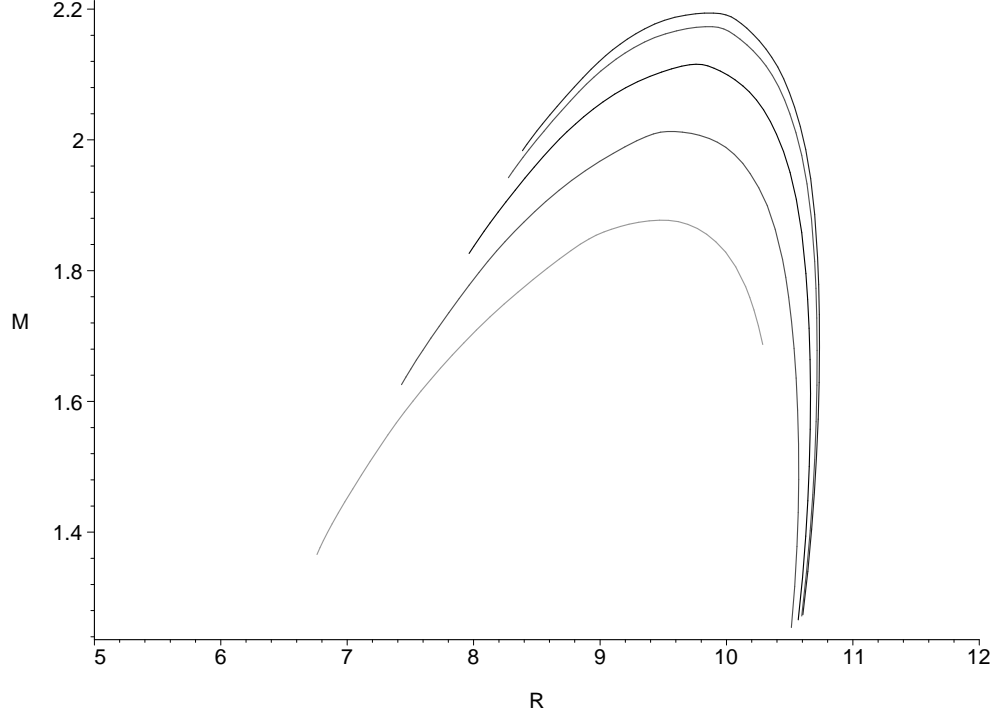


Figure 4.5: Total mass versus R for the Hm equation of state for P_0 up to 100 and c_{14} values 0, 0.05, 0.2, 0.5, and 1. The vertical axis is units of solar masses and the horizontal in km. The GR curve reaches its maximum mass of 2.20 solar masses at slightly more than 10 km. For $c_{14} = 0.05$ the curve is slightly inside GR curve. As c_{14} increases to 1 the maximum masses decrease and the value of the radius at these maxima falls to about 9.5 km.

peaks and then gradually fall off. The region of the curves for small P_0 and larger R up to the mass maximum describe stable equilibrium configurations. Beyond the maximum the neutron stars are unstable. In ae-theory the minimum radius where the equilibrium configuration is stable decreases as c_{14} increases.

A plot of the maximum mass values for the six equations of state considered in this paper is shown in Fig.4.6. Horizontal lines mark the certain lower bound of $1.44 M_{\odot}$ and a benchmark value of $2.0 M_{\odot}$. The dependence of the maximum mass on c_{14} is very close to linear for the quark models, with the mass changing by

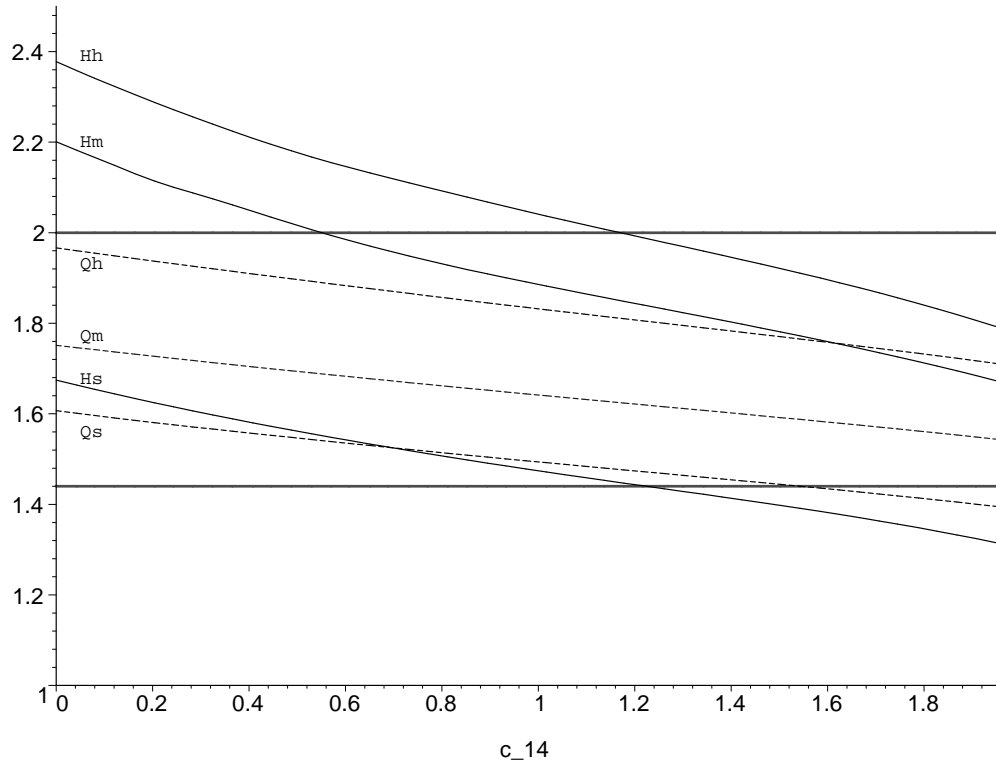


Figure 4.6: Maximum mass vs. c_{14} for the six equations of state. The hadronic models are plotted with solid lines, while the quark models are dashed. The thick solid horizontal lines represent the bare minimum constraint of $1.44 M_{\odot}$ and a possible constraint value of $2 M_{\odot}$.

roughly 6% as c_{14} increases from 0 to 1. For the hadronic models it is roughly linear but steeper, decreasing by roughly 15% over the same range of c_{14} .

4.4.2 Maximum mass constraints

The most straightforward constraint on ae-theory comes from comparing the maximum mass values generated with the six equations of state to observations of neutron star masses in binary pulsars. These masses are not directly measured, but inferred from the timing data from a binary pulsar system. This data contains information on the Keplerian and post-Keplerian parameters of the system, which

depend on the unknown masses m_A and m_B of the neutron stars. A determination of the Keplerian and two post-Keplerian parameters, such as the secular rate of periastron advance and the magnitude of the Shapiro delay, result in two curves in a (m_A, m_B) mass plane. The value of the two masses is the intersection of these curves. Since we are considering the subset of Einstein-aether theories that satisfies the post-Newtonian constraints, any corrections to how the post-Keplerian parameters depend on the pulsar masses would only appear at higher order and therefore should be very small. Thus, the masses can be inferred as in GR to a good approximation. If the maximum mass predicted by Einstein-aether theory is smaller than an observed neutron star mass then the theory is ruled out. Currently the largest reliable observed mass value is $1.44 M_\odot$ from the PSR 1913+16 Hulse-Taylor binary system.

There are, however, suggestions from various data that neutron star masses can be at least $\sim 2 M_\odot$. The neutron star in Vela X-1 has an estimated mass of $1.88 \pm 0.13 M_\odot$ [77], and PSR J0751, a pulsar in a detached low-mass binary, has a reported mass of $2.1 \pm 0.2 M_\odot$ [78]. Furthermore, there are indications (although not as definitive) for neutron star masses greater than or of order two solar masses in several low-mass X-ray binaries based on the inference of the orbital frequency at the ISCO from their kilohertz quasi-periodic brightness oscillations (QPO's)[79, 80, 81, 82]; for an alternative view, see [83]. At the < 700 Hz spin frequencies of these stars, the dimensionless angular momentum is only 0.1 to 0.3 [72], so this would imply that the ISCO is obtained from a near-Schwarzschild spacetime. Since the ISCO we find in Section 4.2.1.2 is very close to the GR value, the derived mass should be the same

in ae-theory as in GR to a good approximation. As a benchmark, we will consider the limits on c_{14} that would result from a measured gravitational mass of $2 M_{\odot}$.

Fig.4.6 shows that in GR ($c_{14} = 0$) all six equations of state respect the lower bound of $1.44 M_{\odot}$ solar masses. For four of the equation of state models the $1.44 M_{\odot}$ mass cutoff does not yield any constraint on c_{14} . For the Hs and Qs EOS there are weak constraints that c_{14} be less than about 1.2 and 1.5 respectively. The $2 M_{\odot}$ constraint is more restrictive. In this case the Hs, Qh, Qs, and Qm EOS are ruled out, while for Hm and Hh c_{14} must be less than about 0.56 and 1.16 respectively.

As the maximum observed neutron star mass is pushed upwards, and more is learned about the nuclear EOS, the observational upper bound on c_{14} will come down. If we assume the existence of a non-rotating neutron star of $2 M_{\odot}$, then even for the hardest equation of state we have considered we obtain the bound $c_{14} < 1.16$.

4.4.3 Surface redshift constraints

There is not yet a definitive detection of an atomic spectral line from the surface of a neutron star. The strongest current case comes from stacked observations of thermonuclear X-ray bursts from EXO 0748–676, from which [84] inferred a surface redshift of 0.35 based on identification of some absorption-like features as being produced by highly ionized iron. The mass of this star is not certain, but Özel [85] used simplifying assumptions about the constancy of the peak flux of the bursts and radiative transfer to infer that the mass of this object is probably not less than $1.8 M_{\odot}$.

Measurements such as these, once confirmed, can provide a joint constraint on c_{14} and the equation of state via the dependence of surface redshift on mass in ae-theory. Note however that the lower bound value of $1.8 M_{\odot}$ is gravity theory dependent [86] and will be modified in ae-theory. We have checked that the mass inferred using the method of Ref. [85] differs from the GR value by less than 2% when $c_{14} = 1$, so the leading order effect of c_{14} is only in the relation between radius and mass, or equivalently redshift and mass. Fig. 4.7 shows a plot of z versus c_{14} for 1.8 solar mass stars using the Hm, Hh, and Qh EOS. These are the three hardest equation of state models and have equilibrium configurations at this mass. (As shown in Fig. 4.6, the other three softest equation of state models do not have equilibrium configurations at this mass.) The surface redshifts increase by roughly 10% as c_{14} ranges from 0 to 1.

If in the future surface redshifts together with masses can reliably be determined, then tight constraints on the equation of state in GR may be obtained by combining measurements for a collection of stars. It is also possible that single measurements may provide stringent constraints. For example, as revealed in Fig. 4.7, the proposed surface redshift 0.35 of EXO 0748–676[84] is compatible with 1.8 solar masses only for the hardest EOS (Hh) among those we considered. In general, the parameter c_{14} could not be constrained without separate knowledge of the equation of state. However, in the example just mentioned one could serendipitously tightly constrain both the equation of state and the value of c_{14} , since a redshift of 0.35 is the lower limit of all the curves at this mass.

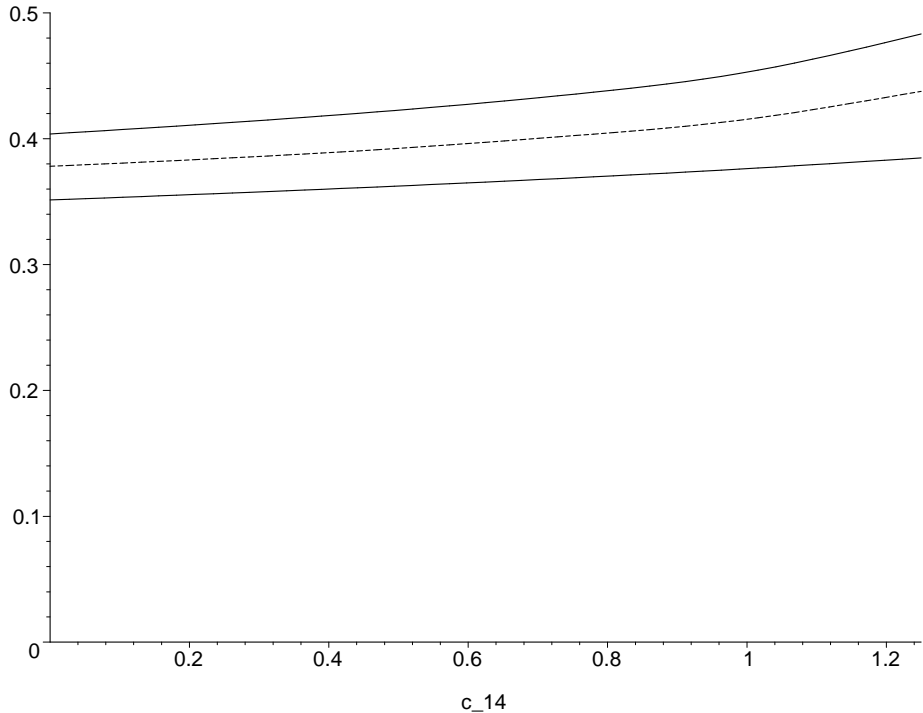


Figure 4.7: Redshift factor z versus c_{14} for 1.8 solar mass neutron stars using the hardest equations of state. Hm (solid) is on top, Qh (dashed) is in the middle and Hh (solid) is on the bottom. Note that the GR value of 0.35 for the hardest eos, Hh, is consistent with the proposed redshift of 0.35 [84]. The Hm and Qh lines begin to curve up near $c_{14} = 1.1-1.2$ because the maximum mass for these equations of state is approaching 1.8 solar masses.

4.5 Discussion

The structure of non-rotating neutron stars in Einstein-aether theory is fairly close to that in GR, but there are quantitative differences. Depending on the equation of state, the maximum masses range from about 6-15% smaller than in GR when the ae-theory parameter c_{14} is equal to 1. The corresponding surface redshifts are roughly 10% larger than in GR. Measurements of high gravitational masses or precise surface redshifts have the potential to yield strong joint constraints on the equation of state and on deviations from GR. Therefore, as laboratory experiments and other observations narrow down the equation of state of cold matter at sev-

eral times nuclear density, neutron star observations may be a valuable resource for exploring deviations from general relativity in strong gravity.

There are several lines of further work that would be interesting to pursue. Perhaps the stability analysis [64] discussed at the end of the previous chapter could also be applied to static solutions in the presence of perfect fluid matter with the goal of providing a firm condition on c_{14} for stability. Second, the fluid star solutions we considered are at rest with respect to the asymptotic aether. Although corrections due to motion with respect to the aether are not significant for the present paper, as was noted in Section 1.3, they are important for the high precision predictions of radiation damping in compact binaries. In particular, the missing ingredient in the analysis of [44] is the value of the “sensitivity” parameter measuring the velocity dependence of the mass. It should be possible to compute this parameter for different masses and different equations of state by determining the velocity perturbations of the solutions found here, or by finding the exact nonlinear solutions with finite velocity. Finally, the work described in this chapter only applies for non-rotating stars. For other astrophysical applications it would be necessary to examine the structure of rotating solutions. The preferred frame effects of ae-theory may be more significant in this case, leading to more noticeable discrepancies from GR predictions.

We considered in this chapter only neutron star phenomenology. What is the situation for black holes? These solutions will be discussed in detail in the next chapter.

Chapter 5

Black Holes

5.1 Introduction

The literature on black hole solutions in alternative theories of gravity has been relatively sparse until recently. In the early 1970's, it was shown stationary black holes in scalar-tensor theories are described by the GR solution plus a constant scalar field, so they yield no new predictions [87]. However, over the past few years non-trivial black hole solutions have been considered in the ghost condensate theory [88], and spherically symmetric solutions in Bekenstein's TeVeS (tensor-vector-scalar) theory [6] were studied in [89]. Work on this subject in ae-theory was begun several years ago in special cases [25].

Studying these solutions is the first step in comparing ae-theory with astrophysical observations of black holes. As in the case of neutron star observations, concrete tests of the gravitational theory are not possible due to the current uncertainties in other astrophysical processes near the black hole. For example, spectral profiles of Fe $K\alpha$ fluorescence lines in active galactic nuclei and stellar-mass black holes are consistent with the expectations of gas streamlines near rapidly rotating black holes, but precision tests are not yet possible because of unknowns about the emission profile and other complications [90]. However, in the future, the *Constellation-X* project [66] may be able to track the motion of individual emitting

elements in a disk, mapping out the spacetime near a rotating black hole. Similar results are likely to come from detections of gravitational waves from black hole mergers seen with ground-based interferometers such as LIGO [91], and later with space-based instruments such as LISA [92].

Ae-theory black holes are also a window on the theoretical implications of a Lorentz violating theory. In particular, what is the fate of black hole thermodynamics or even Hawking radiation in these theories? Foster [49] has already demonstrated the difficulties in extending the first law of black hole mechanics and the definition of entropy to ae-theory. In addition, these solutions are of purely mathematical interest as an example of unusual black hole behavior with non-linear self-gravitating fields.

The vacuum and fluid star static aether solutions discussed in Chapters 3 and 4 depend only on the single combination c_{14} , but this is not the case for the black hole solutions. Moreover, unlike those solutions, the black hole solutions cannot (as far as we know) be obtained analytically, so all of the results here are numerically obtained. We do not make an exhaustive study here for all values of the c_i , but rather just attempt to determine the generic behavior of the black hole solutions.

We begin in Section 5.2 with a discussion of the definition of a black hole in ae-theory, and the conditions for the existence of regular black hole solutions. The qualitative reasons for the existence of a one parameter family of such solutions are explained. In preparation for the subsequent detailed analysis, the field redefinition properties of the theory are reviewed in Section 5.3. This is followed in Section 5.4 by a demonstration using the power series solution of the field equations about

a metric horizon that such horizons are generically regular, i.e. there is a three parameter family of solutions in the neighborhood of such a horizon, just as in the neighborhood of any generic point. We then show that spin-0 horizons are generically singular, but a two-parameter family of solutions is regular and the additional condition of asymptotic flatness further reduces this to a one-parameter family. In Section 5.5, we study the properties of typical examples of this one parameter family of black holes, imposing regularity by a power series expansion about the spin-0 horizon and numerically integrating out to infinity, determining the asymptotically flat solutions by tuning the data at the horizon. These black holes are rather similar to Schwarzschild outside the horizon, and like Schwarzschild they have a spacelike curvature singularity inside at (or very near) zero radius. Unlike the static aether solutions, u^a is not aligned with the static Killing field in these black hole solutions. The aether flows into the black hole, but differs significantly from the 4-velocity of freely-falling geodesics at rest at infinity. We also note that some functions constructed from the metric and aether exhibit oscillatory behavior in the interior as they approach the singularity. Section 5.6 discusses new results [93] showing a scalar field pulse collapses into the black hole solutions discussed above as long as the c_i are not too large. We also briefly discuss other recent work [94] showing Lorentz violating black hole solutions can be used to violate the Generalized Second Law (GSL) of thermodynamics. The chapter concludes by examining various other questions for further research.

5.2 General properties of black holes in ae-theory

The relevant notion of a black hole in ae-theory is not immediately clear. To trap matter influences a black hole must have a horizon with respect to the causal structure of g_{ab} , the metric to which matter couples universally (or almost universally, according to observations). We call this a “metric horizon”. This is not the only relevant notion of causality however. For general values of the coupling coefficients c_i , ae-theory has multiple characteristic hypersurfaces. In particular, perturbing around flat spacetime it was found in [41] that there are spin-2, spin-1, and spin-0 wave modes, with squared speeds relative to the aether given in Table 2.1. The speeds s_i are generally different from each other and from the metric speed of light 1. Only in the special case where $c_4 = 0$, $c_3 = -c_1$, and $c_2 = c_1/(1 - 2c_1)$ do all the modes propagate at the same speed. In general, the characteristic surfaces for a mode of speed s_i are null with respect to the effective metric $\eta_{ab} + (s_i^2 - 1)\underline{u}_a\underline{u}_b$, where η_{ab} is the flat metric and \underline{u}_a the constant background aether.

In the nonlinear case characteristics can be defined as hypersurfaces across which the field equations admit a discontinuity in first derivatives [95]. For this paper we presume that these characteristics define the relevant notion of causal domain of dependence for the ae-theory field equations. This seems quite plausible, although no rigorous study has been attempted. The characteristic hypersurfaces are determined by the highest derivative terms in the field equations, so can also be identified by examination of high frequency solutions to the linearized equations about a given background [95]. For such solutions the gradients in the background

are irrelevant, so one can infer that the nonlinear characteristics are null surfaces of the effective metrics,

$$g_{ab}^{(i)} = g_{ab} + (s_i^2 - 1)u_a u_b. \quad (5.1)$$

We refer to the horizons associated with these metrics as the spin-0, spin-1, and spin-2 horizons. If a black hole is to be a region that traps all possible causal influences, it must be bounded by a horizon corresponding to the fastest speed. The coupling coefficients c_i determine which speed is the fastest.

A horizon is potentially a location where a solution to the field equation can become singular. This is because at a characteristic surface the coefficient of a second derivative term usually present in the equation vanishes. As such a surface is approached, the smallness of that coefficient may generically produce a solution in which some second derivative grows without bound, leading to singular behavior. This does not occur at spin-1 and spin-2 horizons in spherically symmetric solutions to ae-theory, presumably since there are no spherically symmetric spin-1 or spin-2 modes. However there is a spherical spin-0 mode, and we find that spin-0 horizons are generically singular.

The requirement that the spin-0 horizon be regular reduces the general three parameter family of local stationary, spherically symmetric solutions discussed in Section 3.2.1 to a two parameter family, which reduces to a one parameter family when asymptotic flatness is imposed. Hence there is just a one parameter family of regular static, spherically symmetric black hole solutions in ae-theory, just as in GR. Unlike outside a star, the aether in these solutions is *not* aligned with the Killing

vector but rather flows into the black hole.

The fact that the aether is not aligned with the Killing vector in a static black hole solution is no accident. It cannot be so aligned, since it is everywhere a timelike unit vector and the Killing vector is null on the horizon. Thus at a regular horizon the aether must be “infalling”, although it is nevertheless invariant under the Killing flow. The static aether solution found in Chapter 3 has aether aligned with the Killing vector, and can be thought of as an extremal black hole with a singular horizon on which the aether becomes infinitely stretched.

While the aether can be regular at a generic point on the horizon, it cannot smoothly extend to the bifurcation sphere \mathcal{B} , i.e. the fixed point set of the Killing flow at the intersection of the past and future horizons [26]. The Killing flow acts as a Lorentz boost in the tangent space of any point on \mathcal{B} , so it is impossible for the aether to be invariant under the flow there. This implies that the aether must blow up, becoming an infinite null vector as \mathcal{B} is approached. This in turn raises the concern that there may be no regular metric horizon, since regularity on a future horizon is typically linked to regularity at \mathcal{B} . Indeed Racz and Wald [96] have established, independent of any field equations, conditions under which a stationary spacetime with regular Killing horizon can be extended to a spacetime with a regular bifurcation surface, and conditions under which matter fields invariant under the Killing symmetry can also be extended. In spherical symmetry these conditions are satisfied for the metric, but the aether vector field breaks the required time reflection symmetry so it need not be regular at the bifurcation surface (although all scalar invariants must be, as must the aether stress tensor if the field equations hold).

Another potential obstruction to the existence of regular ae-theory black hole horizons arises from the form of the aether stress tensor. At a regular stationary metric horizon the Raychaudhuri equation for the horizon congruence with null generator k^a implies that $R_{ab}k^ak^b$ must vanish, hence the Einstein equation implies that the matter stress tensor component $T_{ab}k^ak^b$ must also vanish. With common matter fields, e.g., scalar fields, Maxwell or Yang-Mills fields, and nonlinear sigma model fields, it is easy to show from examination of the form of the stress tensors that this condition is automatically satisfied locally for any field invariant under the Killing flow, independent of field equations. This property does not seem to hold kinematically for the aether stress tensor, but since we find a full three-parameter family of regular metric horizons, it is evidently imposed by the field equations.

The fact that $T_{ab}k^ak^b$ does not vanish kinematically might appear to contradict the following general argument. For a Killing horizon with non-zero surface gravity it is not necessary to examine the form of the stress tensor to arrive at the inference that the horizon component of a matter stress tensor vanishes. If χ^a is the horizon-generating Killing vector, then the vanishing of the scalar $T_{ab}\chi^a\chi^b$ on the horizon is guaranteed by the facts that (i) it is invariant along the flow, (ii) χ^a vanishes at the bifurcation surface, and (iii) T_{ab} is regular at the bifurcation surface (as guaranteed by the Racz-Wald extension theorem). But this argument too seems to fail for the aether stress tensor, because (as noted above) there is no purely kinematic way to argue that it (and therefore its stress-tensor) is regular at the bifurcation surface. So, again, the field equations seem to play an essential role in ensuring the existence of regular metric horizons.

5.3 Field Redefinitions

In this section we address in more detail the field redefinitions [71] briefly mentioned in Section 4.2. These redefinitions will play an important role in the analysis of subsequent sections below. In spherical symmetry the c_4 term in vacuum action for ae-theory (3.1)

$$\begin{aligned}
L = & -R - c_1(\nabla_a u_b)(\nabla^a u^b) - c_2(\nabla_a u^a)^2 - c_3(\nabla_a u_b)(\nabla^b u^a) \\
& - c_4(u^c \nabla_c u^a)(u^d \nabla_d u_a) - \lambda(g_{ab} u^a u^b - 1)
\end{aligned} \tag{5.2}$$

can again be absorbed by making the replacements

$$c_1 \rightarrow c_1 + c_4, \quad c_3 \rightarrow c_3 - c_4, \quad c_4 \rightarrow 0. \tag{5.3}$$

because the aether is still hypersurface orthogonal (although it is now not aligned with the Killing vector).

It is sometimes convenient to re-express the theory in terms of a new metric and aether field, related to the original fields by a field redefinition of the form

$$g'_{ab} = g_{ab} + (\sigma - 1)u_a u_b \tag{5.4}$$

$$u'^a = \frac{1}{\sqrt{\sigma}}u^a. \tag{5.5}$$

The constant σ is restricted to be positive so the new metric remains Lorentzian. In effect, the field redefinition “stretches” the metric tensor in the aether direction by a factor σ . The Lagrangian (5.2) for (g'_{ab}, u'^a) takes the same form as that for (g_{ab}, u^a) up to the values of the coefficients c_i . The c_i coefficients for the action expressed in terms of the new fields (5.4)-(5.5) are [71]

$$c'_1 = \frac{\sigma}{2} \left((1 + \sigma^{-2})c_1 + (1 - \sigma^{-2})c_3 - (1 - \sigma^{-1})^2 \right) \tag{5.6}$$

$$c'_2 = \sigma(c_2 + 1 - \sigma^{-1}) \quad (5.7)$$

$$c'_3 = \frac{\sigma}{2} \left((1 - \sigma^{-2})c_1 + (1 + \sigma^{-2})c_3 - (1 - \sigma^{-2}) \right) \quad (5.8)$$

$$c'_4 = c_4 - \frac{\sigma}{2} \left((1 - \sigma^{-1})^2 c_1 + (1 - \sigma^{-2})c_3 - (1 - \sigma^{-1})^2 \right). \quad (5.9)$$

Certain combinations of the coefficients change by a simple scaling under the field redefinitions:

$$c'_{14} = c_{14} \quad (5.10)$$

$$c'_{123} = \sigma c_{123} \quad (5.11)$$

$$c'_{13} - 1 = \sigma(c_{13} - 1) \quad (5.12)$$

$$c'_1 - c'_3 - 1 = \sigma^{-1}(c_1 - c_3 - 1). \quad (5.13)$$

The field redefinition relates solutions to the field equations coming from the two actions.

Using a field redefinition the general form of the action can be simplified [71] by eliminating one of the c_i or a combination of the c_i . If one chooses $\sigma = (s_2)^2 = 1/(1 - c_{13})$, then c'_{13} vanishes, i.e. $c'_3 = -c'_1$. In this case the two corresponding terms in the Lagrangian combine to make a Maxwell-like lagrangian, for which the Levi-Civita connection drops out. (This choice of σ is positive and therefore preserves Lorentzian signature provided the original coefficients satisfy $c_{13} < 1$.) In the context of spherical symmetry, one may also exploit the hypersurface orthogonality of the aether to absorb the c_4 term in (5.2) by the replacements (5.3) as explained above. After these two changes, the Lagrangian takes a much simpler reduced form

characterized by only two c_i coefficients,

$$L_{\text{ae}} = -R - \frac{c'_1}{2} F^{ab} F_{ab} - c'_2 (\nabla_a u^a)^2 - \lambda (g_{ab} u^a u^b - 1), \quad (5.14)$$

where $F_{ab} = 2\nabla_{[a} u_{b]}$. In the next section we will use this reduced form of the action to investigate the general behavior of stationary spherically symmetric solutions, addressing the existence of solutions around a metric horizon, asymptotic flatness, and the regularity of the spin-0 horizon.

Another useful choice of field redefinition is to arrange for the new metric in (5.4) to coincide with the effective metric for one of the wave modes (5.1) by choosing $\sigma = s_i^2$. In this way we transform to a “frame” where one of the spin-2, spin-1, or spin-0 horizons coincides with the metric horizon. Under the field redefinition all the squared speeds become $s_i'^2 = s_i^2/\sigma$, since the metric tensor in the aether direction is stretched by the factor σ . In Section 5.5 we use this method to make the spin-0 and metric horizons coincide, which simplifies the expansion of the field equations around the spin-0 horizon.

5.4 Generic behavior of horizons and spatial infinity

In this section we demonstrate that, for generic values of the c_i coefficients (at least for the reduced theory (5.14)), (i) metric horizons are generically regular in the three-parameter family of local solutions, (ii) asymptotic flatness imposes one condition on this family, and (iii) regularity of the spin-0 horizon imposes another condition, leaving a one-parameter family of black hole solutions with regular spin-0 horizons.

5.4.1 Metric horizon expansion

One way to determine the number of independent solutions with a regular metric horizon is to expand the field equations in a power series about a candidate horizon and solve algebraically order by order. We did this using the Maple computer application to carry out the algebra. The computation was prohibitively complicated using our methods with general values of the c_i , so we restricted attention to the reduced theory (5.14). The determination of the solution space can also be done more “experimentally,” by numerical integration of the field equations with varying initial data. With the latter method no special restriction on the c_i is required.

The field equations from varying (5.2)

$$G_{ab} = T_{ab}^{(u)} \quad (5.15)$$

$$\nabla_a J^a_m - c_4 \dot{u}_a \nabla_m u^a = \lambda u_m, \quad (5.16)$$

$$g_{ab} u^a u^b = 1, \quad (5.17)$$

where

$$J^a_m = K^{ab}{}_{mn} \nabla_b u^n. \quad (5.18)$$

The aether stress tensor is given by

$$\begin{aligned} T^{(u)}{}_{ab} &= \nabla_m (J^m{}_{(a} u_{b)}) - J_{(a}{}^m u_{b)} + J_{(ab)} u^m \\ &+ c_1 [(\nabla_a u_m)(\nabla_b u^m) - (\nabla_m u_a)(\nabla^m u_b)] \\ &- c_4 \dot{u}_a \dot{u}_b \\ &- [u_n (\nabla_m J^{mn}) - c_4 \dot{u}^2] u_a u_b \\ &- \frac{1}{2} L_u g_{ab}, \end{aligned} \quad (5.19)$$

where $L_u = -K^{ab}{}_{mn} \nabla_a u^m \nabla_b u^n$.

For the study of spherical black holes we adopt Eddington-Finkelstein (EF) type coordinates (v, r, θ, φ) with line element

$$ds^2 = N(r)dv^2 - 2B(r)dvdr - r^2d\Omega^2 \quad (5.20)$$

with advanced (null) time coordinate v and radial “area coordinate” r . Note that the functions $N(r)$ and $B(r)$ are different from the Schwarzschild coordinate functions of previous chapters. The time-translation Killing vector is ∂_v , and a metric horizon corresponds to $N(r) = 0$. These coordinates are regular at metric and other horizons so are useful for studying black holes and their interiors. Using these coordinates a stationary spherical aether field takes the form

$$u^a = a(r)\partial_v + b(r)\partial_r \quad (5.21)$$

and the unit constraint (5.17) becomes

$$Na^2 - 2Bab = 1. \quad (5.22)$$

The field equations (5.15) and (5.16) become a set of coupled, second order ordinary differential equations (ODE’s) involving the functions N, B, a, b . We use the constraint (5.22) to solve for b in terms of the other three functions. Even for the reduced case $c_{13} = c_4 = 0$ the equations are sufficiently complicated that it does not seem useful to display them here.

Regularity at the metric horizon can be imposed by making a power series expansion about the radius r_h where $N(r_h) = 0$,

$$N(r) = N'(r_h)(r - r_h) + \frac{1}{2}N''(r_h)(r - r_h)^2 + \dots \quad (5.23)$$

$$B(r) = B(r_h) + B'(r_h)(r - r_h) + \frac{1}{2}B''(r_h)(r - r_h)^2 + \dots \quad (5.24)$$

$$a(r) = a(r_h) + a'(r_h)(r - r_h) + \frac{1}{2}a''(r_h)(r - r_h)^2 + \dots \quad (5.25)$$

Inserting these expansions in the field equations, one can solve order by order for the power series coefficients. This allows the set of free parameters in the initial data at the horizon to be identified. At zeroth order in $(r - r_h)$ the field equations imply that $a'(r_h)$ is a function of $N'(r_h)$, $B(r_h)$, $a(r_h)$, and r_h . The specific result is sufficiently complicated that it too does not seem useful to display here. Solving to higher orders we find that all remaining coefficients in the series expansion are determined by these four initial data parameters. Using the scaling freedom in the v coordinate ($v \rightarrow \lambda v$ where λ is a constant) one of the initial values at the horizon can be fixed arbitrarily. Thus, there is a three-parameter family of local solutions with a regular metric horizon. As discussed in Chapter 3, we also found a three-parameter family of local solutions expanding about an arbitrary radius (i.e. not imposing a horizon). Hence we conclude that regularity of the metric horizon generically imposes no restriction on the solutions.

5.4.2 Asymptotic expansion

In addition to regularity at all the horizons, the black hole solutions must be asymptotically flat. To determine the form of such solutions one can change to the inverse radius variable $x = 1/r$ and expand around $x = 0$, as was done in [36] (where isotropic coordinates were employed) and Section 3.2.2 (using Schwarzschild

coordinates). In the reduced theory (5.14) this yields the solutions

$$N(x) = 1 + N_1 x + \frac{1}{48} c'_1 N_1^3 x^3 + \dots \quad (5.26)$$

$$B(x) = 1 + \frac{1}{16} c'_1 N_1^2 x^2 - \frac{1}{12} c'_1 N_1^3 x^3 + \dots \quad (5.27)$$

$$a(x) = 1 - \frac{1}{2} N_1 x + a_2 x^2 + \left(-\frac{1}{96} c'_1 N_1^3 + \frac{1}{16} N_1^3 - N_1 a_2\right) x^3 + \dots \quad (5.28)$$

where $N_1 = N'(x=0)$ and $a_2 = a''(x=0)$, and the freedom to rescale v has been exploited to set $N(x=0) = 1$. No more free parameters appear at higher orders, so the asymptotically flat solutions are determined by the two free parameters N_1 and a_2 .

An asymptotically flat solution can be determined by using a simple shooting method, numerically integrating outward from an interior radius where there are three free initial data parameters. As in Chapter 3, we find that to match the asymptotic form (5.26)-(5.28) requires tuning just one of the three initial parameters, as expected since there are two free parameters in the asymptotic form. We conclude that in particular there is a two-parameter family of asymptotically flat “black hole” solutions with metric horizon fixed to lie at a given radius r_h . In practice, to integrate outward from a metric horizon we found it necessary to first use the perturbative solution about the horizon to generate from the horizon data an initial data set some small radial distance away. This is because the ODE’s have a singular point at the horizon.

A more direct way to generate such asymptotically flat black hole solutions is to start the numerical integration near infinity and integrate inward using the inverse radius coordinate x . Since $x = 0$ is a singular point of the ODE, it is necessary to

start the integration at some small non-zero x value. The expansions (5.26)-(5.28) can be used to generate initial data as a function of N_1 and a_2 . We again find this way that regularity at the metric horizon does not impose any conditions on N_1 and a_2 . The functions N , B , and a evolve smoothly through a point where N goes to zero.

5.4.3 Asymptotically flat solutions and spin-0 horizon regularity

So far we have shown that there is a two-parameter family of asymptotically flat black hole solutions with a regular metric horizon. Normally one expects just one black hole parameter, the total mass, unless there are conserved charges that can be additional parameters. In ae-theory there seems to be no such conserved charge, so the situation is puzzling. Another puzzling aspect of these black hole solutions not yet discussed here is that some have internal singularities at nonzero radius, rather than just at $r = 0$ like most known black holes. Moreover, in some solutions we found that such singularities can occur externally, i.e. not inside a metric horizon. All these puzzles are resolved by the recognition that the singularities in question occur precisely at the location of the spin-0 horizon. Imposing regularity at the spin-0 horizon eliminates one free parameter, leaving a conventional one-parameter family of asymptotically flat black holes.

In the rest of this subsection the full range of behavior of asymptotically flat solutions is discussed. In particular it is demonstrated that when a spin-0 horizon occurs it is singular for generic values of the two initial data parameters N_1 and a_2

at infinity. Evidence is given that by tuning one of these parameters to a special value a regular spin-0 horizon can be obtained. In the next section we show by a power series expansion around the spin-0 horizon that such regular solutions do indeed exist.

For the reduced theory (5.14), the spin-2 and spin-1 speeds are both unity, but the spin-0 mode has squared speed $s_0^2 = (c'_2/c'_1)(2 - c'_1)/(2 + 3c'_2)$ (relative to the aether), which is generically different from unity. At the spin-0 horizon the mode propagates at fixed radius, hence the surface of constant r at that location is null with respect to the effective metric $g_{ab}^{(0)}$ defined in (5.1). This implies the condition $g_{vv}^{(0)} = 0$ in EF coordinates, which occurs where

$$Na^2 = \frac{1 - s_0}{1 + s_0} \quad \text{or} \quad \frac{1 + s_0}{1 - s_0}. \quad (5.29)$$

The first root is less than 1 so according to (5.22) occurs when $b < 0$, i.e. when the aether tips inward. For the second root the aether tips outward. The combination $f = Na^2$ is independent of the arbitrary scale for the v coordinate and equal to one at infinity. Inserting the expansions (5.26) and (5.28) we find the asymptotic form

$$f(x) = N(x)a(x)^2 = 1 + 2(a_2 - \frac{3}{8}N_1^2)x^2 - N_1(a_2 - \frac{3}{8}N_1^2)x^3 + O(x^4) \quad (5.30)$$

Curiously, this expansion is independent of both c'_1 and c'_2 through order x^3 (but not beyond) and depends linearly on $a_2 - \frac{3}{8}N_1^2$ through order x^5 . This pattern suggests an analytic solution may be possible, but we will not pursue this here. The static aether solution studied in Chapter 3 corresponds to the case where $f(x) = 1$ for all x , which occurs when $a_2/N_1^2 = 3/8$.

As in the previous subsection, we study solutions obtained by integration inwards starting from an asymptotically flat spatial infinity. Since the theory has no length scale, the solution with data (N_1, a_2) is trivially related to that with data $(\lambda N_1, \lambda^2 a_2)$ (as are Schwarzschild solutions with different mass trivially related). If one thinks of the line element ds^2 as giving a numerical value specified with respect to a given length unit, then to go from one solution to another one need only change the unit of length. Thus without loss of generality units with $N_1 = \pm 1$ can be fixed. The solutions then depend on the choice of theory through c'_1, c'_2 , on the parameter a_2 , and on the sign of N_1 . A systematic study of these solutions is beyond the scope of this paper; here we just indicate the various behaviors we have encountered, and then focus on the regular positive mass black holes.

Let us first consider positive mass solutions, i.e. $N_1 = -1$. As the radial coordinate decreases, N decreases from 1, while the combination Na^2 increases or decreases according as a_2 is greater or less than $3/8$. There are solutions where $f(r)$ does not reach 0 or $(1 \mp s_0)/(1 \pm s_0)$ and therefore neither a metric nor spin-0 horizon is attained. In some of these $N(r)$ re-curves out to positive infinity, $a(r)$ approaches zero and the solution reaches a curvature singularity near $r = 0$. There are also solutions similar to the static aether of Chapter 3, where $B(r)$ goes to infinity as $N(r)$ approaches a finite value, indicating a minimal area two-sphere. In some cases the larger root for a spin zero horizon in (5.29) is reached by $f(r)$. In other solutions $f(r)$ may reach a metric horizon, but does not attain the value corresponding to a spin-0 horizon. This can only happen when $s_0 > 1$. $N(r)$ again re-curves out to infinity and $a(r)$ approaches zero near $r = 0$ and there are outer and inner metric

horizons. In still other solutions, the functions and their derivatives are regular up to the point where $f(r)$ reaches the spin-0 horizon, but generically the spacetime is singular at that point. If $s_0 > 1$, $f(r_h)$ is negative and the singularity is located inside a metric horizon. If $s_0 < 1$ the singularity occurs without any metric horizon.

For a specific example of this last type we choose parameters $c'_1 = 0.051$ and $c'_2 = 0.116$, for which the spin-0 speed is 1.37. (These arise from starting with coefficients that satisfy all the observational constraints described in [38] and performing the field redefinition to the reduced action (5.14).) Figure 5.1 shows

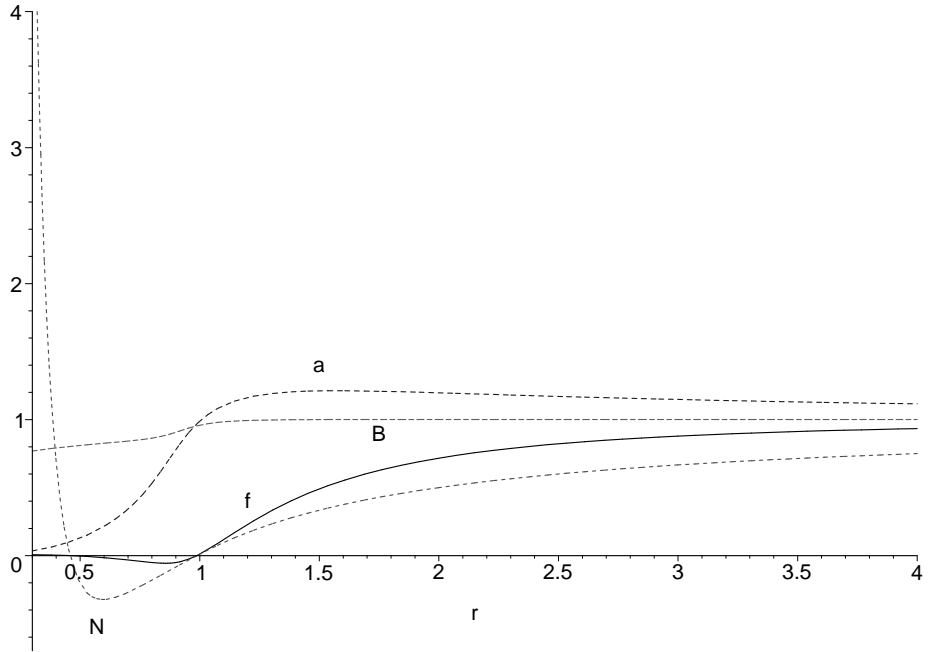


Figure 5.1: Solution for reduced theory (5.14) with $c'_1 = 0.051$ and $c'_2 = 0.116$, determined by data $N_1 = -1$ and $a_2 = -0.1$ at spatial infinity. There is both an outer and inner metric horizon where N vanishes, but f does not decrease enough to reach a spin-0 horizon. The functions N and f go to zero slightly inside $r = 1$ which would be the horizon radius of the corresponding Schwarzschild solution. As a_2 increases the minimum of $f(r)$ decreases until the solution acquires a spin-0 horizon, where it is generically singular.

the behavior of N , B , and a for $N_1 = -1$ and $a_2 = -0.1$. In this case there are

“outer” and “inner” metric horizons where $N = 0$, but $f(r)$ does not reach as low as -0.158 , which is required by (5.29) in this case for a spin-0 horizon. For values of $a_2 < -0.1$ the minimum value of N shifts upward and eventually N never reaches zero, i.e. the metric horizon disappears. On the other hand, for $a_2 > -0.1$ the minimum value of f decreases until the spin-0 horizon is reached. At this point a' goes to negative infinity, N' blows up to positive infinity, and there is a curvature singularity. In contrast, note that in Figure 5.1 $a'(r)$ has a maximum value while $N'(r)$ goes to *negative* infinity. This suggests that at some special value of a_2 there is a transition where the concavity of $a'(r)$ and $N'(r)$ changes and the derivatives are finite at a spin-0 horizon. Regularity at the spin-0 horizon seems thus to impose one condition on the asymptotic values N_1 and a_2 .

In the negative mass case one might expect only solutions analogous to negative mass Schwarzschild, with N increasing from 1 at spatial infinity and no spin-0 or metric horizon. While the solution does take this form for all a_2 in the theory with $c'_1 = 0.051$, $c'_2 = 0.116$, for other values of $c'_{1,2}$ there are ranges of a_2 where N increases from 1 at infinity, but then decreases to a metric horizon at finite r , and all the functions and their derivatives are regular until $f(r)$ reaches the value less than zero required for a spin-0 horizon. This peculiar behavior of a negative mass solution with metric and spin-0 horizons remains to be studied more closely. In particular, it is not clear whether a negative mass solution with a regular spin-0 horizon could exist.

5.5 Black holes with regular spin-0 horizons

In this section we discuss the behavior of black hole solutions possessing regular spin-0 horizons. Rather than imposing regularity at the spin-0 horizon by the shooting method integrating in from infinity, we instead expand the field equations in a power series about a non-singular spin-0 horizon.

5.5.1 Horizon expansion

Due to the complexity of the field equations and their singular nature at the horizon, we were unable to implement the power series solution about a spin-0 horizon in the generic reduced theory (5.14) (even with computer aided algebra). It might be possible to obtain the perturbative solution by a more well-adapted method, but instead we simplified the computation by making a field redefinition to a new metric for which the spin-0 and metric horizons coincide. Starting from an arbitrary set of coefficients c_i , this is implemented by the choice $\sigma = s_0^2$ in (5.5), after which we have $s_0 = 1$ without loss of generality in the theory. As before we can also then exploit spherical symmetry to absorb c_4 by making the replacements (5.3), which do not disrupt the coincidence of the spin-0 and metric horizons since this is just a re-expression of the same Lagrangian without changing the field variables ¹.

¹The spin-0 speed is invariant under (5.3), as guaranteed by this argument. The spin-1 speed is *not* invariant, but this does not contradict the argument since there is no spherically symmetric spin-1 mode. Note however that in diagnosing whether spin-1 perturbations are trapped in a given black hole it is important to use the value of the spin-1 speed written in (2.1) *before* the c_4 coefficient has been absorbed.

This reduces the distinct parameter space to just (c_1, c_3) (omitting the prime in the notation for $c_{1,3}$). After this field redefinition the coefficient c_2 is given by

$$c_2 = \frac{-2c_3 - c_1^3 - 2c_3c_1^2 - c_1c_3^2}{2 - 4c_1 + 3c_1^2 + 3c_3c_1}. \quad (5.31)$$

A further simplification of the equations is achieved by trading the metric function N for the combination of metric and aether functions $f = Na^2$. We have no insight into why this simplifies the expansion of the field equations about the common metric and spin-0 horizon at $N = 0 = f$, although as stated above the combination Na^2 is invariant under a rescaling of the v coordinate. The field equations in this set of field variables involve $a, a', a'', f, f', f'', B,$ and B' . At the horizon $f(r)$ vanishes linearly, $f(r) = f'(r_0)(r - r_0) + \dots$ By a constant rescaling of v we can furthermore set $B(r_h)$ equal to 1. Using this along with (5.24) and (5.25) the field equations can be expanded and solved order by order for the coefficients of the power series.

Solving the field equations for this theory as algebraic equations for the expansion coefficients we find that at zeroth order in $(r - r_h)$ the quantities $a(r_h), a'(r_h), a''(r_h),$ and $f''(r_h)$ are determined by free parameters $r_h, f'(r_h), B'(r_h)$. We succeeded in solving the equations to the next order in $(r - r_h)$ only in the special cases $c_3 = 0, c_3 = c_1,$ and $c_3 = -c_1$. In these cases we find that $B'(r_h)$ is determined by r_h and $f'(r_h)$. Hence, consistent with the expectation of the previous section, there is a two-parameter family of local solutions around the regular spin-0 horizon. These solutions are generically not asymptotically flat.

5.5.2 Asymptotically flat black holes

To produce asymptotically flat solutions we numerically integrate outward, starting with the horizon data and matching onto (5.26), (5.27), and (5.28) by tuning $f'(r_h)$ until $f(r)$ is constant and equal to 1 at very large r values. The asymptotic flatness boundary condition at infinity thus reduces the number of free parameters to one, namely the horizon radius itself. Solutions with different horizon radii are trivially related. Since r_h is a singular point of the ODE's, it is necessary to start the integration with initial data at some small positive value of $r - r_h$. We used the series solution determined by a given r_h and $f'(r_h)$ to generate this initial data. To examine the solution inside the horizon, we numerically integrated inward, starting at a small negative value of $r - r_h$ with data generated by the same series solution.

Here we will discuss the properties of the solutions for the $c_3 = 0$ theory only, whose behavior is typical of the three special cases $c_3 = 0, \pm c_1$. Figure 5.2 displays the solution for $c_1 = 0.3$, $c_2 = -.025$, $c_3 = c_4 = 0$, together with $S(r) = 1 - 2/r$, the Schwarzschild version of $N(r)$ with the same mass. For this plot we use the scaling freedom of v to convert the numerical solution to a “gauge” where the metric functions and v component of the aether are all equal to 1 at infinity. The two metric functions $B(r)$ and $N(r)$ in GR and ae-theory are in very close agreement outside the horizon, while inside they differ noticeably.

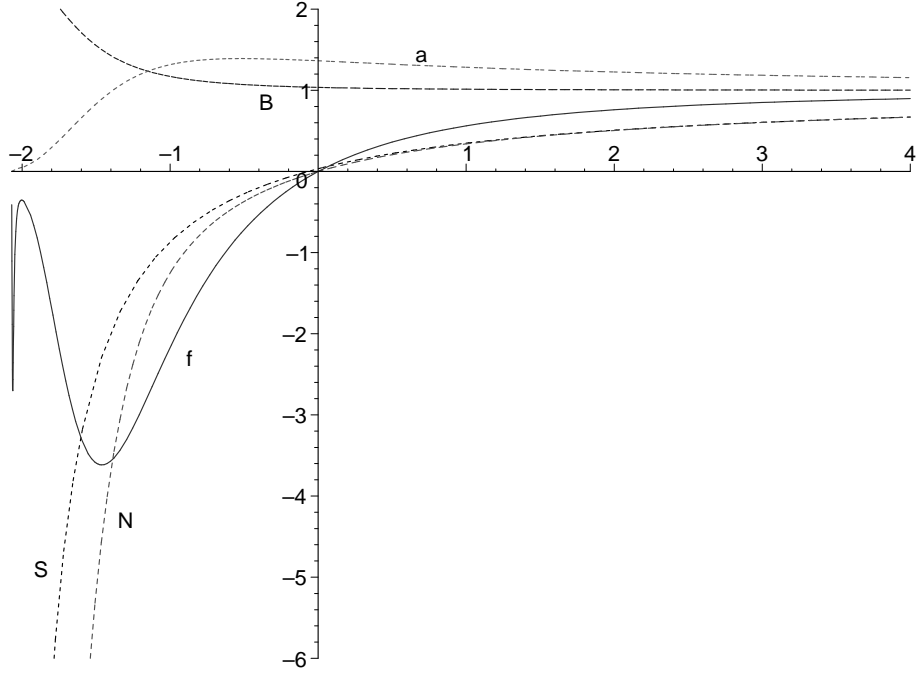


Figure 5.2: Plots of f , N , B , a , and S (the Schwarzschild version of N) vs. $z = r - r_h$ for $c_1 = 0.3$, in units with $r_0 = 2$. The horizon radius is $r_h \approx 2.07$ for the ae-theory black hole, so $S = 0$ at $z \approx -0.07$. The solutions agree closely outside the horizon. Deviations are noticeable near the horizon and become significant in the interior, where N blows up more rapidly. Near the singularity f begins to oscillate rapidly.

5.5.2.1 Black hole mass

The ADM mass M_{ADM} of an asymptotically flat spacetime whose asymptotic metric takes the Schwarzschild form at $O(1/r)$ is directly determined by the coefficient $r_0 = 2GM_{ADM}$ of the $O(1/r)$ part of g_{tt} . We found in Chapter 2 that in ae-theory the relation between M_{ADM} and the total energy E of the spacetime is $GM_{ADM} = G_N E$, where $G_N = G/(1 - c_{14}/2)$ is the Newton constant appearing in the force law between two weakly gravitating masses [34]. We will refer to the quantity $r_0/2$ with dimensions of length as the “mass” in what follows, and denote it by M . For a Schwarzschild black hole in GR, r_0 is equal to the horizon radius r_h . In ae-theory the ratio r_0/r_h is a constant (since there is only one length scale)

determined by the coupling coefficients c_i .

The EF line element (5.20) transforms to Schwarzschild form

$$ds^2 = N dt^2 - (B^2/N) dr^2 - r^2 d\Omega^2 \quad (5.32)$$

with time coordinate t defined by $dt = dv - (B/N)dr$. The asymptotic form of B (5.27) shows that $B = 1 + O(1/r^2)$, so up through $O(1/r)$ the line element (5.32) has the standard asymptotic form if N and B are normalized to 1 at infinity. In generating an asymptotically flat numerical solution we fixed the scale freedom of the v coordinate by imposing $B(r_h) = 1$ at the horizon however, so the asymptotic form of N is $N_\infty + N_1/r + O(1/r^2)$. The mass is given by $M = r_0/2 = N_1/2N_\infty$, which can be extracted from the numerical solution at large r .

5.5.2.2 Horizons

The solution displayed in Figure 5.2 has metric and spin-0 horizons at $z = 0$, but how about spin-1 and spin-2 horizons? Is the fastest speed actually trapped? The condition for a horizon corresponding to a speed s_0 is given in (5.29). As the speed approaches infinity the horizon value of f approaches -1 from above. In Figure 5.2 (and for all values of c_1 that we studied up to 0.7), the minimum value of $f(r)$ is less than -1 , which is sufficient to trap any wave mode. The fact that $f(r)$ curves back to being greater than -1 indicates that an inner horizon might exist for some wave modes in certain parameter ranges of c_i .

In the theory under discussion we have $c_3 = c_4 = 0$ and $c_2 = -c_1^3/(2 - 4c_1 + 3c_1^2)$, so the squared mode speeds in (2.1) are given by $1/(1 - c_1)$ for spin-2 and

$(1 - c_1/2)/(1 - c_1)$ for spin-1. With $0 < c_1 < 1$ both of these are greater than 1, and the spin-2 speed is the highest. In the particular case shown in the figure, the spin-1 speed is 1.10 and the spin-2 speed is 1.20, which correspond to horizons at $f = -0.049$ and $f = -0.089$ respectively, which do not seem to be reached a second time.

5.5.2.3 Oscillations

A notable aspect of the black hole interior displayed in Figure 5.2 is the oscillation in f . The function $h = Ba$ also oscillates in a similar manner, but is 180 degrees out of phase. In addition, there are related oscillations in the curvature scalar and aether congruence behavior discussed below. These oscillations are reminiscent of the interior behavior found in Einstein-Yang-Mills black holes [97], where the metric functions and derivative of the Yang-Mills potential oscillate an infinite number of times before the singularity.

While N decreases monotonically and B increases monotonically, a goes to zero, so the oscillations of Na^2 and Ba arise because of variations in the magnitude of their derivatives. Since the oscillations inside $z = -2$ are not clearly visible in Figure 5.2, a zoomed in graph of $f(z)$ is provided in Figure 5.3. From this graph it is clear that f smoothly turns over at least once more before the singularity. Although the number of oscillations before the singularity appears finite, it is possible that the numerical integration employed is not capable of resolving additional or even infinitely more oscillations. More information may be obtained

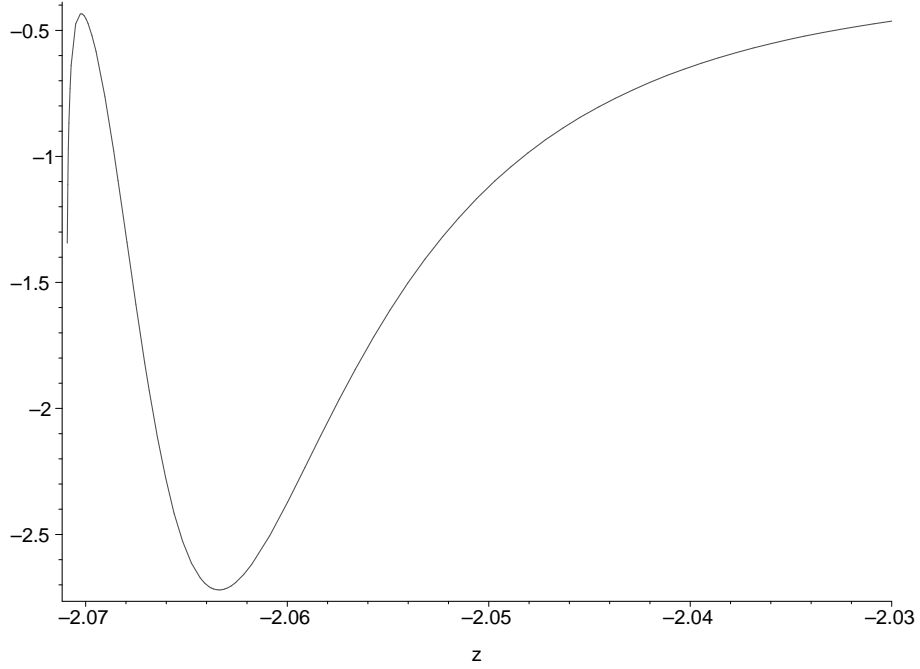


Figure 5.3: Oscillations of $f = Na^2$ near the singularity inside the black hole solution shown in Figure 5.2, plotted vs. $z = r - r_h$ in units with $M = 1$.

in the future by improved numeric methods or analytic methods around $r = 0$.

5.5.2.4 Curvature singularity

There appears to be a spacelike curvature singularity at or near $r = 0$, as in the Schwarzschild solution of GR. In Figure 5.2, the approach of N to negative infinity near $r = 0$ suggests a singularity. In Figure 5.4 the logarithm of the Kretschmann scalar $K = R_{abcd}R^{abcd}$ is plotted vs. $\ln r$ for the ae-theory solution together with its value in the corresponding Schwarzschild solution with the same mass. In the latter case $K = 48/r^6$ in units with $M = 1$, so $\log K = -6 \ln r + \ln 48$. The rate $d \ln K / d \ln r$ for the ae-theory solution seems to alternate between roughly -6 and -4.5 . The location of the transitions may be correlated with the oscillations

discussed above. The location of the singularity seems to be at $r = 0$ for all the

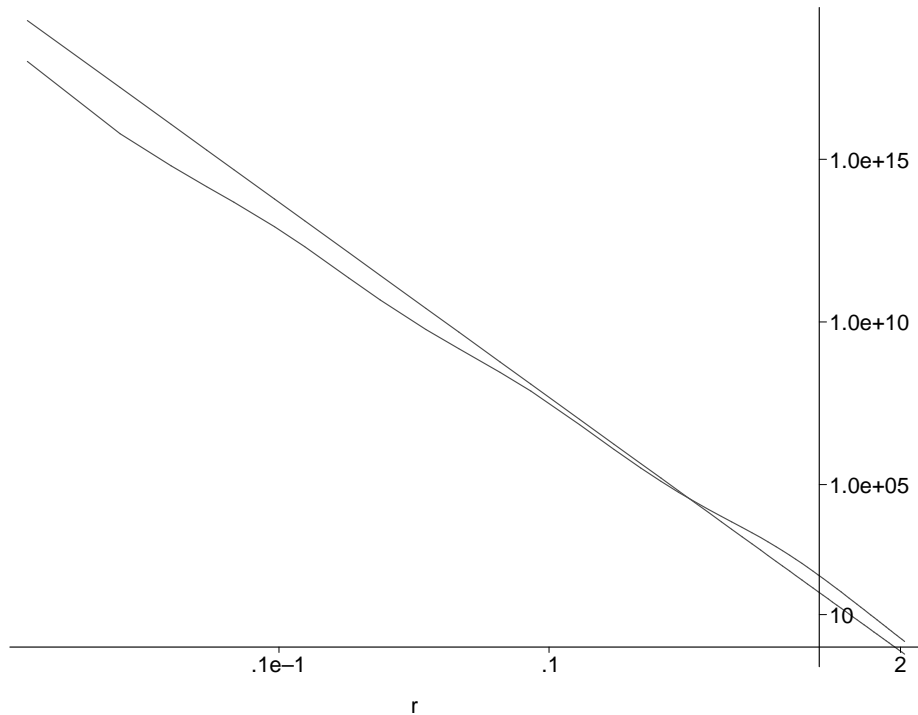


Figure 5.4: Plot of $\ln R_{abcd}R^{abcd}$ vs. $\ln r$ for $c_1 = 0.3$ ae-theory black hole (wiggly curve) and Schwarzschild black hole (straight line) of the same mass, in units with $M = 1$. r is plotted on a logarithmic scale. The slope for the GR case is -6 , while for the ae-theory case it alternates between roughly -6 and -4.5 .

values of c_1 , although the numerical solutions do not permit a determination of the exact location.

5.5.2.5 Aether congruence

The aether field defines a congruence of radial timelike curves at rest at infinity and flowing into the black hole. It is interesting to compare this with the static frame and with the congruence of freely falling radial geodesics with 4-velocity v^a that are also at rest at infinity. Being unit vector fields, at each point u^a and v^a can be fully characterized by their Killing energy, i.e. their inner product with the Killing

vector. The free-fall congruence has a conserved energy that is equal to one if the Killing vector is normalized to one at infinity. The aether does not fall as quickly outside the black hole. In fact it remains rather aligned with the Killing vector up until quite close to the horizon.

To characterize and contrast the free-fall and aether congruences we plot in Figure 5.5 the derivative $dr/d\tau$ of radius with respect to proper time along each congruence. Let us call this the quantity the “proper velocity”.² The aether and free-fall are both at rest at infinity, but only as the horizon is approached is the aether finally pulled away from the Killing direction. As close as $r = 3r_h$ ($z \approx 4$), the proper velocity of the aether is still about fifteen times smaller than that of free-fall. Inside the horizon the aether proper velocity is equal to the free-fall one around $z = -1.3$, but the 4-velocities do not agree there. The aether is still going inward faster, but its proper time is “running slower” so it can have the same proper velocity.

To compare the aether and free-fall motions inside the horizon we plot in Figure 5.6 the inward 3-velocity of the aether with respect to the free-falling frame.

The relative velocity is initially negative, meaning that the aether is not falling in as fast as the free-fall frame. It is clear from this plot at around $z = -1.3$ the

²The magnitude of this quantity is affected both by the radial motion and the behavior of the proper time. For instance as the particle becomes lightlike the proper time goes to zero and this derivative diverges. However we could think of no better measure of the radial velocity. One might use the 3-velocity relative to a static observer outside the black hole, but since the static observer becomes lightlike at the horizon, this 3-velocity will be equal to one at the horizon for *any* finite timelike 4-velocity, so it does not distinguish different motions there.

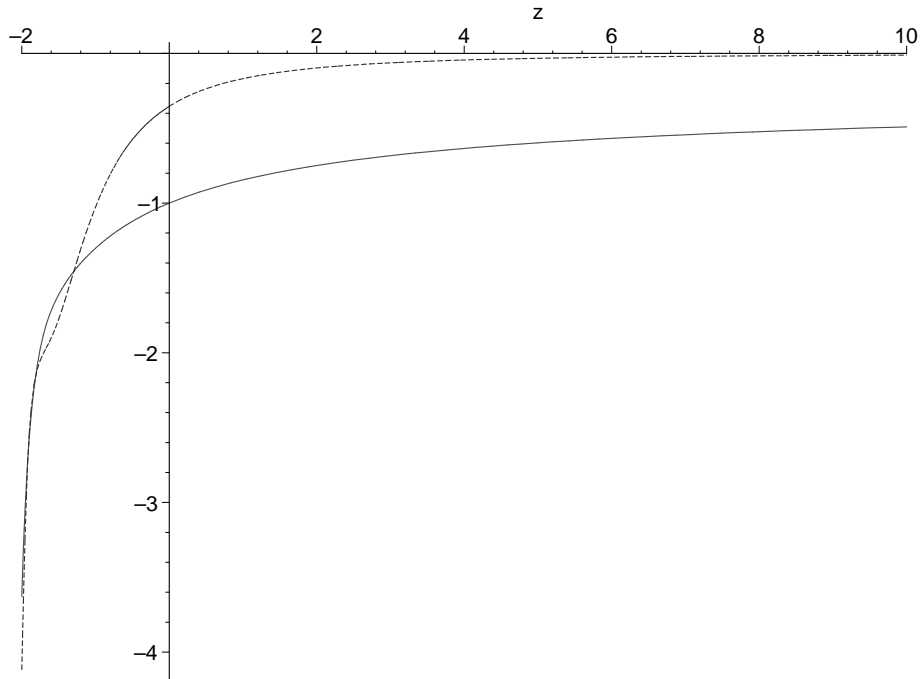


Figure 5.5: Radial proper velocity $dr/d\tau$ of free-fall (lower, solid curve) and aether (upper, dashed curve) vs. $z = r - r_h$, in units with $M = 1$, for $c_1 = 0.3$. In contrast to the free-falling geodesics, the aether does not begin to fall significantly inward until close to the horizon.

aether still lags well behind free-fall. However, around $z = -1.9$ the relative velocity is zero, and after that it oscillates a couple of times (at least) before reaching the singularity.

5.5.2.6 Surface gravity and the first law of black hole mechanics

The laws of black hole mechanics have been shown to apply to a wide class of generally covariant metric theories of gravity coupled to matter [98]. There appears to be no straightforward extension of the first law and the concept of black hole entropy to ae-theory however [49], a difficulty that is tied to the fact that there is no smooth extension of the aether to the bifurcation surface of the Killing horizon.

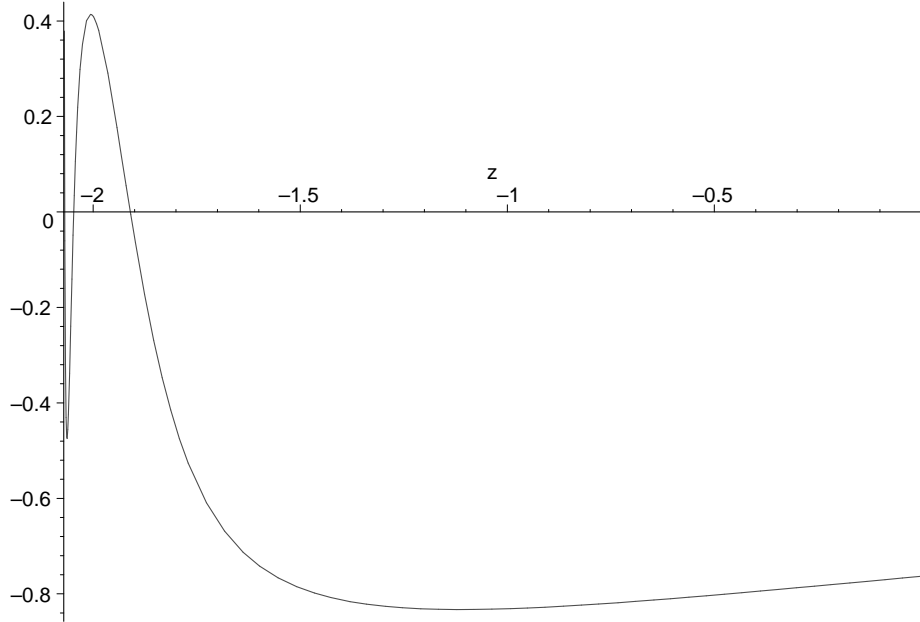


Figure 5.6: Inward 3-velocity of the aether relative to free-fall inside the horizon for $c_1 = 0.3$. The velocity is initially negative and the aether lags behind the free-fall. Near the singularity the velocity oscillates between faster and slower than free-fall.

Moreover, it is not clear to which horizon the law should apply, in a theory with multiple characteristic surfaces. For example, in the solutions considered in this section, the spin-2 horizon is inside the spin-1 horizon which is inside the joint spin-0 and metric horizon. One might imagine that the relevant horizon is always the Killing horizon, but recall that by a field redefinition we can make any one of these horizons be the Killing horizon. Some light will be shed on these puzzling issues in the next section, but for now we will just briefly examine the variational relation between mass, surface gravity and area of the spin-0 horizon, for possible future use.

The first law of black hole mechanics for spherically symmetric neutral black holes in GR takes the form

$$\delta M = \alpha \frac{\kappa \delta A}{8\pi G}, \quad (5.33)$$

where $A = 4\pi r_h^2$ is the horizon area, κ is the surface gravity, and $\alpha = 1$. By dimensional analysis such a variational relation must also hold in ae-theory, with some value for the dimensionless constant α that depends on the dimensionless coupling coefficients c_i . Presumably for M we should put the total energy E of the spacetime, and for “ G ” we should put the Newton constant G_N governing the attractive force between distant bodies. Alternatively one might use the ADM mass M_{ADM} and the constant G appearing in the ae-theory action (1.1). As discussed in Section 5.5.2.1, $GM_{ADM} = G_N E = r_0/2$, so these two choices actually yield identical “first laws”. If we express the mass and area in terms of r_0 and r_h respectively, (5.33) thus becomes

$$\delta r_0 = 2\alpha\kappa r_h \delta r_h. \quad (5.34)$$

It was also pointed out in Section 5.5.2.1 that r_0 and r_h are proportional, so one infers that α is determined by the dimensionless combination

$$\alpha = \frac{r_0}{2\kappa r_h^2}, \quad (5.35)$$

which depends on the coefficients c_i defining the theory.

5.5.2.7 Black hole properties for different values of c_1

Various properties of the black hole solutions for different values of c_1 are displayed in Table 5.1. The other coupling coefficients have the values $c_3 = c_4 = 0$ and c_2 is given by (5.31). For each c_1 there is a one-parameter family of black hole solutions with regular spin-0 horizon, labelled by horizon radius. For the values in the table we compare black holes with the same horizon radius, and adopt units

with $r_h = 1$. The Killing vector which enters the definition of κ and α is normalized to unity at spatial infinity.

Table 5.1: Properties of black hole solutions for several c_1 values, in units with $r_h = 1$.

c_1	$f'(r_h)$	$\gamma = u^a v_a$	r_0	κ	α
0.1	2.096	1.619	0.990	0.507	0.976
0.2	2.072	1.608	0.979	0.517	0.947
0.3	2.039	1.592	0.966	0.528	0.914
0.4	1.997	1.568	0.951	0.543	0.876
0.5	1.941	1.535	0.933	0.562	0.830
0.6	1.867	1.490	0.911	0.588	0.787
0.7	1.767	1.429	0.881	0.625	0.704

The values of $f'(r_h)$ that yield asymptotically flat solutions for different choices of c_1 are displayed in the 2nd column. These values decrease as c_1 grows. For $c_1 = 0.8$ and larger we could not find a $f'(r_h)$ that yielded an asymptotically flat solution. The third column shows the gamma factor between the aether and free-fall velocity at the horizon. The fourth column shows $r_0 = 2GM_{ADM}$. This is equal to r_h for $c_1 = 0$ (a Schwarzschild black hole), and decreases by 12% as c_i increases up to 0.7. Conversely, for a given mass the black hole horizon is larger for larger c_1 . The fifth column shows the surface gravity, which for $c_1 = 0$ is $1/2r_h$ and increases by 25% as c_1 increases up to 0.7. The last column is the dimensionless ratio (5.35) appearing in the first law (5.33), which is unity for $c_1 = 0$ and decreases by 30% as c_1 increases to 0.7.

5.6 Recent and related work on ae-theory black holes

This section will summarize recent and related results of further collaborative work on numerical collapse in ae-theory and on Lorentz violation and the GSL.

5.6.1 Numerical simulations of gravitational collapse

From an astrophysical point of view an essential question that emerges from the above work on black holes is what happens when matter collapses. It is a plausible conjecture that nonsingular spherically symmetric initial data will evolve to one of the regular black holes whose existence has been demonstrated here. In [93] David Garfinkle, Ted Jacobson, and I probed this conjecture by numerical evolution of the time-dependent spherically symmetric field equations. We added scalar matter that couples universally to the metric g_{ab} to form a collapsing pulse. A key first step done by Garfinkle was working out the initial value formalism for ae-theory. He specialized to the case (consistent with spherical symmetry, as was discussed previously) where the aether is hypersurface orthogonal. Numerical evolution requires the choice of surfaces of constant time and one can choose the time foliation orthogonal to u^a . Then in the 3+1 space-time decomposition of the metric u^a is identified with the unit normal n^a . This choice satisfies the unit constraint automatically and simplifies the computations of the aether stress tensor components such as $T_{ab}u^au^b$ and $T_{bc}h_a^cu^b$. Since the aether stress tensor (5.19) involves second derivatives of both the aether and metric, the usual form of the Hamiltonian and momentum constraints in GR is not applicable. Instead the metric and aether field

equations must be used together to solve for second time derivative terms, separating out new constraints and evolution equations.

For our study of scalar field collapse we considered a case where the parameters c_i satisfy the combined weak field constraints other than radiation damping

$$c_2 = \frac{c_3^2}{3c_1} - \frac{2c_1 + c_3}{3} \quad (5.36)$$

$$c_4 = \frac{-c_3^2}{c_1} \quad (5.37)$$

$$0 < c_{13} < 1 \quad (5.38)$$

$$0 < (c_1 - c_3) < \frac{c_{13}}{3(1 - c_{13})}. \quad (5.39)$$

We chose $c_1 = 1/3$ and $c_3 = 1/6$ (essentially in the midrange of the inequalities given above) and then determined c_2 and c_4 by the above equalities. This yields the set of coupling constant values

$$c_1 = \frac{1}{3}, \quad c_2 = -\frac{1}{4}, \quad c_3 = \frac{1}{6}, \quad c_4 = -\frac{1}{12}. \quad (5.40)$$

This choice of the constants c_i is different from those used above because the spin-0 speed in this theory is not 1. However, a field redefinition can be used to transform to a “frame” where the metric and spin-0 horizons agree. The results with the parameter choice (5.40) yield a theory with c_{13} and c_4 vanishing and $c_1 = 1/4$ and $c_2 = 1/2$. Since $c_3 = -c_1$, this new set of parameters falls in the $s_0 = 1$ class of time independent, spherically symmetric equations that can be numerically integrated (see Section 5.5.1). Therefore we can make a direct comparison of the black hole solutions discussed above with the end state of our numerical simulations of gravitational collapse.

For initial data Garfinkle used a moment of time symmetry and assumed the scalar field was a thin spherical shell initially at rest. The simulations show that for this data used the collapse does form a regular spin-0 horizon. Furthermore, outside of the spin-0 horizon the metric and aether field do settle down into a time independent state. In addition, all the scalar field either falls into the black hole or escapes, so that outside and near the horizon the time independent state is that of a pure Einstein-aether black hole with no matter other than the aether field u^a . We explicitly verified this by comparing plots of various metric quantities for both the static solution and numerical final state.

Garfinkle also performed simulations for the coupling constant choice used above in Section 5.5.1: Eqn. (5.31) with $c_3 = 0$. We again found good agreement between the final state solutions and the static solutions. Interestingly, regular black holes only formed for $c_i \leq 0.7$. For larger values of c_i the evolution became singular, forming a naked singularity. This is consistent with the results in Table 5.1, where we found the asymptotically flat boundary conditions could not be met for $c_i \geq 0.8$.

5.6.2 Generalized second law violation

As discussed in Section 5.33, there has not been much success in extending the first law of black hole mechanics and a definition of entropy to ae-theory black holes. The ae-theory is not alone in this difficulty. Apparently the root of the problem is the multiple characteristic surfaces that typically appear in Lorentz violating theories of gravity. In [99] Dubovsky and Sibiryakov noted that in these

theories ³ the multiple horizons would have different Hawking temperatures. They consider a situation where two different horizons radiate A and B particles such that $T_{A,\text{Hawking}} < T_{B,\text{Hawking}}$. Then two A and B shells that interact *only* with the A and B particles are placed around the hole. They show it possible to have

$$T_{B,\text{Hawking}} > T_{B,\text{shell}} > T_{A,\text{shell}} > T_{A,\text{Hawking}} \quad (5.41)$$

and balance the energy fluxes of A and B particles between the shells and hole. Thus, the state of the black hole is unchanged and heat must flow from colder A shell into the black hole and then from the black hole to hotter B shell, violating the second law. Dubovsky and Sibiriyakov considered 3 possible conclusions from their construction of the perpetual motion machine. The first was that some subtle, unaccounted for effect causes the state of the system to change such that entropy is actually increased. The second was that the usual derivation of the Hawking effect is incorrect. The third possibility was that the second violation is real and the high-energy completions of Lorentz violating theories have unusual properties.

In [94] I worked with Brendan Foster, Ted Jacobson, and Aron Wall to extend Dubovsky and Sibiriyakov’s work. We noted the perpetual motion machine might fail because: (a) the two A and B shells must interact gravitationally to come to equilibrium or (b) because of some classical or quantum instabilities of the “ergoregion” between the two horizons. We show (a) is ruled out because (5.41) can be maintained while increasing the black hole radius R and decreasing the shell temperatures such that the equilibration rate due to gravity is slower than the pump

³for simplicity they considered the case of the ghost condensate black hole [88]

rate. Since this process is equivalent to turning down the gravitational coupling, we argued the instabilities of (b) will also not be important.

Furthermore, we found that there is a completely classical process analogous to the Penrose process that violates the GSL. We considered a system of positive Killing energy composed of A and B particles falling into the black hole. We assume without loss of generality that A is coupled to the metric g_{ab} while B feels the effective metric $g_{ab} + \kappa u_a u_b$, where $\kappa > 1$ so that the effective B horizon is inside the metric horizon. When the system enters the ergoregion we showed it is possible to arrange a breakup so that the A particle falls into the B horizon with negative Killing energy while the B particle is ejected out of the A horizon. Since energy is conserved the A particle must have more energy than the original system and thus the black hole size is decreased. The GSL is violated by repeating this process many times over.

Since this process is classical and allows for any interactions between A and B particles, it can operate faster than Dubovsky and Sibiryakov's perpetuum mobile while evading any need to invoke the Hawking effect. We concluded that the only way GSL violation might be avoided is for the ultraviolet completion of LV theories to not admit black holes. This would eliminate the notion of a black hole (or more generally, horizon) entropy as a fundamental quantity associated with a causally disconnected region that hides information. Thus it appears that black hole thermodynamics and Lorentz violation cannot be reconciled.

5.7 Discussion

In this chapter we considered the meaning of a black hole in Einstein-Aether theory, arguing that the fastest wave mode must be trapped if the configuration is to qualify as a causal black hole. Regularity at the spin-0 horizon was identified as a key property of black holes in ae-theory. It was found that, for generic values of the coupling constants c_i , regularity at a metric horizon imposes no restrictions on spherically symmetric, static local solutions but regularity at a spin-0 horizon imposes one condition. At least for a class of coupling constants, there is a one-parameter family of asymptotically flat black hole solutions with all horizons (metric and spin-0,1,2) regular. We concluded by summarizing some recent work on numerical collapse in ae-theory and GSL violations associated with Lorentz violating black hole solutions.

It would be useful to pursue predictions of ae-theory that will be relevant for astrophysical settings and observational tests. For example, the nonrotating black hole solutions found here are very similar to the Schwarzschild solution of GR. Hence it is not likely that these could lead to significant constraints. In addition, astrophysical black holes are actually rapidly rotating.

It is quite conceivable that strong deviations from GR will be found for rapidly rotating black hole solutions. This is suggested by the presence of the ergoregion, in which the inertial frames are strongly dragged. The preferred frame aspects of ae-theory may be conspicuous here, due to larger gradients in the aether field. Also, unlike for the spherically symmetric non-rotating case, the spin-1 degrees of freedom

of the aether could be activated in the axially symmetric setting. To explore these issues would require finding numerical solutions describing rotating black holes in Einstein-aether theory.

A less ambitious program would to examine the static solutions beyond the special class of coupling coefficients studied here. This could use either improved analytical techniques or the collapse simulations of Garfinkle. The more mathematical aspects of the solutions, such as the study of negative mass and the oscillating behavior approaching the internal black hole singularity remain open research problems.

Finally, it would be interesting to continue to explore the consequences of our GSL violation, possibly in a quantum setting. A possible toy model that could be of some use is Einstein-aether theory in two-dimensions. This will be examined in the next chapter.

Chapter 6

Einstein-aether theory in two-dimensions

6.1 Introduction

In this chapter we will examine the two dimensional version of Einstein-aether theory. The idea of studying the theory in lower dimensions was initially rooted in hope that the spherical reduction of the four-dimensional theory would yield insights into the structure of the spherically symmetric field equations and their general solutions. The reduction proceeds by assuming the spacetime manifold is a direct product of a two-dimensional manifold and S^2 . In GR the resulting reduced action is that of dilaton gravity [100], depending on the two dimensional Ricci scalar and a scalar dilaton field Φ . In [101], Deser and Tekin discussed the further gauge choice $\Phi \sim r^2$ and special form of the two dimensional metric

$$ds^2 = a(r, t)b(r, t)^2 dt^2 - \frac{dr^2}{a(r, t)}. \quad (6.1)$$

Remarkably, this ansatz produces a simple action, which when varied with respect to $a(r, t)$ and $b(r, t)$ yields the correct field equations and Birkhoff's theorem. In ae-theory a similar reduction leads to dilaton gravity with one extra scalar "matter" field coming from the unit constrained aether. So far in this situation we have not been able to find a functional form of the metric and time independent aether that lead to a simplified set of field equations. Since the field equations are considerably

more complicated than in pure GR or even GR coupled to ordinary matter, it is not surprising that no simple gauge has yet been found.

Since the spherical reduction of ae-theory to two dimensions yields a complicated theory of dilaton gravity plus matter, it is possible that ae-theory in two-dimensions ab initio will be simple, yet non-trivial. A parameter count is useful. In two-dimensions pure GR has no content since since the Einstein-Hilbert action is topological. However, an additional unit vector field in two dimensions has one degree of freedom, so in this respect it is similar to a dilaton field. Like the dilaton, it turns out the presence of the vector field renders the theory non-trivial, but still with no local degrees of freedom.

Although dilaton gravity theories possess no local degrees of freedom, there exist for example black hole solutions [100, 102, 103, 104, 105], and when coupled to matter fields the theories acquire local dynamics. Thus, it is worthwhile to probe the character of 2-d ae-theory. The theory might provide a toy model in which to study aspects of quantum gravity. In particular, the presence of the unit timelike vector field might ameliorate or modify the problem of time in the canonically quantized setting. The vector also defines an intrinsic preferred frame with which for example the impact of Lorentz violation on black hole evaporation could be studied.

In this chapter we will show Einstein-aether theory does provide a different two dimensional gravity model than any previously considered. It possesses both constant and non-constant curvature solutions. Unlike the simple Jackiw-Teitelboim [106] dilaton model the constant curvature is not specified a priori by the action. In this regard it is similar to two-dimensional unimodular gravity [107], but unlike

in unimodular gravity the *sign* of the curvature scalar is determined by the action. Also it has the unit vector field, which defines in each solution a locally preferred frame.

6.2 1+1 dimensional action

The action for Einstein-aether theory in n dimensions is

$$S[g_{ab}, u^a, \lambda] = \frac{-1}{16\pi G} \int d^n x \sqrt{-g} (R + L_u + \lambda(g_{ab}u^a u^b - 1)), \quad (6.2)$$

where R is the Ricci scalar, λ is a Lagrange multiplier enforcing the unit timelike constraint on u^a , and the aether Lagrangian is defined by

$$L_u = c_1(\nabla_a u_b)(\nabla^a u^b) + c_2(\nabla_a u^a)^2 + c_3(\nabla_a u_b)(\nabla^b u^a) + c_4(u^a \nabla_a u^b)(u^c \nabla_c u_b) \quad (6.3)$$

where the c_i are dimensionless coupling constants, and λ is a Lagrange multiplier.

In two-dimensional spacetime the variation of the Einstein-Hilbert term $\sqrt{-g}R$ is a total divergence. The aether part of the action is non-trivial, but only two of the terms are independent. To see this one can express the covariant derivative $\nabla_a u_b$ in the orthonormal basis $\{u^a, s^a\}$, where s^a is a unit spacelike vector orthogonal to u^a . It follows from $u^a u_a = -s^a s_a = 1$ and $u^a s_a = 0$ that $0 = u^b \nabla_a u_b = s^b \nabla_a s_b = u^b \nabla_a s_b + s^b \nabla_a u_b$ everywhere. Using these relations, we find that when the unit constraint is satisfied the covariant derivatives take the form

$$\nabla_a u_b = A s_a s_b + B u_a s_b, \quad (6.4)$$

$$\nabla_a s_b = A s_a u_b + B u_a u_b. \quad (6.5)$$

where A and B are generically spacetime functions. Using (6.4) we obtain

$$(\nabla_a u_b)(\nabla^a u^b) = A^2 - B^2 \quad (6.6)$$

$$(\nabla_a u_b)(\nabla^b u^a) = A^2 \quad (6.7)$$

$$(\nabla_a u^a)^2 = A^2 \quad (6.8)$$

$$(u^a \nabla_a u^b)(u^c \nabla_c u_b) = -B^2 \quad (6.9)$$

$$F_{ab} F^{ab} = -2B^2, \quad (6.10)$$

where $F_{ab} = \nabla_a u_b - \nabla_b u_a$. These expressions may be substituted into the Lagrangian (6.3) without changing the equations of motion, since the Lagrange multiplier term in the action (6.2) implies that the equations of motion are equivalent to the condition that the action be stationary only with respect to variations of u^a that preserve the constraint $u^a u_a = 1$. On the constraint surface the Lagrangian is thus given by

$$L_u = c_{123} A^2 - c_{14} B^2, \quad (6.11)$$

where $c_{123} \equiv c_1 + c_2 + c_3$ and $c_{14} \equiv c_1 + c_4$. Using (6.8) and (6.10) the Lagrangian can therefore be written for example as

$$L_u = \frac{1}{2} c_{14} F^{ab} F_{ab} + c_{123} (\nabla_a u^a)^2, \quad (6.12)$$

without any loss of generality in the theory.

It turns out that if either c_{14} or c_{123} vanishes the theory is under-deterministic. We thus assume in the remainder of this chapter that neither c_{14} nor c_{123} is zero. The classical equations of motion then depend only on the one combination c_{123}/c_{14} of the coupling coefficients.

The action can be further simplified by the field redefinitions discussed in Section 5.3,

$$\begin{aligned} g_{ab} &= g'_{ab} + (\sigma - 1)u'_a u'_b \\ u^a &= \sigma^{-1/2} u'^a, \end{aligned} \tag{6.13}$$

where the coefficient σ must be positive in order to preserve Lorentzian signature. These redefinitions preserve the general form of the action given in (6.2), the overall effect being only a change of the coupling constants,

$$S[g_{ab}, u^a, c_i] = S[g'_{ab}, u'^a, c'_i(c_i, \sigma)]. \tag{6.14}$$

The relation between c'_i and c_i was found by Foster [71], and using this one can show that in any spacetime dimension c_{14} is invariant and c_{123} simply scales by the nonzero factor σ^{-1} . Thus no field redefinition will make one of the terms in (6.11) or (6.12) vanish. On the other hand, the choice $\sigma = c_{123}/c_{14}$ (which is allowed as long as it is positive) will produce $c'_{14} = c'_{123}$, in which case using (6.6) the Lagrangian may be reduced to just one term of the original four-term Lagrangian (6.3),

$$L_{u,\text{reduced}} = c'_{14}(\nabla_a u_b)(\nabla^a u^b) = c'_{14}(F^{ab}F_{ab} + (\nabla_a u^a)^2). \tag{6.15}$$

In terms of the new fields the classical equations of motion are thus totally independent of the coupling parameters. We will obtain the solutions for the general case when c_{123}/c_{14} is positive by applying the field redefinition to solutions of this reduced theory.

6.3 Field equations and solutions

In this section we will study the general two-dimensional theory described by the action with Lagrangian (6.12), to obtain the field equations and the curvature of their solutions.

The Lagrangian takes the form

$$L_u = c_{14} \left(\frac{1}{2} F^{ab} F_{ab} + \beta (\nabla_a u^a)^2 \right), \quad (6.16)$$

where

$$\beta = c_{123}/c_{14}. \quad (6.17)$$

The equations of motion depend on the couplings only through the combination β defined in (6.17). Varying with respect to the inverse metric g^{ab} and the covariant aether vector u_a as independent field variables, one finds the metric field equation

$$\begin{aligned} F_{am} F_b^m &- \frac{1}{2} g_{ab} \left(\frac{1}{2} F^{ab} F_{ab} - \beta (\nabla_c u^c)^2 - 2\beta u^m \nabla_m (\nabla_c u^c) \right) \\ &- 2\beta u_{(a} \nabla_{b)} \nabla_c u^c + \lambda u_a u_b = 0 \end{aligned} \quad (6.18)$$

and the aether field equation

$$\nabla_b F^{ba} + \beta \nabla^a (\nabla_c u^c) - \lambda u^a = 0, \quad (6.19)$$

where λ is a re-scaled Lagrange multiplier (*cf.* eqn. (6.2)). These amount to three equations from (6.18) and two from (6.19). The u^a component of the latter determines λ . Using the expansion of the covariant derivatives (6.4,6.5) to project out the various components of the field equations we find that the remaining four

equations are equivalent to

$$\begin{aligned} uA &= f & sA &= 0, \\ uB &= 0 & sB &= \beta f \end{aligned} \tag{6.20}$$

where (for example) $uA \equiv u^m \nabla_m A$, and

$$f \equiv \frac{1}{2}(A^2 - \beta^{-1}B^2). \tag{6.21}$$

The equations (6.20) are extremely restrictive, and there are just two types of solutions. In the first type both A and B are constant and related by $B^2 = \beta A^2$ so that $f = 0$. In the second type of solution the gradients $\nabla_a A$ and $\nabla_b B$ are both non-zero and independent. In this case A and B may be used as coordinates, so one can immediately write the unique solution,

$$u = f \partial_A \quad \text{and} \quad s = \beta f \partial_B. \tag{6.22}$$

The inverse metric is given by $g^{ab} = u^a u^b - s^a s^b$, hence for this solution the line element is

$$ds^2 = \frac{4}{(\beta A^2 - B^2)^2} (\beta^2 dA^2 - dB^2). \tag{6.23}$$

The scalar curvature R completely characterizes the curvature in two-dimensions.

Using the relation

$$R = 2u^a (\nabla_b \nabla_a - \nabla_a \nabla_b) u^b \tag{6.24}$$

which is valid in two-dimensions, and making use of (6.4) and (6.5), we find

$$R = 2(B^2 - A^2 + uA + sB). \tag{6.25}$$

When the field equations (6.20) are satisfied the scalar curvature is thus given by

$$R = (\beta - 1)A^2 + (1 - \beta^{-1})B^2. \quad (6.26)$$

The solutions with constant A and B have constant curvature. Being two dimensional, they are therefore either Minkowski, de Sitter, or anti-de Sitter space, and have three independent Killing vectors. The solution (6.23) has non-constant curvature unless $\beta = 1$, in which case it is flat. For $\beta \neq 1$ it can be shown that (6.23) has no Killing vectors. For $\beta > 1$ the curvature scalar is positive, for $0 < \beta < 1$ it is negative, and for $\beta < 0$ it is indefinite.

In the case $\beta < 0$ the function f defined in (6.21) can only vanish when both A and B vanish; hence the only solution with constant A and B is the one with $A = B = 0$. In this solution the metric is flat, and according to (6.4) the vector field u^a is then constant. The only other solution in this case is (6.22, 6.23). The curvature scalar for this metric with $\beta < 0$ is zero on the lines $|B| = |A|(1 - \beta)/(1 - \beta^{-1})$, negative for smaller $|B|/|A|$ and positive for larger $|B|/|A|$. It vanishes at $A = B = 0$, which lies at infinite distance diverging as $1/A$ on any non-null line $A/B = \text{const}$. There is a curvature singularity as either A or B goes to infinity, except on the lines where the curvature vanishes, and the geodesic distance to this singularity is finite.

In the next section we summarize the nature of the solutions for the special case $\beta = 1$, and the following section summarizes the case $0 < \beta \neq 1$. Since the Lagrangian with $\beta > 0$ can be reached by a field redefinition from the $\beta = 1$ case, the solutions for general positive β can be obtained by field redefinition from the $\beta = 1$ solutions.

6.4 $\beta = 1$: Flat spacetime solutions

To characterize the solutions in the case $\beta = 1$, for which the curvature vanishes, we adopt null coordinates (w, v) , so

$$ds^2 = dw dv \quad (6.27)$$

$$u = F\partial_w + F^{-1}\partial_v \quad (6.28)$$

where $F(w, v)$ is to begin with an arbitrary function. Using the field equations in the form (6.20) with $\beta = 1$, it follows that the general solution is

$$F = (a + bw)/(c + dv), \quad (6.29)$$

where a, b, c, d are constants. Thus there are four classes of solutions for u^a , corresponding to whether or not the constants b and d vanish. Up to constant coordinate shifts and opposite scalings of w and v (which preserve the Minkowski metric (6.27)) these four solutions have (w, v) components

$$(1, 1) \quad (6.30)$$

$$(kw, (kw)^{-1}) \quad (6.31)$$

$$((kv)^{-1}, kv) \quad (6.32)$$

$$(w/v, (w/v)^{-1}) \quad (6.33)$$

where k is a constant with dimensions of inverse length that sets a physical scale for the solution.

The first solution (6.30) is simply a constant vector field covering the entire Minkowski spacetime. In this solution A and B both vanish. The second and third

solutions (6.31) and (6.32) are equivalent to each other with the roles of w and v reversed. For the solution (6.31) one finds that $A = -B = -k$, so these are solutions of the type with A and B constant. In the solution (6.31) the vector field u^a is non-singular in regions covering one-half of the flat Minkowski manifold, either $w > 0$ or $w < 0$. Fig. 6.1 shows the flow lines of the aether on Minkowski space.

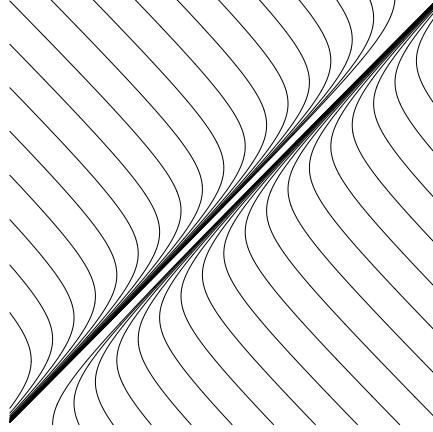


Figure 6.1: Plot of the flow lines of (6.31) in Minkowski space with Cartesian coordinates t (increasing vertically) and x (increasing toward the right). The u^a field approaches the null vector ∂_v along the line $w = t - x = 0$, hence must be infinitely stretched there in order to maintain the unit constraint.

These curves are hyperbolae, as can also be seen from the fact that the acceleration vector $u^a \partial_a u^b$ has a constant squared norm $-k^2$.

The solution (6.31) is further characterized by its symmetries. The commutator of the two flat spacetime Killing vectors that commute with u^a is

$$[w\partial_w - v\partial_v, \partial_v] = \partial_v. \quad (6.34)$$

These generate a non-abelian sub-algebra of the Poincare algebra in 1+1 dimensions. This sub-algebra is isomorphic to the algebra of the affine group $A(1)$ of translations and scalings in one dimension. It will re-appear in the next section as a sub-algebra

of the 2+1 dimensional Lorentz group when we relate this solution to a constant curvature one via a field redefinition.

For the fourth solution (6.33) we find that now

$$\begin{aligned} A &= -w^{-1} - v^{-1} \\ B &= -w^{-1} + v^{-1}. \end{aligned} \tag{6.35}$$

These are not constant, so this solution corresponds to the solution (6.22, 6.23) with $\beta = 1$. A plot showing the aether flow lines in a part of the Minkowski space is shown in Fig. 6.2.

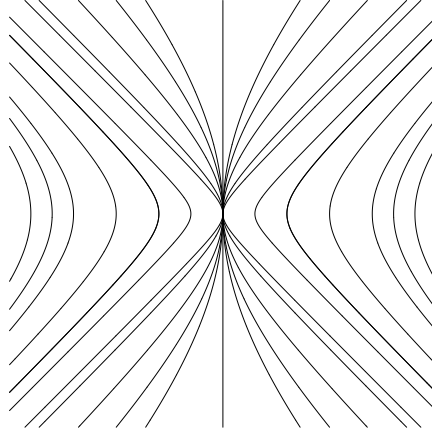


Figure 6.2: Plot of the flow lines of (6.33) in Minkowski space with Cartesian coordinates t and x . Here the aether is singular along the lines $w = t - x = 0$ and $v = t + x = 0$.

The vector field u^a in this solution is singular on both lines $w = 0$ and $v = 0$, stretches infinitely as either v or w goes to infinity and does not have constant acceleration. Unlike the previous case, this u^a field commutes with none of the Killing vectors of the flat metric.

This completes the summary of the solutions in the special case when the

coupling constants satisfy $\beta = 1$, for which the metric is flat. Next we turn to the solutions for general $\beta > 0$.

6.5 $0 < \beta \neq 1$ solutions

To obtain the general solutions for the theory when $0 < \beta \neq 1$ one can use the field redefinition (6.13) with $\sigma = \beta$,

$$\begin{aligned} g_{ab} &= \eta_{ab} + (\beta - 1)u'_a u'_b \\ u^a &= \beta^{-1/2} u'^a. \end{aligned} \tag{6.36}$$

If (η_{ab}, u'^a) is a solution to the theory with $\beta = 1$ then (g_{ab}, u^a) is a solution with arbitrary positive $\beta = c_{123}/c_{14}$. Conversely, every solution of the $\beta \neq 1$ theory can be obtained in this way. We apply this method to the three different types of solutions found in the previous section.

For the constant vector field solution (6.30) the primed metric components remain constant, as do those of the aether, so after the field redefinition one still has the trivial solution of a constant aether in a flat spacetime.

In the next two subsections we consider the solutions obtained by field redefinition from the other two types of solutions, first (6.33) and next (6.31) and (6.32).

6.5.1 Non-constant curvature solution

Using the redefinition (6.36) with the primed solution (6.33) we find

$$ds^2 = \frac{1}{4}(\beta - 1)(w/v)^2 dw^2 + \frac{1}{2}(\beta + 1)dw dv + \frac{1}{4}(\beta - 1)(v/w)^2 dv^2 \tag{6.37}$$

and

$$u = \beta^{-1/2}(w/v\partial_w + (w/v)^{-1}\partial_v). \quad (6.38)$$

This solution corresponds again to the non-constant curvature solution (6.23). The scalar curvature of the new metric (6.37) is

$$R = 2(1 - \beta^{-1})(w^{-2} + v^{-2}). \quad (6.39)$$

As discussed in Section 6.4, none of the flat-spacetime Killing vectors commute with this u^a , from which it follows that no Killing vector of g_{ab} could commute with u^a . Moreover, g_{ab} has no Killing vectors at all, as mentioned previously. Thus, we could find no simple, concise way to characterize this spacetime. According to (6.39) the curvature can be both zero and infinite depending on w and v . When w or v vanishes the metric (6.37) has a curvature singularity. In the same limits u^a aligns with either ∂_w or ∂_v , which are null vectors when respectively w or v equals zero. Thus, for this solution, the scalar curvature becomes singular exactly on the horizons where u^a must be infinitely stretched. One can show that the distances to these regions are infinite.

6.5.2 Constant curvature solutions

Under the field redefinition (6.36) the second type of solution (6.31) produces the metric

$$ds^2 = \frac{1}{4}(\beta - 1)(kw)^{-2}dw^2 + \frac{1}{2}(\beta + 1)dw dv + \frac{1}{4}(\beta - 1)(kw)^2dv^2 \quad (6.40)$$

and re-scaled u^a

$$u = \beta^{-1/2}(kw\partial_w + (kw)^{-1}\partial_v). \quad (6.41)$$

This solution corresponds to the general type with constants $A = -\beta^{-1/2}k$ and $B = k$, and the scalar curvature of the new metric (6.40) is

$$R = 2(1 - \beta^{-1})k^2, \quad (6.42)$$

The curvature is constant, so the geometry is locally that of de-Sitter (dS) for $0 < \beta < 1$ and anti-de-Sitter (AdS) space for $\beta > 1$ (Recall that we use the metric signature $(+-)$, so the scalar curvature for dS is negative while for AdS it is positive.) The nature of these maximally symmetric spaces is well-known, so to fully describe these solutions we need only specify the behavior of the u^a vector field on the dS/AdS background. This behavior is illustrated for the case of de Sitter and anti-de Sitter spaces in Fig. 6.3 and Fig. 6.4. In the remainder of this chapter we will describe the properties of this solution.

First note that since

$$u^a \nabla_a u_b = u^a (A s_a s_b + B u_a s_b) = k s_b \quad (6.43)$$

the magnitude of the acceleration of the flow of u^a with respect to g_{ab} is constant and equal to k , as is that of u'^a with respect to η_{ab} . Since ∂_v is a null vector when $w = 0$ and similarly ∂_w is null when $w \rightarrow \pm\infty$, from (6.41), it is clear that u^a is singular on one of the dS/AdS horizons labelled by $w = 0$, where it is infinitely stretched in order to remain unit timelike as it approaches a null vector. It is also infinitely stretched as w approaches $\pm\infty$. The aether is thus regular in either of the two coordinate patches $w > 0$ or $w < 0$. It is not immediately clear to which regions of dS/AdS these patches correspond. We will address this shortly with the

help of new coordinates better adapted to the dS/AdS metric. We will focus on the dS case first, and indicate the corresponding results for AdS at the end.

6.5.2.1 $\beta < 1$: de Sitter solution in adapted coordinates

One can show that the set of Killing vectors under which the aether is invariant is identical to the Killing vectors of η_{ab} (6.34) that commute with u^a . Therefore these must generate a two dimensional non-Abelian subgroup of $SO(2, 1)$, which is the symmetry group in the 2+1 dimensional embedding space that preserves the 1+1 dimensional dS hyperboloid. The only two-dimensional non-Abelian subalgebras of $SO(2, 1)$ are generated by a boost and a *null rotation*, for example

$$[\mathbf{K}_1, \mathbf{J} + \mathbf{K}_2] = \mathbf{J} + \mathbf{K}_2, \quad (6.44)$$

where \mathbf{J} is the generator of rotations and $\mathbf{K}_{1,2}$ generate boosts. This coincides with the flat spacetime algebra (6.34), and so reveals the geometrical nature of the symmetry group of our solutions. The flow lines of this null rotation on the hyperboloid are the intersections of null planes with the embedded hyperboloid. The idea is to reexpress the dS solution in the “planar” coordinate system adapted to the generator of null rotations. This will help to illustrate the nature of the aether field in this solution and exhibit which patch of dS is covered by a nonsingular aether.

In planar coordinates (t, x) the unit dS hyperboloid $(X^0)^2 - (X^1)^2 - (X^2)^2 = -1$ is described by the embeddings

$$\begin{aligned} X^0 &= -\sinh t - \frac{1}{2}x^2 e^t \\ X^1 &= -\cosh t + \frac{1}{2}x^2 e^t \end{aligned}$$

$$X^2 = xe^t \tag{6.45}$$

[108]. Lines of constant t are the flow lines associated with the null rotation discussed above. The full range of t in $(-\infty, \infty)$ foliates half of the hyperboloid. Using $ds^2 = (dX^0)^2 - (dX^1)^2 - (dX^2)^2$ with (6.45) the induced 1+1 dimensional metric on the hyperboloid is found to be

$$ds^2 = dt^2 - e^{2t} dx^2. \tag{6.46}$$

Thus, in planar coordinates the null rotation symmetry generated by ∂_x is manifest.

One can find a coordinate transformation from the metric (6.40) to the planar form. After this transformation the aether (6.41) takes the form

$$u = (1 - \beta)^{-1/2} (\partial_t - \beta^{1/2} e^{-t} \partial_x), \tag{6.47}$$

with flow lines

$$x - \sqrt{\beta} e^{-t} = \text{const.} \tag{6.48}$$

In terms of the embedding coordinates (6.45), the flow lines are given by the intersections of the planes

$$\frac{X^2 - \sqrt{\beta}}{X^0 + X^1} = \text{const.} \tag{6.49}$$

with the de Sitter hyperboloid.

To further visualize how the aether flow behaves and what part of de Sitter spacetime it covers in a nonsingular manner, we transform to global Robertson-Walker coordinates (T, φ) , which in two-dimensions arise from foliating the hyperboloid with circles. These are related to the embedding coordinates $X^{0,1,2}$ of (6.45)

via

$$\begin{aligned}
X^0 &= \sinh T \\
X^1 &= \cosh T \cos \varphi \\
X^2 &= \cosh T \sin \varphi,
\end{aligned} \tag{6.50}$$

and they yield the line element

$$ds^2 = dT^2 - \cosh^2 T d\varphi^2. \tag{6.51}$$

In these coordinates only the rotation symmetry generated by \mathbf{J} is manifest. The ranges $T \in (-\infty, \infty)$ and $\varphi \in (-\pi, \pi)$ cover the entire manifold.

If we introduce the new coordinate τ via $\cosh T = \sec \tau$, the metric takes the conformally flat form

$$ds^2 = \sec^2 \tau [d\tau^2 - d\varphi^2], \tag{6.52}$$

and the finite range of $\tau \in (-\pi/2, \pi/2)$ covers the entire manifold. In these coordinates the flow lines (6.48) are given by

$$\frac{\sin \varphi - \sqrt{\beta} \cos \tau}{\cos \varphi + \sin \tau} = \text{const.} \tag{6.53}$$

and are plotted in Fig. 6.3.

The aether is regular in the planar coordinate system, which covers the triangle with solid grey edges. On these edges u^a becomes infinitely stretched as it approaches a null direction. The solid grey lines form the past horizon part of the Killing horizon for the boost symmetry under which the aether is invariant, while the dashed grey lines form the future horizon part. The aether cannot possibly be regular at the

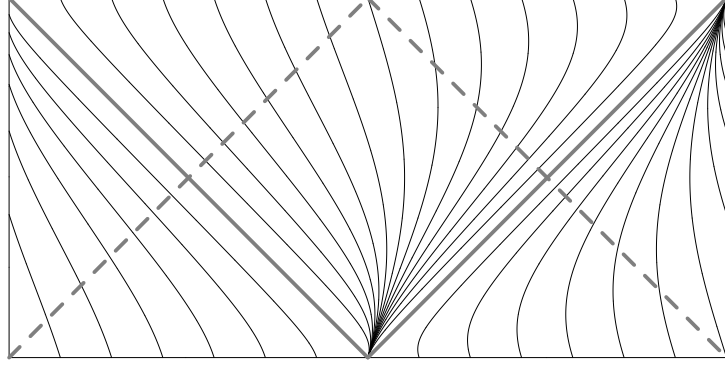


Figure 6.3: Conformal diagram of 1+1 dS spacetime with the flow lines of the aether field. Horizontal lines at the top and bottom represent null infinity, while the two vertical lines at left and right are identified. The solid and dashed grey lines form the past and future horizons of the Killing horizon for the boost symmetry under which the aether is invariant. The slope of the flow lines is $-\beta^{-1/2}$ on all boundaries of the diagram which is drawn for the case $\beta = 0.1$.

bifurcation points where the past and future horizons intersect, since these are fixed points of the Killing flow; hence a unit timelike vector cannot be invariant there. (A similar circumstance occurs in the context of the 3+1 dimensional black hole solutions discussed in Chapter 5.) However, the aether is regular on the horizon to the future of the bifurcation points. This solution therefore provides a setting with a nonsingular aether flowing across a future horizon.

6.5.2.2 $\beta > 1$: Anti-de Sitter solution

When $\beta > 1$ the curvature scalar (6.42) is positive, hence (with our signature choice) the constant curvature solutions for this theory correspond to anti-de Sitter space. In two dimensions dS and AdS are exactly the same spacetime locally, only with a reversal in the identification of what are the timelike and spacelike directions. Rather than going through the details we simply remark here that the aether solution

for the AdS case can be obtained from the dS case by interchanging the planar t and x coordinates. This leads to the AdS metric in Poincaré coordinates, covering the so-called “Poincaré patch”, and to the u^a field appropriate to the AdS space. The flow lines of the aether are again given in the embedding coordinates by (6.49), only now with $\beta > 1$. In Fig. 6.3 we plot this flow and the Killing horizons in a conformal diagram for AdS. To avoid closed timelike curves we can pass to the covering space as is usually done, in which case the diagram should be extended infinitely in the vertical direction.

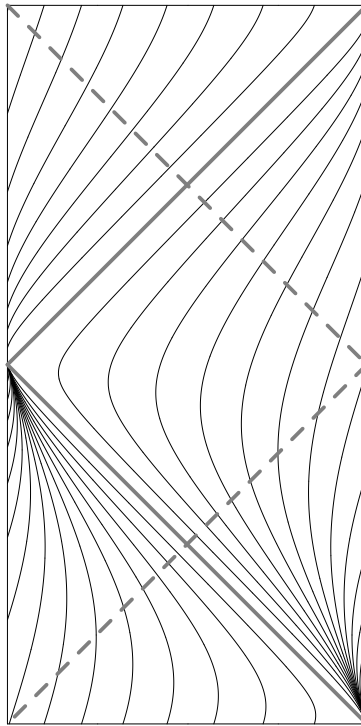


Figure 6.4: Conformal diagram of 1+1 AdS spacetime with the flow lines of the aether field. The two vertical lines at left and right are at null infinity, and the diagram should be continued infinitely in the vertical direction. The aether is regular in the Poincaré patch bounded by the solid grey lines and null infinity. The dashed grey lines are the rest of the boost Killing horizon. The diagram is drawn for the case $\beta = 10$.

6.6 Discussion

In this chapter we have shown that the general Einstein-aether action can be parameterized by two coupling constants in 1+1 dimensional spacetime, and the classical equations of motion depend only on one combination β of these. Hence there is a one-parameter family of classical theories. Using a field redefinition of the metric, we demonstrated that for $\beta > 0$ the theory can be reduced to a form involving only one coupling constant which does not affect the classical solutions. The only solutions to this reduced theory are a flat metric together with one of three distinct types of solutions for the aether field. Via the inverse field redefinition these produce all solutions for the generic theory, namely (i) flat spacetime with constant aether, (ii) constant curvature spacetimes with a uniformly accelerated u^a invariant under a two-dimensional symmetry group generated by a boost and a null rotation, and (iii) a non-constant curvature spacetime that has no Killing symmetries and contains singularities. The sign of the curvature is determined by whether the coupling β is less or greater than one. For $\beta < 0$ only the solutions (i) and (iii) are present.

Unlike in dilaton gravity, there are no asymptotically flat black hole solutions, although the de Sitter and anti-de Sitter solutions possess Killing horizons that could allow issues of black hole thermodynamics to be studied. This classical study of the behavior of Einstein-aether theory in 1+1 dimensions may provide a starting point for further investigations into semiclassical and fully quantum toy models of quantum gravity with a dynamical preferred frame.

Chapter 7

Conclusion

7.1 Summary of Results

This work focused first on energy in ae-theory and then examined non-linear spherically symmetric solutions, particularly those that describe neutron stars and black holes. Comparing neutron star properties to observations results in a tentative constraint on c_{14} . Since stationary black holes in ae-theory have properties very similar to Schwarzschild black holes in GR, no new constraints are currently available. We also studied the solutions to Einstein-aether theory in two-dimensions, which could be a toy model for future work on gravitational Lorentz violation. To summarize the contents explicitly:

In Chapter 2, we studied pseudotensor methods and described their relationship to Wald’s covariant Noether charge approach. The modified Weinberg and Einstein pseudotensors appropriate for ae-theory were used to find the energy density of the linearized “massless” wave modes characterized by Jacobson and Mattingly [41]. Constraining the four dimensionless coupling parameters c_i such that these energy densities are positive yields an important constraint. When combined with other weak field constraints [38, 43], only a one parameter family of theories is observationally viable.

We also used the Einstein pseudotensor to find the total energy of an as-

ymptotically flat spacetime. The result is that the ADM mass of GR is simply renormalized by a c_{14} dependent factor. However, a general positive energy theorem for this energy remains an open question. To initialize work on this difficult problem we probed some special cases.

In Chapter 3, we started work on the vacuum non-linear solutions to the theory by considering the case of time independent spherical symmetry. We demonstrated Birkhoff's theorem does not apply here and showed generically there is a three parameter family of solutions and a two parameter subset of these is asymptotically flat. We then specialized to the simplest case where the aether field is aligned with the timelike Killing vector. These static aether solutions are quite similar to the Schwarzschild solution of GR asymptotically, but in the interior they have an interesting wormhole-like behavior before reaching a null singularity on a Killing horizon.

In Chapter 4, we demonstrated that the static aether solutions are the unique vacuum solutions outside stars and the interior must also be static for the solutions to match across the stellar surface. We used numerical integration in the interior to find various properties for constant density stars and six realistic neutron star equations of state. The key results are that maximum stellar masses are smaller than in GR while surface redshifts are larger as the coupling constant combination c_{14} increases. If the equation of state of dense matter were known to good accuracy these results could be used to put a firm constraint on c_{14} . Future data from large X-ray telescopes may be able to measure masses and radii of various neutron stars, possibly providing a joint constraint on the equation of state and c_{14} .

In Chapter 5, we used numerical integration to find that ae-theory has regular black hole solutions, at least for some range of the c_i coupling constants. In these solutions the aether field is not aligned with the static Killing vector. In the exterior, the geometry is close to Schwarzschild even for fairly large c_i : for example, the ISCO radius for $c_1 = 0.3$ differs only by about 1%. In the interior, the geometry approaches a spacelike singularity at the origin, yet there is some interesting mathematical behavior, involving oscillations of certain functions.

Recent work with collaborators on further research into the nature and consequences of the black hole solutions was also summarized. In [93] we found that the endstates of the time dependent collapse of simple scalar pulses are the static black holes found earlier in Chapter 5. This is a further test showing that realistic astrophysical black holes could form in the theory. Also consistent with the static results is the discovery that if the c_i are too large the collapse forms a naked singularity. In [94] my collaborators and I discussed a general classical Penrose-like process in Lorentz violating black hole systems that violates the GSL. This seems to show that LV is not compatible with black hole thermodynamics, a result which could have deep implications for the theoretical consistency of Lorentz violating theories.

In Chapter 6, we investigated two-dimensional Einstein-aether theory, finding a set of non-trivial solutions. These included constant curvature solutions where the aether is uniformly accelerated and non-constant curvature solutions with exotic geometries. The constant curvature dS/AdS solutions could be used as a toy model for studying Hawking radiation and quantization in the LV setting.

7.2 Reflections and Future Directions

Since ae-theory violates Lorentz symmetry and has a complicated derivatively coupled structure where a number of theoretical inconsistencies could arise, the ability of a class of theories to pass a variety of observational and theoretical tests is remarkable. It has been an excellent “sparring partner” for Einstein’s GR, providing insights into Lorentz violating physics. At the end of the individual chapters we discussed a variety of specific areas for future research, including some more mathematically motivated problems. Here we will discuss what I feel are the most important future directions in observation and theory.

Other non-linear solutions to ae-theory will be crucial to new strong-field tests, although it will probably require more involved numerical work to solve the field equations. Rapidly rotating black hole solutions analogous to the Kerr solution, if they exist, should have properties that deviate more strongly from GR. In addition, since compact objects in the cosmos are rotating, direct comparisons to black holes and neutron stars could be made in the near future by observations of gravitational waves and X-ray sources. Another important class of solutions are ones that have translational motion with respect to the preferred frame. These would connect to the studies of binary pulsar systems carried out by Foster [44] since the currently unknown values of the “sensitivities” characterizing the velocity dependence of mass can be extracted from these solutions. I expect that Einstein-aether theory will be tightly constrained (and probably ruled out) by this future battery of compact object and binary pulsar timing tests.

From a theoretical perspective it would also be interesting to probe further the GSL violation discussed [94]. It is exciting that one may be able to rule out LV in quantum gravity simply by studying low-energy behavior such as black hole thermodynamics. The investigation of LV in the Hawking effect or even quantization may yield further insights. Finally, even if our universe ultimately does not exhibit some type of LV, the remarkable robustness of Einstein-aether theory indicates it may have an application in future physics as a model describing some other complex system.

Bibliography

- [1] M. Takeda *et al.*, “Energy determination in the Akeno Giant Air Shower Array experiment,” *Astropart. Phys.* **19**, 447 (2003) [arXiv:astro-ph/0209422].
- [2] K. Griesen, *Phys. Rev. Lett.* **16** 748 (1966).
- [3] G. T. Zatsepin and V. A. Kuzmin, “Upper limit of the spectrum of cosmic rays,” *JETP Lett.* **4**, 78 (1966) [*Pisma Zh. Eksp. Teor. Fiz.* **4**, 114 (1966)].
- [4] S. R. Coleman and S. L. Glashow, “High-energy tests of Lorentz invariance,” *Phys. Rev. D* **59**, 116008 (1999) [arXiv:hep-ph/9812418].
- [5] R. Abbasi *et al.* [HiRes Collaboration], arXiv:astro-ph/0703099.
- [6] J. D. Bekenstein, “Relativistic gravitation theory for the MOND paradigm,” *Phys. Rev. D* **70**, 083509 (2004) [Erratum-ibid. *D* **71**, 069901 (2005)] [arXiv:astro-ph/0403694].
- [7] T. G. Zlosnik, P. G. Ferreira and G. D. Starkman, “Modifying gravity with the aether: An alternative to dark matter,” *Phys. Rev. D* **75**, 044017 (2007) [arXiv:astro-ph/0607411].
- [8] M. A. Clayton and J. W. Moffat, “Scalar-Tensor Gravity Theory For Dynamical Light Velocity,” *Phys. Lett. B* **477**, 269 (2000) [arXiv:gr-qc/9910112].
- [9] O. Bertolami, R. Lehnert, R. Potting and A. Ribeiro, “Cosmological acceleration, varying couplings, and Lorentz breaking,” *Phys. Rev. D* **69**, 083513 (2004) [arXiv:astro-ph/0310344].
- [10] S. Kanno and J. Soda, “Lorentz violating inflation,” *Phys. Rev. D* **74**, 063505 (2006) [arXiv:hep-th/0604192].
- [11] R. Gambini and J. Pullin, “Nonstandard optics from quantum spacetime,” *Phys. Rev. D* **59**, 124021 (1999) [arXiv:gr-qc/9809038].
- [12] J. Alfaro, H. A. Morales-Tecotl and L. F. Urrutia, “Loop quantum gravity and light propagation,” *Phys. Rev. D* **65**, 103509 (2002) [arXiv:hep-th/0108061].
- [13] G. Amelino-Camelia, J. R. Ellis, N. E. Mavromatos and D. V. Nanopoulos, “Distance measurement and wave dispersion in a Liouville-string approach to quantum gravity,” *Int. J. Mod. Phys. A* **12**, 607 (1997) [arXiv:hep-th/9605211].

- [14] G. Amelino-Camelia, J. R. Ellis, N. E. Mavromatos, D. V. Nanopoulos and S. Sarkar, “Potential Sensitivity of Gamma-Ray Burster Observations to Wave Dispersion in Vacuo,” *Nature* **393**, 763 (1998) [arXiv:astro-ph/9712103].
- [15] A. Connes, M. R. Douglas and A. S. Schwarz, “Noncommutative geometry and matrix theory: Compactification on tori,” *JHEP* **9802**, 003 (1998) [arXiv:hep-th/9711162].
- [16] S. M. Carroll, J. A. Harvey, V. A. Kostelecky, C. D. Lane and T. Okamoto, “Noncommutative field theory and Lorentz violation,” *Phys. Rev. Lett.* **87**, 141601 (2001) [arXiv:hep-th/0105082].
- [17] G. E. Volovik, “Superfluid analogies of cosmological phenomena,” *Phys. Rept.* **351**, 195 (2001) [arXiv:gr-qc/0005091].
- [18] M. Novello, M. Visser and G. Volovik, *Artificial Black Holes*, (World Scientific 2002)
- [19] G. E. Volovik, *The Universe in a Helium Droplet*, (Clarendon Press, 2003).
- [20] C. Barcelo, S. Liberati and M. Visser, “Analogue gravity,” *Living Rev. Rel.* **8**, 12 (2005) [arXiv:gr-qc/0505065].
- [21] V. A. Kostelecky and S. Samuel, “Spontaneous Breaking of Lorentz Symmetry in String Theory,” *Phys. Rev. D* **39**, 683 (1989); V. A. Kostelecky and S. Samuel, “Phenomenological Gravitational Constraints on Strings and Higher Dimensional Theories,” *Phys. Rev. Lett.* **63**, 224 (1989).
- [22] D. Colladay and V. A. Kostelecky, “Lorentz-violating extension of the standard model,” *Phys. Rev. D* **58**, 116002 (1998) [arXiv:hep-ph/9809521].
- [23] for a review, see T. Jacobson, S. Liberati and D. Mattingly, “Lorentz violation at high energy: Concepts, phenomena and astrophysical constraints,” *Annals Phys.* **321**, 150 (2006) [arXiv:astro-ph/0505267].
- [24] D. Mattingly, “Modern tests of Lorentz invariance,” *Living Rev. Rel.* **8**, 5 (2005) [arXiv:gr-qc/0502097].
- [25] T. Jacobson and D. Mattingly, “Gravity with a dynamical preferred frame,” *Phys. Rev. D* **64**, 024028 (2001) [arXiv:gr-qc/0007031].

- [26] C. Eling, T. Jacobson and D. Mattingly, “Einstein-aether theory,” in *Deserfest*, eds. J. Liu, M. J. Duff, K. Stelle, and R. P. Woodard (World Scientific, 2006) arXiv:gr-qc/0410001.
- [27] C.M. Will and K. Nordtvedt, Jr., “Conservation Laws and Preferred Frames in Relativistic Gravity. I. Preferred-Frame Theories and an Extended PPN Formalism,” *Astrophys. J.* **177**, 757 (1972); K. Nordtvedt, Jr. and C.M. Will, “Conservation Laws and Preferred Frames in Relativistic Gravity. II. Experimental Evidence to Rule Out Preferred-Frame Theories of Gravity,” *Astrophys. J.* **177**, 775 (1972); R.W. Hellings and K. Nordtvedt, Jr., “Vector-metric theory of gravity,” *Phys. Rev.* **D7**, 3593 (1973).
- [28] See, for example, M. Gasperini, “Classical Repulsive Gravity And Broken Lorentz Symmetry,” *Phys. Rev. D* **34**, 2260 (1986); “Singularity prevention and broken Lorentz symmetry”, *Class. Quantum Grav.* **4**, 485 (1987); “Repulsive gravity in the very early Universe”, *Gen. Rel. Grav.* **30**, 1703 (1998); and references therein.
- [29] N. Arkani-Hamed, H. C. Cheng, M. A. Luty and S. Mukohyama, “Ghost condensation and a consistent infrared modification of gravity,” *JHEP* **0405**, 074 (2004) [arXiv:hep-th/0312099].
- [30] B. M. Gripaios, “Modified gravity via spontaneous symmetry breaking,” *JHEP* **0410**, 069 (2004) [arXiv:hep-th/0408127].
- [31] R. Bluhm and V. A. Kostelecky, “Spontaneous Lorentz violation, Nambu-Goldstone modes, and gravity,” *Phys. Rev. D* **71**, 065008 (2005) [arXiv:hep-th/0412320].
- [32] V. A. Rubakov, “Phantom without UV pathology,” arXiv:hep-th/0604153.
- [33] H. C. Cheng, M. A. Luty, S. Mukohyama and J. Thaler, “Spontaneous Lorentz breaking at high energies,” *JHEP* **0605**, 076 (2006) [arXiv:hep-th/0603010].
- [34] S. M. Carroll and E. A. Lim, “Lorentz-violating vector fields slow the universe down,” *Phys. Rev. D* **70**, 123525 (2004) [arXiv:hep-th/0407149].
- [35] for a complete review see C. M. Will, *Theory and Experiment in Gravitational Physics*, (Cambridge University Press, 1993).
- [36] C. Eling and T. Jacobson, “Static post-Newtonian equivalence of GR and gravity with a dynamical preferred frame,” *Phys. Rev. D* **69**, 064005 (2004) [arXiv:gr-qc/0310044].

- [37] M. L. Graesser, A. Jenkins and M. B. Wise, “Spontaneous Lorentz violation and the long-range gravitational preferred-frame effect,” *Phys. Lett. B* **613**, 5 (2005) [arXiv:hep-th/0501223].
- [38] B. Z. Foster and T. Jacobson, “Post-Newtonian parameters and constraints on Einstein-aether theory,” *Phys. Rev. D* **73**, 064015 (2006) [arXiv:gr-qc/0509083].
- [39] D. Mattingly and T. Jacobson, “Relativistic gravity with a dynamical preferred frame,” arXiv:gr-qc/0112012.
- [40] E. A. Lim, “Can We See Lorentz-Violating Vector Fields in the CMB?,” *Phys. Rev. D* **71**, 063504 (2005) [arXiv:astro-ph/0407437].
- [41] T. Jacobson and D. Mattingly, “Einstein–Aether waves,” *Phys. Rev. D* **70**, 024003 (2004) [arXiv:gr-qc/0402005].
- [42] J. W. Elliott, G. D. Moore and H. Stoica, “Constraining the new aether: Gravitational Cherenkov radiation,” *JHEP* **0508**, 066 (2005) [arXiv:hep-ph/0505211].
- [43] B. Z. Foster, “Radiation damping in Einstein-aether theory,” *Phys. Rev. D* **73**, 104012 (2006) [arXiv:gr-qc/0602004].
- [44] B. Z. Foster, Ph.D. Thesis, University of Maryland-College Park, 2007.
- [45] E. Witten, *Comm. Math. Phys.* **80**, 381 (1981); R. Schoen and S.-T. Yau, *Phys. Rev. Lett.* **48**, 369 (1982).
- [46] D. L. Lee, A. P. Lightman, and W.-T. Ni, *Phys. Rev. D* **10**, 1685 (1974).
- [47] C. C. Chang, J. M. Nester, and C. M. Chen, *Phys. Rev. Lett.* **83** 1897-1901 (1999) [arXiv:gr-qc/9809040]
- [48] R. M. Wald, “Black hole entropy in the Noether charge,” *Phys. Rev. D* **48**, 3427 (1993) [arXiv:gr-qc/9307038]; V. Iyer and R. M. Wald, “Some properties of Noether charge and a proposal for dynamical black hole entropy,” *Phys. Rev. D* **50**, 846 (1994) [arXiv:gr-qc/9403028].
- [49] B. Z. Foster, “Noether charges and black hole mechanics in Einstein-aether theory,” *Phys. Rev. D* **73**, 024005 (2006) [arXiv:gr-qc/0509121].
- [50] S. Weinberg, *Gravitation and Cosmology* (Wiley, New York, 1972).

- [51] C. W. Misner, K. Thorne, and J. A. Wheeler, *Gravitation* (Freeman, San Francisco, 1973).
- [52] R. M. Wald, *General Relativity*, (University of Chicago Press, 1984), Ch.4 Problem 5.
- [53] B. Julia and S. Silva, *Class. Quant. Grav.*, **15**, 2173-2215 (1998) [arXiv:gr-qc/9804029].
- [54] Ph. Freud, *Ann. of Math.* **40** 417 (1938).
- [55] R. M. Wald, "Local symmetries and constraints," *J. Math. Phys.* **31**, 2378 (1990).
- [56] R. Portugal and S. Sautu, *Computer Physics Communications*, **105**, 233 (1997). Also see <http://www.cbpf.br/~portugal/Riemann.html>.
- [57] M. A. Clayton, "Causality, shocks and instabilities in vector field models of Lorentz symmetry breaking," arXiv:gr-qc/0104103.
- [58] R. M. Wald, *General Relativity*, (University of Chicago Press, 1984), Ch. 11.
- [59] U. K. De and A. K. Raychaudhuri, "Static Distribution of Charged Dust in General Relativity," *Proc. Royal Soc. A* **303** 47 (1968).
- [60] W. B. Bonnor, "Equilibrium of charged dust in general relativity," *Gen. Rel. Grav.* **12** 453 (1980).
- [61] P. Jetzer, "Boson stars," *Phys. Rept.* **220**, 163 (1992).
- [62] R. Bartnik and J. Mckinnon, "Particle - Like Solutions Of The Einstein Yang-Mills Equations," *Phys. Rev. Lett.* **61**, 141 (1988).
- [63] M. S. Volkov and D. V. Gal'tsov, "Gravitating non-Abelian solitons and black holes with Yang-Mills fields," *Phys. Rept.* **319**, 1 (1999) [arXiv:hep-th/9810070].
- [64] M. D. Seifert, "Stability of spherically symmetric solutions in modified theories of gravity," arXiv:gr-qc/0703060.
- [65] M. D. Seifert and R. M. Wald, "A general variational principle for spherically symmetric perturbations in diffeomorphism covariant theories," *Phys. Rev. D* **75**, 084029 (2007) [arXiv:gr-qc/0612121].

- [66] N. White, “The Constellation-X Mission,” High Resolution X-ray Spectroscopy: towards XEUS and Con-X, Proceedings of the international workshop held at the Mullard Space Science Laboratory of University College London, Holm-bury St Mary, Dorking, Surrey, UK, March 27 - 28, 2006, Ed. G. Branduardi-Raymont, E41 (2006).
- [67] J. van Paradijs, *Ap. J.* **234** 609 (1979).
- [68] A. Salmona, *Phys. Rev. D* **154** 1218 (1967); W. Hillebrant and H. Heintzmann, *Gen. Relativ. Gravitation* **6** 663 (1974)
- [69] T. Damour and G. Esposito-Farese, “Nonperturbative strong field effects in tensor - scalar theories of gravitation,” *Phys. Rev. Lett.* **70**, 2220 (1993).
- [70] S. DeDeo and D. Psaltis, “Towards New Tests of Strong-field Gravity with Measurements of Surface Atomic Line Redshifts from Neutron Stars,” *Phys. Rev. Lett.* **90**, 141101 (2003) [arXiv:astro-ph/0302095].
- [71] B. Z. Foster, “Metric redefinitions in Einstein-aether theory,” *Phys. Rev. D* **72**, 044017 (2005) [arXiv:gr-qc/0502066].
- [72] G. B. Cook, S. L. Shapiro and S. A. Teukolsky, “Rapidly rotating neutron stars in general relativity: Realistic equations of state,” *Astrophys. J.* **424**, 823 (1994).
- [73] J. B. Hartle, *Gravity: An Introduction to Einstein’s General Relativity*, (Addison Wesley, 2002), Chapter 22.
- [74] A. Akmal, V. R. Pandharipande and D. G. Ravenhall, “The equation of state for nucleon matter and neutron star structure,” *Phys. Rev. C* **58**, 1804 (1998) [arXiv:nucl-th/9804027].
- [75] E. Farhi and R. L. Jaffe, “Strange matter,” *Phys. Rev. D* **30**, 2379 (1984).
- [76] Sudip Bhattacharyya and Cole Miller, private communication.
- [77] H. Quaintrell et al., “The mass of the neutron star in Vela X-1 and tidally induced non-radial oscillations in GP Vel,” *A&A* **401**, 313 (2003).
- [78] D. J. Nice et al., “A $2.1 M_{\odot}$ Pulsar Measured by Relativistic Orbital Decay,” *ApJ* **634**, 1242 (2005).

- [79] D. Barret, J.-F. Olive and M. C. Miller, “Drop of coherence of the lower kilohertz QPO in neutron stars: Is there a link with the innermost stable circular orbit?,” *AN* **326**, 808 (2005).
- [80] D. Barret, J.-F. Olive and M. C. Miller, “An abrupt drop in the coherence of the lower kHz quasi-periodic oscillations in 4U 1636-536,” *MNRAS* **361**, 855 (2005).
- [81] D. Barret, J.-F. Olive and M. C. Miller, “The coherence of kilohertz quasi-periodic oscillations in the X-rays from accreting neutron stars,” *MNRAS* **370**, 1140 (2006).
- [82] D. Barret, J.-F. Olive and M. C. Miller, “Supporting evidence for the signature of the innermost stable circular orbit in Rossi X-ray data from 4U 1636-536,” *MNRAS* **376**, 1139 (2007).
- [83] M. Méndez, “On the maximum amplitude and coherence of the kilohertz quasi-periodic oscillations in low-mass X-ray binaries,” *MNRAS* **371**, 1925 (2006).
- [84] J. Cottam, F. Paerels and M. Méndez, “Gravitationally redshifted absorption lines in the X-ray burst spectra of a neutron star,” *Nature* **420**, 51 (2002).
- [85] F. Özel, “Soft equations of state for neutron-star matter ruled out by EXO 0748-676,” *Nature* **441**, 1115 (2006).
- [86] D. Psaltis, “Testing General Metric Theories of Gravity with Bursting Neutron Stars,” arXiv:0704.2426 [astro-ph].
- [87] J. D. Bekenstein, “Nonexistence of baryon number for static black holes,” *Phys. Rev. D* **5**, 1239 (1972); S. W. Hawking, “Black holes in the Brans-Dicke theory of gravitation,” *Commun. Math. Phys.* **25**, 167 (1972).
- [88] S. Mukohyama, “Black holes in the ghost condensate,” *Phys. Rev. D* **71**, 104019 (2005) [arXiv:hep-th/0502189].
- [89] D. Giannios, “Spherically symmetric, static spacetimes in TeVeS,” *Phys. Rev. D* **71**, 103511 (2005) [arXiv:gr-qc/0502122].
- [90] for a review, see C. S. Reynolds and M. A. Nowak, “Fluorescent iron lines as a probe of astrophysical black hole systems,” *Phys. Rep.* **377**, 389 (2003).
- [91] B. C. Barish, “The Laser Interferometer Gravitational-Wave Observatory LIGO,” *Adv. Space Res.* **25**, 1165 (2000).

- [92] K. Danzmann, “LISA Mission Overview,” *Adv. Space Res.* **25**, 1129 (2000).
- [93] D. Garfinkle, C. Eling and T. Jacobson, “Numerical simulations of gravitational collapse in Einstein-aether theory,” *Phys. Rev. D* **76**, 024003 (2007) [arXiv:gr-qc/0703093].
- [94] C. Eling, B. Z. Foster, T. Jacobson and A. C. Wall, “Lorentz violation and perpetual motion,” *Phys. Rev. D* **75**, 101502 (2007) [arXiv:hep-th/0702124].
- [95] R. Courant and D. Hilbert *Methods of Mathematical Physics*, (New York: Interscience Publishers, 1962).
- [96] I. Racz and R. M. Wald, “Global extensions of space-times describing asymptotic final states of black holes,” *Class. Quant. Grav.* **13**, 539 (1996) [arXiv:gr-qc/9507055].
- [97] E. E. Donets, D. V. Galtsov and M. Y. Zotov, “Internal structure of Einstein Yang-Mills black holes,” *Phys. Rev. D* **56**, 3459 (1997) [arXiv:gr-qc/9612067].
- [98] R. M. Wald, “The thermodynamics of black holes,” *Living Rev. Rel.* **4**, 6 (2001) [arXiv:gr-qc/9912119].
- [99] S. L. Dubovsky and S. M. Sibiryakov, “Spontaneous breaking of Lorentz invariance, black holes and perpetuum mobile of the 2nd kind,” *Phys. Lett. B* **638**, 509 (2006) [arXiv:hep-th/0603158].
- [100] D. Grumiller, W. Kummer and D. V. Vassilevich, “Dilaton gravity in two dimensions,” *Phys. Rept.* **369**, 327 (2002) [arXiv:hep-th/0204253].
- [101] S. Deser and B. Tekin, “Shortcuts to high symmetry solutions in gravitational theories,” *Class. Quant. Grav.* **20**, 4877 (2003) [arXiv:gr-qc/0306114].
- [102] J. D. Brown, M. Henneaux and C. Teitelboim, “Black holes in two space-time dimensions,” *Phys. Rev. D* **33**, 319 (1986).
- [103] V. P. Frolov, “Two-dimensional black hole physics,” *Phys. Rev. D* **46**, 5383 (1992).
- [104] C. G. Callan, S. B. Giddings, J. A. Harvey and A. Strominger, “Evanescent black holes,” *Phys. Rev. D* **45**, 1005 (1992) [arXiv:hep-th/9111056].
- [105] A. Achucarro and M. E. Ortiz, “Relating black holes in two-dimensions and three-dimensions,” *Phys. Rev. D* **48**, 3600 (1993) [arXiv:hep-th/9304068].

- [106] C. Teitelboim, “Gravitation and hamiltonian structure in two space-time dimensions,” *Phys. Lett. B* **126**, 41 (1983); R. Jackiw, “Liouville field theory: a two-dimensional model for gravity?”, in *Quantum Theory of Gravity*, ed. S. Christensen (Hilger, Bristol, 1984).
- [107] A. Einstein, “Spielen Gravitationsfelder im Aufbau der materiellen Elementarteilchen eine wesentliche Rolle?,” *Sitzungsberichte der Koniglich Preussischen Akad. d. Wissenschaften*, 349-356 (1919); translated as “Do gravitational fields play an essential part in the structure of the elementary particles of matter?,” in *The Principle of Relativity*, by A. Einstein *et. al.* (Dover, New York, 1952); J. L. Anderson and D. Finkelstein, “Cosmological constant and fundamental length,” *Am. J. Phys.* **39**, 901 (1971); see also S. Weinberg, “The cosmological constant problem,” *Rev. Mod. Phys.* **61**, 1 (1989), and references therein.
- [108] M. Spradlin, A. Strominger and A. Volovich, “Les Houches lectures on de Sitter space,” arXiv:hep-th/0110007.